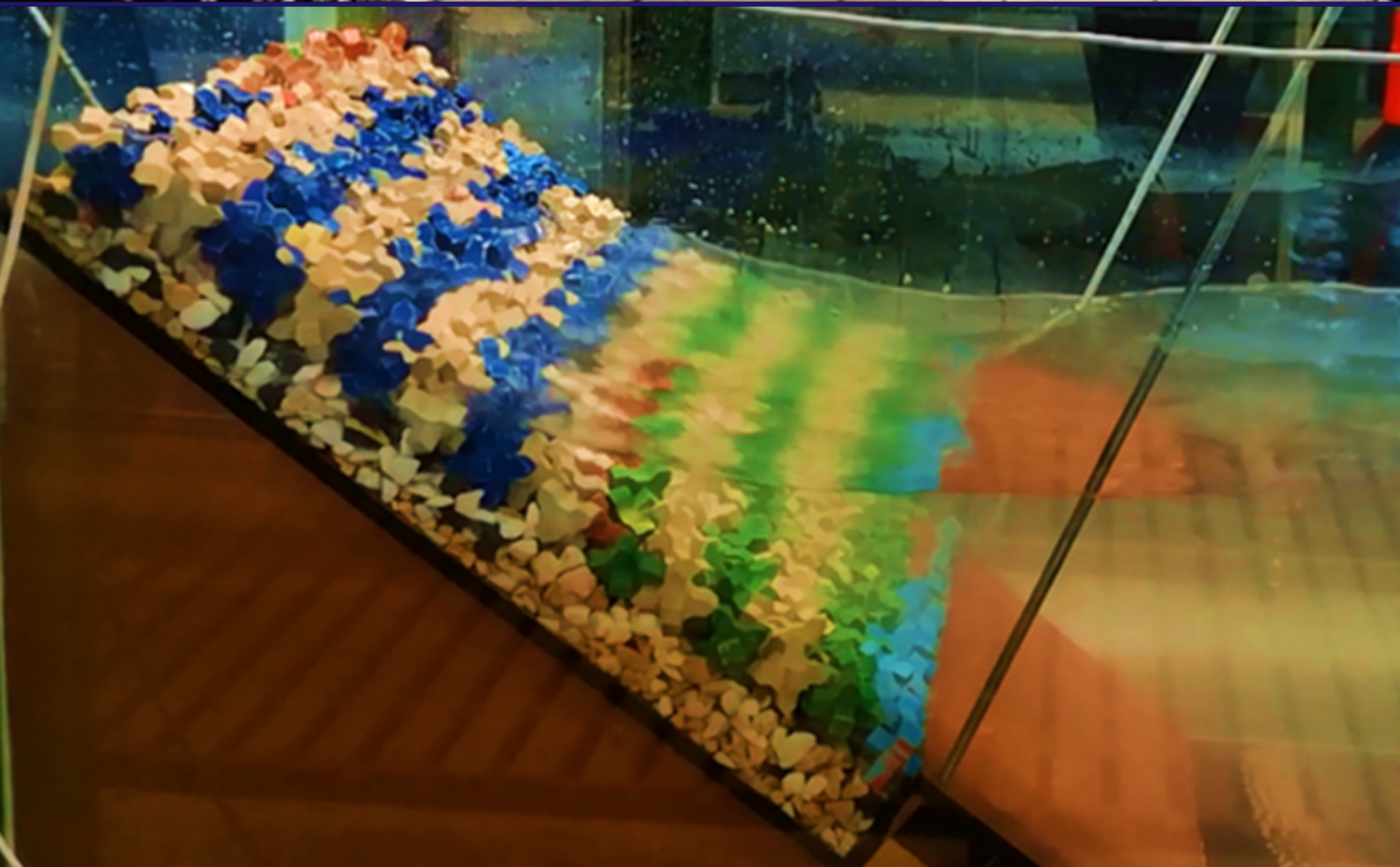


# Rocking of Single Layer Armour Units

## Rocking Revisited III

H.P.G.M Caldera

Delft University of Technology



ERASMUS +: ERASMUS MUNDUS MOBILITY PROGRAMME

Master of Science in

COASTAL AND MARINE ENGINEERING AND  
MANAGEMENT

CoMEM

**ROCKING OF SINGLE LAYER ARMOUR UNITS  
ROCKING REVISITED III**

Delft University of Technology  
16 July 2019

H.P.G.M, Caldera

The Erasmus+: Erasmus Mundus MSc in Coastal and Marine Engineering and Management is an integrated programme including mobility organized by five European partner institutions, coordinated by Norwegian University of Science and Technology (NTNU).

The joint study programme of 120 ECTS credits (two years full-time) has been obtained at two or three of the five CoMEM partner institutions:

- Norges Teknisk- Naturvitenskapelige Universitet (NTNU) Trondheim, Norway
- Technische Universiteit (TU) Delft, The Netherlands
- Universitat Politècnica de Catalunya (UPC). BarcelonaTech. Barcelona, Spain
- University of Southampton, Southampton, Great Britain
- City University London, London, Great Britain

During the first three semesters of the programme, students study at two or three different universities depending on their track of study. In the fourth and final semester an MSc project and thesis has to be completed. The two-year CoMEM programme leads to a multiple set of officially recognized MSc diploma certificates. These will be issued by the universities that have been attended by the student. The transcripts issued with the MSc Diploma Certificate of each university include grades/marks and credits for each subject.

Information regarding the CoMEM programme can be obtained from the programme coordinator:

Øivind A. Arntsen, Dr.ing.  
Associate professor in Marine Civil Engineering  
Department of Civil and Environmental Engineering  
NTNU Norway  
Mob.: +4792650455 Fax: + 4773597021  
Email: oivind.arntsen@ntnu.no

CoMEM URL: <https://www.ntnu.edu/studies/mscomem>

Disclaimer:

*"The European Commission support for the production of this publication does not constitute an endorsement of the contents which reflects the views only of the authors, and the Commission cannot be held responsible for any use which may be made of the information contained therein."*

## CoMEM Thesis

This thesis was completed by:

*H.P.G.M, Caldera*

Under supervision of:

*Prof. dr.W.S. J.Uijtewaal*

*Assoc.Prof. dr.ir. B. Hofland*

*Assoc.Prof. dr. A. Antonini*

*Dr. ir. M. R.A.van Gent*

*Ir.J.C.van der Lem*

*Dr.ir. M. Muttray*

As a requirement to attend the degree of

*Erasmus+: Erasmus Mundus Master in Coastal and Marine Engineering and Management (CoMEM)*

Taught at the following educational institutions:

*Norges Teknisk- Naturvitenskapelige Universitet (NTNU)*

*Trondheim, Norway*

*Technische Universiteit (TU) Delft*

*Delft, The Netherlands*

*University of Southampton,*

*Southampton, Great Britain*

At which the student has studied from August 2017 to July 2019.

# Rocking of Single Layer Armour Units

## Rocking Revisited III

by

**H.P.G.M Caldera**

in partial fulfillment of the requirements for the degree of

### **Master of Science**

in Coastal and marine Engineering and Management (CoMEM)

at the Delft University of Technology,  
to be defended publicly on Thursday July 18, 2019 at 1:00 PM.

Graduation committee:	Prof. dr. W. S. J. Uijtewaal,	TU Delft
	Assoc.Prof. dr. ir. B. Hofland,	TU Delft/Deltares
	Assoc.Prof. dr. A. Antonini,	TU Delft
	Dr. ir. M. R. A. van Gent,	Deltares
	Ir. J. C. van der Lem,	Royal Haskoning DHV
	Dr. ir. M. Muttray,	DMC

An electronic version of this thesis is available at <http://repository.tudelft.nl/>.

# Preface

The present report is my final thesis for the partial fulfillment of the requirement for the degree in Masters of Science in Coastal and Marine Engineering and Management (CoMEM). First of all I extend my sincere gratitude to EU and the CoMEM board for giving me this wonderful opportunity to study in three leading universities in the world which is one of the best experiences I ever had in my life.

This thesis is supervised by prof. dr. ir. W.S.J. Uijtewaal (TU Delft), dr. ir. B. Hofland (TUDelft), dr. A. Antonini (TU Delft), dr. ir. M.R.A. van Gent (Deltares), ir. J.C. van der Lem (Royal HaskoningDHV) and dr.ir. M. Muttray (DMC). This would not be successful without the continuous support of them. Therefore I would like to thank my supervisory committee for their input and guidance during my Master's thesis. Specially, I am grateful to my daily supervisor, Bas Hofland for giving me the opportunity to take part in this research and kind input and guidance throughout the thesis work . Also I would like to thank Pieter Bakker (DMC) for his kind support to success the work.

Many thanks Christian van Nieuwenhuizen (Deltares) for the friendly support given to make the instrumented unit. Also, I would like to thank Jelle Molenaar and Wim Taal (Deltares) for their help and advice for making the instrumented units. I am also very thankful to Sander de Vree (TU Delft) and all the other supporting staff from the TU Delft water lab for their constant support during the experiments.

I also would like to thank my dear parents, and the family for loving me so much and encouraging me being my pillars of strength. Last but not least, I would like to thank all my friends specially to J.Sirisena and K. Ihalagedara for their unconditional support and to all my CoMEM friends for making these two years memorable.

*H.P.G.M Caldera  
Delft, July 2019*

# Abstract

After the failure of several large breakwaters in late 1970's and early 1980's where the role of rocking and breakage of armour became apparent, the importance of understanding this rocking phenomenon is given a great emphasis. Single layer randomly placed armour units are widely used in breakwater designs as they are more economical due to the less volume requirement. But these single layer units have a much more "brittle" behaviour and strength of the units becomes a critical factor. As the stresses developed after the impact is difficult to measure directly in the scale models, currently percentage rocking is used as a design criterion. But a clear relationship between this quantity and breakage has not been identified. Even though the single layer armour unit types are widely used the knowledge on the rocking behaviour of this type of units are limited.

Therefore to get a better insight into the rocking behaviour of single layer armour units a previously proposed technique of instrumented unit with embedded sensor was adopted. This technique was found to be promising in detecting the rocking motion in stand alone mode. However, one issue of that technique was relatively lower sampling frequency. Because of that, enough data could not be captured to resolve the rocking motion in time very accurately.

Therefore, in this report the measurements with standalone IMU sensor embedded in 3D printed model armour unit has been developed further. Firstly, different techniques were adopted to get the optimum sampling frequency and sampling frequency was increased from 25 Hz to 100 Hz.

Then 2D physical model testings were performed with two instrumented model units. The model units were placed on the loosely placed underlayer which was supported by glued stones layer and a wooden base. This set up represents a breakwater section with a impermeable core in reality. The water level was kept constant during the testings. Tests were performed for two days and only wave heights and periods were changed during the testings while keeping the constant wave steepness. Initially, both units were placed at the water level. But, when the instrumented units seem well interlocked with neighbouring units the spacing around the units were intentionally increased by disturbing the natural interlocking pattern. Otherwise, evaluating the effectiveness of the technique will be difficult without having sufficient movements. During the second day of testings after rebuilding the slope, initially both instrumented units were placed at the water level but later on units' positions were changed to obtain sufficient motions so that a good record of data to analyze.

Then the data were analyzed and processed based on a matlab routing. This report includes further details on the processing method and obtained results. It is the first time that stand alone rocking motions are reported for single layer armour units. By increasing the sampling frequency from 25 Hz to 100 Hz, rocking events can now be resolved in time by 5-10 measurements points. Gyroscope data and accelerometer data were combined to separate the linear acceleration from raw accelerometer data. Upward and downward rotational motions were distinguished and impact velocities were calculated based on both accelerometer and gyroscope. By analyzing the data it was observed that the angle of rotation during the rocking event is small and usually unit returns to its original position after a full rotation.

According to the final results, calculated characteristic impact velocities are in the same order of magnitude with the previously conducted researches. Also the results show that the magnitude of the characteristic impact velocity and number of collisions are not solely depend on the wave height or the stability number, as same order of magnitude of the impact velocities and number of collisions can be observed with the smaller waves if the interlocking is less effective. Therefore it can be concluded that for the single layer armour units, interlocking effect can significantly influence the magnitude of the impact velocity and number of collisions.

Also highest impact velocities were observed during the upward movement compared with the impact velocities of the downward movement. Also results show that both vertical position and horizontal position of the unit on the slope can influence the both impact velocities and the number of collisions. Also testing results showed that amount of first settlement of top rows can also affect the rocking motion of below rows due to the additional pressure provided by the settled units.

However, impact velocities resulted from accelerometer integration is relatively higher than the impact velocities obtained from the gyroscope. As the impact velocity estimation from the accelerometer has several uncertainties, the impacts velocity given by the gyroscope is more trustworthy.

The proposed technique is promising in detecting the rocking motion. After analyzing the data it was realized that some rocking motions that was not identified during the visual observations (basically due to higher foaminess and turbulence) were also detected by the instrumented units. Therefore it is recommended to use the technique in future researches to further study on the rocking motion.

# Contents

<b>List of Symbols</b>	<b>x</b>
<b>1 Introduction</b>	<b>1</b>
1.1 Background	1
1.2 Problem Description	2
1.3 Objective	3
1.4 Approach	4
<b>2 Literature Review</b>	<b>5</b>
2.1 Rocking motion of armour units	5
2.1.1 CUR C70 1989	5
2.1.2 Rocking of a single Cube on a breakwater slope	7
2.1.3 Measurement on rocking of Cubes in a double Layer on a breakwater	9
2.2 Stability of single layer armour units	11
2.2.1 The influence of the wave height distribution on the stability of single layer armour units.	11
2.3 Different applications of Inertial Measurement Units (IMU)	12
2.3.1 Smartstones: a small e-compass, accelerometer and gyroscope embedded in stones	12
2.3.2 Inertial forces on shipping containers from a broken tsunami bore	12
2.3.3 Smart pebble for monitoring riverbed sediment transport.	13
2.3.4 Forces and pressures on Core-Loc armour units in rubble mound breakwaters measured via instrumented smart units.	13
<b>3 Experimental studies -Instrumented Xbloc Unit</b>	<b>15</b>
3.1 Instrumented units construction and development	15
3.1.1 Model unit construction	15
3.1.2 Instrumentation	16
3.1.3 Assembly and Fabrication	16
3.2 Hardware/Software improvements	20
3.2.1 Improving Sampling Frequency	20
3.2.2 Performances with different classes of SD cards	21
3.2.3 Comparison of the different techniques used to improve the data recording speed.	24
3.3 Sensor Calibration and Validation.	24
3.3.1 Complementary filter	26
<b>4 Experimental studies -Model Setup</b>	<b>29</b>
4.1 Scaling Laws	29
4.1.1 Dimensionless Scaling.	30
4.2 Test Programme	30
4.2.1 Phenomena that affect the stability of the armour layer	30
4.2.2 Hydraulic test parameters	32
4.3 Model layout.	34
4.3.1 Main dimensions	34
4.3.2 Armour layer	35
4.3.3 Under layer	35
4.3.4 Armour layer placement.	36

<b>5</b>	<b>Experimental studies -Model Testings</b>	<b>39</b>
5.1	Test Facility . . . . .	39
5.2	Data Collection . . . . .	39
5.3	Observations during the testings . . . . .	40
5.3.1	Test Series 1. . . . .	40
5.3.2	Test Series 2. . . . .	41
<b>6</b>	<b>Data Processing and Analyzing</b>	<b>43</b>
6.1	Possible movements . . . . .	43
6.2	Data Processing. . . . .	45
6.2.1	Impact Velocity Calculation. . . . .	49
6.3	Results Analysis . . . . .	51
6.3.1	Probability of exceedance of impact velocity . . . . .	51
6.3.2	Upward movement with run up . . . . .	52
6.3.3	Downward movement with rundown . . . . .	54
6.3.4	Number of collisions . . . . .	58
<b>7</b>	<b>Discussion and Conclusions</b>	<b>61</b>
7.1	Measurement and processing technique . . . . .	61
7.2	Order of magnitude of Impact velocity . . . . .	61
7.3	Difference with respect to unit position on the slope . . . . .	62
7.4	Number of collisions . . . . .	62
7.5	Amount of rotation during the rocking motion . . . . .	62
7.6	Impact velocity from gyroscope and the accelerometer. . . . .	62
<b>8</b>	<b>Recommendations</b>	<b>63</b>
8.1	Data Processing. . . . .	63
8.1.1	Frame of reference . . . . .	63
8.1.2	Rotation angle of the unit during the rocking . . . . .	63
8.1.3	Corrections of the sensor . . . . .	63
8.1.4	Minimizing the slowing down of the sensor . . . . .	63
8.1.5	Improving the method of integration of accelerometer data . . . . .	63
8.1.6	Distance between point of rotation and location of impact . . . . .	63
8.2	Use of the proposed technique . . . . .	64
8.2.1	Impact velocity of single layer armour units . . . . .	64
8.2.2	Synchronize the wave data with the measurements . . . . .	64
8.2.3	Translation and settlement . . . . .	64
<b>A</b>	<b>Input and output wave conditions</b>	<b>65</b>
<b>B</b>	<b>Photos taken during the model testing</b>	<b>67</b>
<b>C</b>	<b>Analyzing the data during the impact</b>	<b>73</b>
<b>D</b>	<b>Probability of exceedance of impact velocities before collision</b>	<b>77</b>
	<b>List of Figures</b>	<b>83</b>
	<b>List of Tables</b>	<b>85</b>
	<b>Bibliography</b>	<b>87</b>

# List of Symbols

## Generic Symbols

$D_n$	Nominal Diameter	[m]
$H_{m0}$	Significant wave height from wave energy spectrum	[m]
$H_s$	Significant Wave Height	[m]
$N$	Number of Waves	[-]
$N$	Number of waves	[-]
$N_{col}$	Number of collisions in the test	[-]
$N_{o<0.5D}$	Number of units that was moved over a distance of less than 0.5 times the diameter related to a width of $1D_n$ in cross-section	[-]
$N_{o>0.5D}$	Number of units that was moved over a distance of greater than 0.5 times the diameter related to a width of $1D_n$ in cross-section	[-]
$N_{od}$	Number of displaced units out of the layer related to a width of $1D_n$ in cross-section	[-]
$N_{otol}$	Total number of units that was moved related to a width of $1D_n$ in cross-section	[-]
$V$	Velocity center of armour unit before collision	[m/s]
$\Delta$	Relative Buoyant Density	[-]
$\rho_s$	Density of Armour Unit	[kg/m <sup>3</sup> ]
$\rho_w$	Density of Water	[kg/m <sup>3</sup> ]
$S_m$	Fictitious wave steepness based on $H_s$ and $T_m$	[-]
$S_{m-1.0}$	Fictitious wave steepness based on $H_{m0}$ and $T_{m-1.0}$	[-]
$\omega$	Angular Velocity	[rad/s]
$T_{m-1.0}$	Wave period based on the ratio of the wave energy spectral moments $m_{-1}$ and $m_0$	[s]
$T_p$	Peak Wave Period	[s]
$[y/D_n]$	Position of the cube relative to the water level	[-]
$I_0$	Moment of Inertia	[kgm <sup>2</sup> ]
$\alpha$	filter coefficient	[-]
$\alpha_g$	angle from gyroscope data	[rads <sup>-1</sup> ]

$\nu$	Kinematic Viscosity	$[m^2s^{-1}]$
$\omega_{gyro}$	the angular velocity from the gyroscope	$[rads^{-1}]$
$\sigma$	Surface tension	$[Nm^{-1}]$
$\tau$	filter time coefficient	[-]
$C$	Correction factor on weight of the unit	[-]
$Fr$	Froude Number	[-]
$H_D$	Significant design wave height	$[m]$
$H_{0.1\%}$	the wave height with a probability of exceedance of 0.1%	$[m]$
$H_{2\%}$	the wave height with a probability of exceedance of 2%	$[m]$
$L$	Characteristic Length	$[m]$
$L_{op}$	Deep water wave length based on peak wave period	$[m]$
$m_i$	mass of the $i$ th element	$[g]$
$r_i$	radius to the $i$ th element	$[cm]$
$Re$	Reynolds Number	[-]
$S$	Empirically derived value for the stability number	[-]
$s_{op}$	Fictitious wave steepness	[-]
$t$	Duration	$[s]$
$We$	Weber Number	[-]
$\alpha_a$	angle from accelerometer data	$[rads^{-1}]$
$\theta_{angle}$	the tilting angle	$[rads^{-1}]$
$\zeta_{op}$	Iribarren number	[-]
$a_x$	acceleration in X direction	$[ms^{-1}]$
$a_y$	acceleration in Y direction	$[ms^{-1}]$
$a_z$	acceleration in Z direction	$[ms^{-1}]$
$a_{Acc}$	angle obtained through the data from accelerometer	$[rads^{-1}]$
$D$	Height of Xbloc	$[m]$
$I$	Moment of Inertia of the unit	$[gcm^2]$
$U$	Particle velocity	$[m^{-1}]$
$[H_s / \Delta D_n]$	Stability Number	[-]

# 1

## Introduction

The focus of this research is to understand the rocking motion of Xbloc which is a commonly used single layer armour unit type. This chapter will provide better insight into the purpose, motivation and objectives of this research.

### 1.1. Background

Breakwaters are worldwide popular structures that are built on the coast to provide protection against waves and currents. Primarily, these are constructed at the entrance of the ports and harbours to provide safe navigation and sheltered basin. But these can also serve as shore parallel structures that protect habitats in the hinterland and beach against erosion. Additionally, in some cases breakwaters avoid or reduce the siltation of navigation channels and accommodate loading facilities for cargo or passengers.

A conventional breakwater consists of three main layers, core from fine material, underlayer(s) to act as filter layer to protect the core material being washed away and armor layer mainly to dissipate wave energy (Figure 1.1).

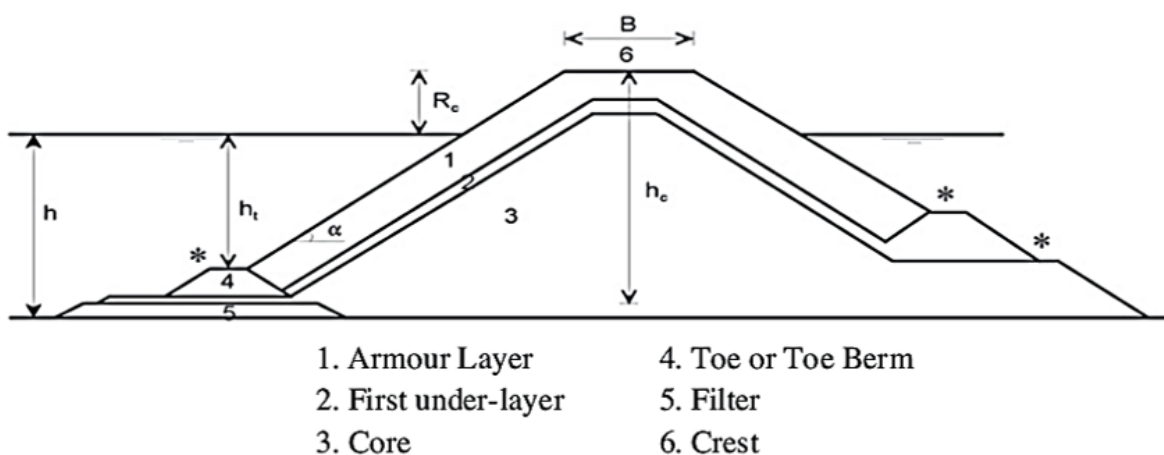


Figure 1.1: Typical cross section of a rubble mound breakwater (Verhagen et al., 2008)

Traditionally, large natural rocks and very heavy concrete blocks were used as armour units which obtain stability by self-weight. But with the availability problems of natural rocks and massive material requirement of the concrete blocks, interlocking type armour units were introduced to optimize the concept. Among them classical units such as Dolosse, Tetrapods, and etc were used in double layers until the armor units such as Xbloc, Accropode, and Coreloc have been developed to use in a single

layer (Figure 1.2).

Randomly placed armour units				Uniformly placed armour units	
Double layer placement		Single layer placement			
Stability factor: Own weight	Own weight and interlocking		Interlocking		Friction
Cube 	Tetrapode France, 1950 	Accropode France, 1980 	Cob UK, 1969 		
Modified Cube USA, 1959 	Akmon NL, 1962 	Core-loc <sup>®</sup> USA, 1996 	Diahitis Ireland, 1998 		
Antifer Cube France, 1973 	Tribar USA, 1958 	A-Jack USA, 1998 	Seabee Australia, 1978 		
Haro Belgium, 1984 	Stabit UK, 1961 	Xbloc NL, 2003 	Shed UK, 1982 		
Tripod NL, 1962 	Dolos South Africa, 1963 				

Figure 1.2: Different types of armour units (Reedijk & Muttray, 2009)

Xbloc units are randomly placed armour blocks (Figure 1.3) invented by Delta Marine Consultants (DMC). Due to the angular shape of the Xblocs, the porosity of the Xbloc armour layer is high and the concrete consumption is low. Xblocs are best suited for breakwater slopes with a steepness of 3V:4H.



Figure 1.3: Xbloc placement on a breakwater

## 1.2. Problem Description

Designing of the armour layer of breakwaters predominantly based on the hydraulic stability and knowledge on incorporating the strength (structural stability) of the armour units in breakwater design procedure remains poor. But during a large storm rocking and collision between armour units are inherent

and consequent breakage of the armour units can be observed.

After the failure of several large breakwaters in late 1970's and early 1980's where the role of rocking and breakage of armour became apparent, the importance of understanding this phenomenon is given a great emphasis.

Single layer randomly placed armour units are widely used in breakwater designs as they are more economical due to the less volume requirement. But these single layer units have a much more "brittle" behaviour and strength of the units becomes a critical factor. As the stresses developed after the impact is difficult to measure directly in the scale models, currently percentage rocking is used as a design criterion. But a clear relationship between this quantity and breakage has not been identified [Hofland et al. \(2018\)](#).

As the shape, placement and slope are different for each armour unit type, the rocking mechanism is also different for each armour unit type. Even though the single layer armour unit types are widely used the knowledge on the rocking behaviour of this type of units are limited. Especially, the magnitude of the impact velocity and the stochastic and spatial distribution of this impact velocity has not been addressed which are known as the important parameters of the rocking behaviour [Hofland et al. \(2018\)](#).

### Measurement technique

In current practice percentage rocking is included in the design guidelines by means of both number of events per element, and number of elements that move. These are usually taken from visual observations and results are very subjective to the observer. Also, it is a laborious process and by visually observing the measurements like impact velocity that can ultimately be related to the breakage of the units, is difficult to calculate. Even though this technique is possible to use in 2D modelling to observe rocking, it can not be adopted in 3D modelling to calculate the rocking.

High-speed photography technique that captures a series of photographs taken at a high frame rate also an alternative method to detect movements and frequency of the movements of the armour units clearly. But this technique alone does not help in estimating impact velocity correctly and especially when dominant mode of rocking is rotation rather than translation it requires to capture the motions in different angles. Also, laborious and time consuming when processing the data. Next to that, with higher turbulence generated after violent breaking it would be difficult to detect movements using photos practically.

Also, rocking motions are completely random in nature and difficult to give an accurate representation using numerical modelling. Modelling turbulence, and rocking motion need high level of programming and super computers to run the model. Hence, numerically modelling of rocking is also difficult.

Developing a standalone measurement device with embedded sensor seems to be more realistic to measure the impact velocity. But measuring this during the impact itself would require a device with very high sampling frequency as the impact time is in the order of 1ms. But measuring the impact velocity before the impact can be achieved with much smaller sampling frequency as the accelerations in the movement before the impact are related to the wave period in the order of the 1s duration [Hofland et al. \(2018\)](#). A state of the art measuring device with a 9 axis IMU sensor is used in the previous study by [Arefin \(2017\)](#) appears to be a promising method to measure impact velocity before the impact with the maximum sensor frequency of 100 Hz.

## 1.3. Objective

The objective of the study follows the problem description sated in Section [1.2](#).

### Objective

- Determining magnitude, spatial and stochastic distribution of impact velocities of Xblocs, that are rocking under the wave action.

In order to achieve this main objective, following sub objectives are defined.

Sub-Objectives:

- Further improve and validate the dedicated measurement technique for rocking analysis
- Determine the parameters related to rocking of Xblocs and methods to derive these parameters efficiently and accurately from these devices.
- Compare and validate the parameters with previous studies

### 1.4. Approach

In order to fulfill the above objectives, following methodology will be applied.

- Analysis of previously conducted studies on rocking motion of armour units and stability of Xblocs.
- Update and optimize the hardware settings by increasing the sampling frequency, water tightness and etc.
- Develop an instrumented Xbloc unit and validate the required minimum sampling frequency to achieve accurate measurement for impact velocity.
- Develop a physical model and measure the rocking behavior of Xblocs subjected to varying wave height.
- Take measurements for acceleration and rotation with improved sampling frequency together with video recordings to detect movements of the units.
- Process and Analyze the data.
- Compare the results from the current research project with the results from previously conducted research.

# 2

## Literature Review

This chapter summarizes the previous studies to contextualize the current thesis work under three different sections. First section presents the research works relevant to understanding the behaviour of both single layer and double layer armour units, rocking motion, determination of impact velocities and incorporating the strength of the armor units in the breakwater design procedure. The second section presents the research work on stability of concrete armour units particularly on Xbloccs and is followed by different applications of IMU sensors.

### 2.1. Rocking motion of armour units

In the 1980 's the Centre for Civil Engineering Research and Codes (CUR) paid the attention in incorporating the strength of the armor units in the breakwater design procedure by initiating a comprehensive joint industry research programme. This was followed by two other research works performed by Tuan Le (2016) and Syed Arefin (2017) in TU Delft for their master theses.

#### 2.1.1. CUR C70 1989

Owing to the emphasis on the problem of damaged breakwaters with large slender concrete units, basic research project was developed under the coordination of the Centre for Civil Engineering Research and Codes work group C70.

##### Overview

Being a very extensive research on strength of concrete armour units, several topics were studied during this project including loading, strength of concrete armour units, measuring impact velocities and measuring load time relationship for the colliding concrete bodies. The final aim of all these studies was to develop an overall design procedure for the practical applications.

In order to fulfill this objective model tests were performed on breakwater sections armoured with Cubes and Tetrapods which are typically considered as double layer armour units. Test programme was divided into two parts; stability tests and tests on acceleration measurements. Stability tests resulted in prediction of the number of moved units and the number of impacts as a function of wave height, period and location on the slope. Based on these estimations the number of failed units on the breakwater was calculated. Measurements on acceleration during impacts resulted in a description of the distribution of impact velocities at the centre of the unit. The test results were transferred into an applicable format by developing a numerical application, known as "Rocking" in which the calculation procedure was conducted as a Monte Carlo simulation.

### Test programme

Each of the tests was conducted considering random waves with about 2000 waves and with increasing wave height from about 0.08m up to 0.20m. Number of units displaced from their initial positions were determined by both visual counting and overlay technique. Additionally, single-frame-technique was used to determine the frequency of the rocking of the moving units.

In order to measure the accelerations in the rocking unit, instrumented units were developed for both armour unit types by placing an accelerometer in the centre of the units. This accelerometer can only measure in one direction and had a natural frequency of 100kHz. Four different positions of armour units along the slope were considered;  $2D_n$  over the still water line, at the still water line,  $2D_n$  under the still water line and  $4D_n$  under the still water line, where  $D_n$  is the nominal diameter of the particular armour unit ( $y/D_n = +2, 0, -2$  and  $-4$ ).

### Number of moved units and Collisions

As for the double layer armour certain number of displaced units are allowed during design conditions, the total number of moved units ( $N_{total}$ ) was calculated taking into account the number of displaced units ( $N_{od}$ ), number of units moved more than 0.5 times the diameter ( $N_{o>0.5D}$ ) and the number of units moved less than 0.5 times the diameter ( $N_{o<0.5D}$ ). After analyzing the data it was found that the 0.50 reduction in stability number ( $H_s / \Delta D_n$ ) in the stability formula derived by Van der Meer for Cubes and Tetrapodes ( equation 2.1 and 2.2) in a double layer gives the satisfactory representation for the total number of moving units. The total number of collisions were roughly assumed as three times the total number of moving units.

Stability formula for cubes in a double layer:

$$\left(\frac{H_s}{\Delta D_n}\right) = [(6.7 \frac{N_{od}^{0.4}}{N^{0.3}}) + 1] S_m^{-0.1} \quad (2.1)$$

Stability formula for Tetrapodes:

$$\left(\frac{H_s}{\Delta D_n}\right) = [(3.75 \frac{N_{od}^{0.5}}{N^{0.25}}) + 0.85] S_m^{-0.2} \quad (2.2)$$

Where,  $N$  is the number of waves and  $S_m$  denotes the wave steepness.

### Impact velocity

Determination of stresses after the impact is important to decide whether the armour unit tends to break or not. Therefore, to calculate the resulting stress step by step approach was adopted. Firstly, acceleration of units during the impact was measured and impact velocity was determined from accelerometer measurements. Then resulting stress was estimated by calculating the momentum during collision together with impact velocities and the type of movement.

When processing the data only acceleration peaks larger than one third of the maximum peak values were used to calculate the impact velocities. A relation between hydraulic conditions and acceleration peaks were used instead of using the integrating the acceleration signal over time to determine the impact velocity. The largest impacts were measured near still water level. The impact velocity was used together with the rocking mode to calculate the momentum. The rocking mode (translation or rotation) determined the type of calculation. It was assumed that in 50% of the cases the Tetrapodes rotate and in the remaining percentage the Tetrapodes translate. In addition, only translations were assumed for cubes in a double layer.

As accelerations were measured in the center of the unit, following relationships were used to translate these measurements to the velocity at the position where collision is considered. For translating unit:

$$Momentum = MV \quad (2.3)$$

$$V_{collision} = V \quad (2.4)$$

Where,  $M$  is the mass and  $V$  is the velocity from the impulse of impact of the armour unit. For rotation:

$$Momentum = \left( \frac{I_0 \omega}{arm_r} \right) \quad (2.5)$$

$$\omega = \left( \frac{V}{0.65h} \right) \quad (2.6)$$

$$V_{collision} = \left( \frac{Momentum}{M} \right) \quad (2.7)$$

Where, the moment of inertia is  $I_0$ ,  $\omega$  is the angular velocity and the distance between the place of collision and the center of rotation is  $arm_r$ .

### Summary

According to aforementioned details this research has addressed several important topics extensively. But some aspects that need careful attention are discussed below.

It is arguable that rocking also results in collisions with neighbouring armour units and under layer. Hence, estimation of number of collisions by total number of moving units might have underestimate the number of colliding units. Further, analysis of changes in the unit's position before and after the test does not give satisfactory results in cases where the units rotate and fall back to its original position with rocking. Also, the number of collision calculated using the average number of collision was only a rough assumption and should be further addressed in future research works.

The tests were conducted using non directional wired accelerometer and these measurements were accurate when the acceleration is in the direction of the installed accelerometer. Connection with wires might have influenced the degrees of freedom of the armor units at least for some extent. Next to that, mode of movement is restricted to either rotation or translation for simplicity but no attention has paid if the rotation or translation both causes movement. Further, measuring acceleration during the impact itself might have led to scale effects in small scale model [Van der Meer & Heydra \(1991\)](#).

### 2.1.2. Rocking of a single Cube on a breakwater slope

[Le \(2016\)](#)

As the existing knowledge on rocking motion of single layer armour units is limited, a study to understand the behaviour of single layer armour units was performed by Tuan Le for his master thesis.

#### Overview

Firstly, a theoretical assessment is conducted for an exposed cube, which rotates around a hinge. The magnitude of movement is expressed with Newton's second law, in which the acceleration is calculated as a function of the sum of forces and mass of the element. The resulting velocity of the cube is estimated by integration of the acceleration over time. However, due to the assumptions made for the simplification the theoretical model overestimates the impact velocities and therefore, found as too conservative. Further, an experimental set up was developed along with the theoretical analysis to have a better insight in the physical processes.

The effect of wave steepness to the rocking motion was also addressed during the research which has not been addressed in CUR C70 (1989). The tested parameters are: degree of exposure of cube, wave height, wave steepness and position on slope in relation to the water level. Instead of measuring accelerations due to the mechanical impacts the accelerations due to movement are measured.

### Test programme

The wave flume experiments were conducted with the purpose of reviewing and updating the results from computer application "Rocking". Aforementioned parameters were selected as most important variables. Additional tests are done with a more representative configuration for breakwaters using an embedded cube.

The tests were carried out considering following hydraulic conditions. Model wave height ( $H_{m0}$ ) of 0.06-0.16 m, wave steepness ( $S_{m-1.0}$ ) of 0.02 -0.04 and a range of wave periods ( $T_{m-1.0}$ ) of 1.1-2.5 s. Due to time limitations, the cube was placed at only three positions relative to the water level:  $y/D_n = +2, 0$  and  $-2$ .

The measurement was done using a three-axis accelerometer (ADXL335) to calculate the angular acceleration of the center of the armor unit. The accelerometer can measure in three directions with a measurement range from  $\pm 5g$  to  $\pm 15g$ . The maximum sampling frequency is 1600 Hz for the x and y direction and 550 Hz for the z direction. The device was placed in the center of the armor unit and connected to thin wires. As the accelerations are linked to the wave conditions, wave gauges (Deltares Wave Height Meters) were used to measure the wave conditions. To determine the applicability of the accelerometer for measuring movement of an armor unit, validation tests were conducted.

### Number of collisions

Due to crosstalk, only the signals from the accelerometer z axis were available and the velocities of the cube were obtained by processing the data of this axis.

The collisions are taken into account only if a full rotation is observed and one impact is counted as one collision. The start of collision is regarded as the wave condition prior to the wave condition in which collisions are observed and relations between number of collisions and the stability number are derived. The results of the research however show that the number of collisions is dependent on the wave height, wave steepness and position on the slope. Also it was found that the start of collisions is independent from the wave steepness. In addition, position  $y/D_n = -2$  gave the highest probability of exceedance.

### Impact velocity

A synthetic model is used to calculate the impact velocities, which takes the time period of movement and the angle of the cube before and after movement as input values. The measured signal in the accelerometer is approximated, with an iteratively fitted tangential acceleration of the cube in time. The resulting approximations for tangential and normal acceleration are imposed in the equation of motion for the rotating cube. Afterwards, the output was obtained as the angle of the cube in time. Differentiation of the angle in time results in the angular velocities where the impact velocity is taken to be equal to the velocity before collision.

It has been found that the wave steepness influences the magnitude of impact velocities significantly. In addition, the probability of exceedance of a certain angular velocity is influenced by the positioning of the cube relative to the water level and position  $y/D_n = -2m$  resulted in the highest probability of exceedance.

### Summary

With the purpose of having a better insight into behaviour of single layer armour units and the rocking motion, this research was conducted. Most realistic observation for the test program was with the embedded Cubes. But some limitations can also be identified in the experimental set-up, for instance, the breakwater porosity is not represented and the slope roughness is not equal to the roughness of a prototype breakwater. Moreover, this study recommended to develop a wireless device that contains an accelerometer and a gyroscope, to capture and process the armour unit movements accurately.

### 2.1.3. Measurement on rocking of Cubes in a double Layer on a breakwater Arefin (2017)

This research was performed to estimate the order of the magnitude of the impact velocity and distribution of the impact velocity and then to compare, validate and conclude the new findings those did not address in CUR C70 (1989) research.

#### Overview

As there was no any research carried after CUR C70 study to validate their findings, this study was carried out using a state of the art measurement technique developed at Deltares and TU Delft. Measurements were taken using 9-axis IMU sensors that measure acceleration, rotation rate (gyroscope), and magnetic field (compass).

To check the applicability of the new measurement technique in this type of studies physical model tests were carried out using two different types of armour units; Tetrapodes and Cubes. The maximum sampling frequency of the sensors is 100 Hz. Therefore, with this relatively slow sampling rate this study adopted a different principle to obtain the impact velocity. As the typical mode of movement is identified as rotation rather than rocking, the gyroscope readings were used instead of the accelerometer readings. This approach comparing with previous approaches is illustrated below (Figure 2.1). The vertical dashed lines indicate the required sampling frequency for a direct (angular) velocity measurement of prior to the impact, and the required sampling frequency to resolve the acceleration or angular velocity during the impact Hofland et al. (2018).

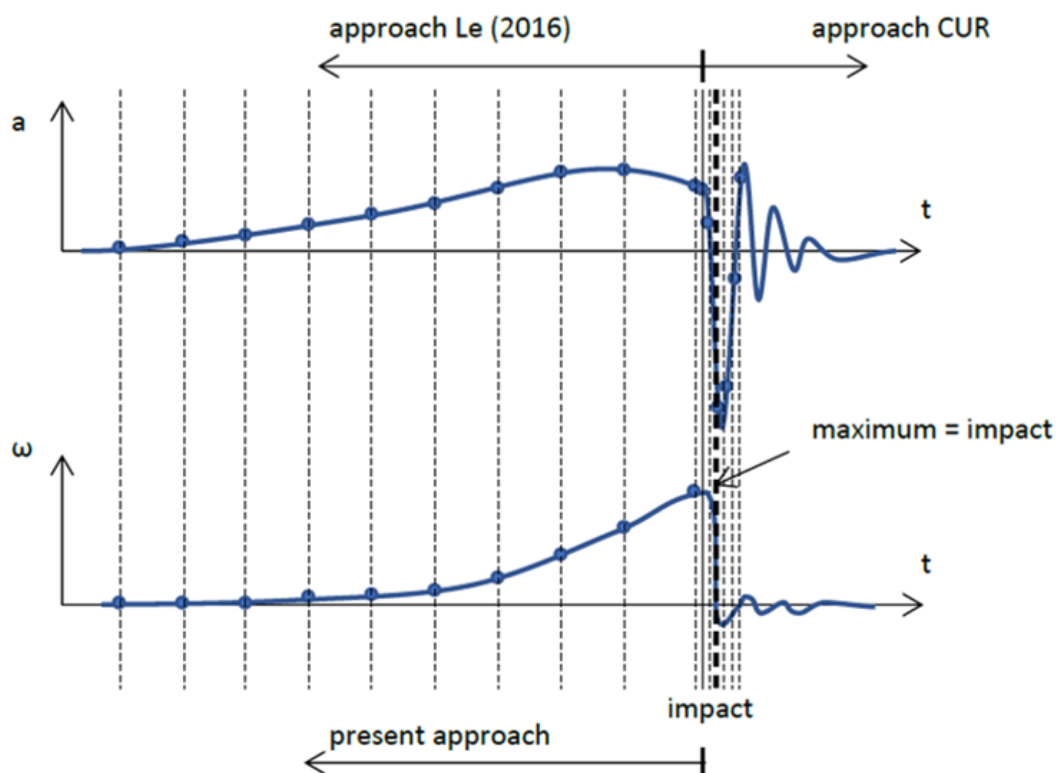


Figure 2.1: Schematic representation of the time variations of acceleration  $a$  and angular velocity  $\omega$  during rocking and collision, starting at vertical solid line (Hofland et al., 2018)

#### Test programme

A first test was performed with a stand-alone instrumented Tetrapod unit. As data was written into a SD card the actual sampling frequency is even smaller than the sensor frequency. Therefore, the data

were capture with 32.5Hz frequency. Two test series were performed with  $H_{mo} = 0.09\text{m}$  and  $0.11\text{m}$ ,  $T_p = 1.84\text{s}$  and  $1.81\text{s}$  respectively.

Tests with Cubes were performed using eight instrumented cubes. Cubes were connected with flexible wires and collected real-time data with 50Hz frequency. The tests were performed with stability numbers up to the initiation of damage. Three different positions of cubes were considered  $y/D_n = 0, -2$  and  $-4$  by changing the water level. The test duration was set as 1000 waves per test.

To validate the sensors they were placed on a bar that was rotated over 90 degrees (Figure 2.2). It is clearly showed that the gyroscope shows less noise than the accelerometer measurement. Overall the sensors seemed accurate enough.

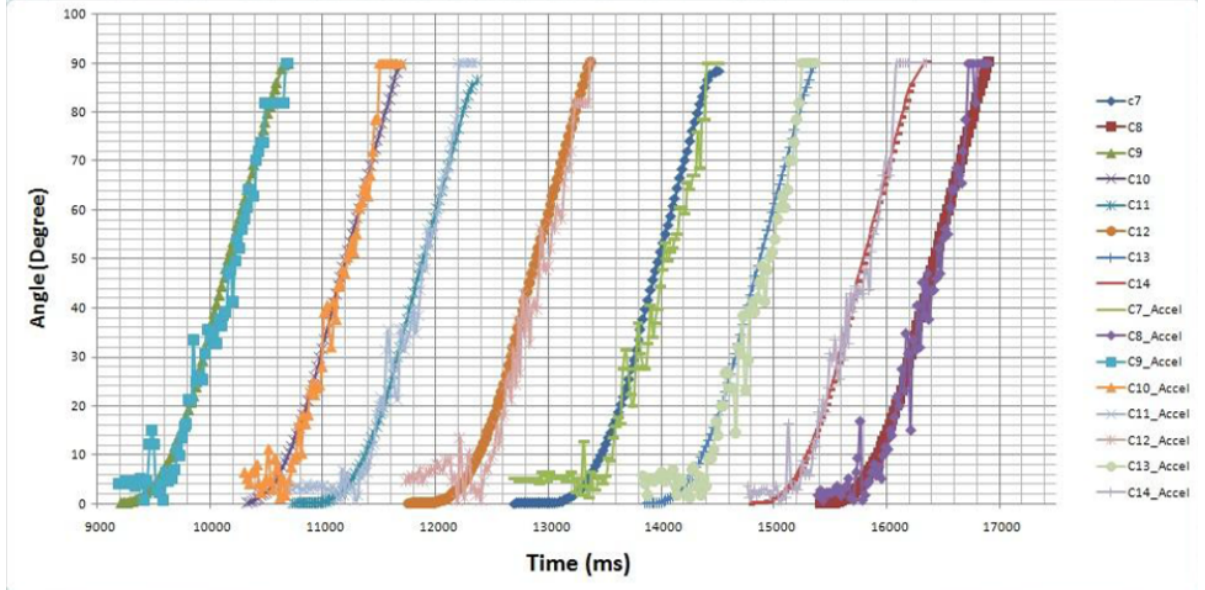


Figure 2.2: Change in angle over time due to falling test of eight sensors (Arefin, 2017)

### Number of collisions

To estimate the number of collisions it was assumed that it is equal to the number of peaks in the time signal of the absolute angular velocity  $|\omega|$ . Then the relationship between number of collisions and the stability number was identified by plotting the two variables together. For the cubes it was observed that the number of collisions increases with the stability number. Further, it was observed that the number of collisions is largest below the waterline, at the  $y/D_n = -2$  location, and the fraction of collisions increases with wave steepness.

### Impact velocity

In order to calculate the impact velocity absolute value of angular velocity was calculated using angular velocity components measured for x, y and z directions (equation 2.8).

$$|\omega| = \sqrt{\omega_x^2 + \omega_y^2 + \omega_z^2} \quad (2.8)$$

Then peaks of this signal above a selected threshold was considered and the impact velocity ( $v_i$ ) was calculated assuming pure rotation (equation 2.9).

$$v_i \approx D_n |\omega| \quad (2.9)$$

Then the exceedance curve was made and the exceedance probability was estimated as using the equation 2.10. Where,  $N_{col}$  is the number of collisions in the test and  $v_{i,1}$  is the largest impact velocity.

$$P(v_i > v_{i,n}) = \frac{n}{N_{col}} \quad (2.10)$$

The results clearly showed that the measured impact velocities are in the same order of magnitude as those obtained in the CUR research (1989, 1990-a,b). Moreover, it was also found that the impact velocity magnitude depends on the wave steepness.

### Summary

This study creates good future opportunities by introducing and validating embedded IMU sensor to measure an important engineering parameter, the impact velocity. However, the proposed methodology can further be improved to distinguish upward and downward motion. Also spatial distribution of impact velocities need to be addressed. However, by assuming number of collisions are equal to the number of peaks in the absolute angular velocity signal, number of collisions might be overestimated [Hofland et al. \(2018\)](#).

## 2.2. Stability of single layer armour units

A research was carried out by Zwanenburg (2012) in which the stability of single layer armours units were evaluated according to the rocking behaviour of them.

### 2.2.1. The influence of the wave height distribution on the stability of single layer armour units.

#### Zwanenburg (2012)

This study was focused on evaluating the influence of the wave height distribution on the stability of single layer armour units according to rocking.

#### Overview

During this study, the influence of the wave height distribution on the stability of single layer interlocking armour units has been investigated in general and experimental study was performed particularly for Xbloccs and influence of exceptional larger waves on the stability of Xbloccs was tested.

Rocking has considered as the most reliable stability indicator than the armour units displacement. The outcome of the tests resulted in relation between rocking probability and wave height of Xbloccs.

#### Stability of Xbloccs

This study has found that the wave height is the main parameter that influence the probability of rocking [Zwanenburg et al. \(2014\)](#). Further, study concluded that most suitable indicator for the rocking is not the significant wave height ( $H_s$ ) but the wave height with a probability of exceedance of 2% ( $H_{2\%}$ ). As it was found that the stability of single layer interlocking armour units can be described by the stability number, a new stability formula was derived for the Xbloccs based on the results of experiments (Equation 2.11).

$$\frac{H_s}{\Delta D_n} \leq \min\left[2.77; 4.26 \frac{H_s}{H_{2\%}}; 5.12 \frac{H_s}{H_{0.1\%}}\right] \quad (2.11)$$

Also, the influence of the relative packing density on rocking was found as significant whereas a weak relation was found between wave steepness and rocking.

### Rocking analysis

According to design criterion of Xblocs, during the design conditions in a model test, not more than 2% of the units are allowed to move during more than 2% of the waves. During the 2D physical model testings, rocking was observed visually and was recorded by manually activating a pulse on one channel of the data collection device. Then the total number of rocking units was estimated for each pulse by video analysis. The probability of rocking for the armour layer of the model tests can be described according to the equation 2.12 where  $H$  is the wave height (when the influence of wave groupiness is omitted).

$$f_{rocking}(H) = \frac{1}{1 + e^{10.2 - 0.0385H}} \quad (2.12)$$

### Summary

The influence of the larger waves on the stability of Xblocs has been investigated in this study and new stability formula for Xblocs has been proposed based on a rocking criterion. It is expected that for other interlocking single layer armour units, rocking probability will be similar. However, the rocking behaviour can be influenced by the interlocking mechanism of different types of armour units, thus the suggested coefficients can be different. Therefore, further model testing is recommended to determine the rocking probability functions for other types of armour units.

## 2.3. Different applications of Inertial Measurement Units (IMU)

IMU sensors initially restricted only to bulk applications like in aircraft navigation because of its constraints mainly in size, cost, and power consumption. But recently the demand has increased to wider area of usage with the invention of micro-electromechanical system (MEMS) and IMU is introduced with a very attractive feature of low cost, compact, and low processing power. Among its wider range of applications, IMUs are also being used as measuring devices in various scientific studies.

### 2.3.1. Smartstones: a small e-compass, accelerometer and gyroscope embedded in stones

Gronz et al. (2015)

The movement of pebbles is important in a variety of engineering disciplines. In this research, a sufficiently small probe is introduced: the Smartstone probe. It consists of a metal cylinder (diameter 8 mm, length 55 mm) with a flexible antenna and contains a Bosch BMX055 sensor composed of a triaxial accelerometer, magnetometer and gyroscope, respectively. Additional components inside the probe are memory to store data, active RFID (Radio-frequency identification) technique to transmit data and two button cells as power supply.

In the device's first software version, all three sensors – acceleration, compass, and gyroscope were used. The acquisition of all values resulted in a sampling rate of 10 Hz. But as the acquisition of the gyroscope's value does not allow for higher sampling rates in the second version only compass and accelerometer were used and sampled every 12 ms. For data analysis, the high-speed camera images were merged with the device data using a MATLAB script. The pebble's orientation is derived from compass and accelerometer data using sensor fusion and algorithms for tilt compensated compasses. The results show that the device is able to capture the movement of the pebble such as rotation (including the rotation axis), sliding or saltation and method is promising. Further improvements are to be carried out to minimize the errors by using different filtering techniques.

### 2.3.2. Inertial forces on shipping containers from a broken tsunami bore

Goseberg et al. (2016)

The paper investigates the motion of debris entrained by broken surge flow. The main objective was

to derive the inertial forces exerted on the debris outer hull. To track the motion of debris and to measure the velocities and accelerations, a measurement concept called 'smart debris' was introduced. It is composed of a water proof rectangular device with embedded accelerometer, gyroscope and magnetometer. Inside this container model, motion sensors were used to record the three dimensional orientation of debris by using sensor fusing and Kalman filtering of integrated accelerometers, gyroscopes and magnetometers. In order to determine the debris positions a real time locating system was also installed.

### 2.3.3. Smart pebble for monitoring riverbed sediment transport

[Akeila et al. \(2010\)](#)

In this research a smart pebble was developed to study and monitor the behaviour of sediment particles in riverbed. Mainly to capture the initial motion of particles which lift them up in the water column. This device is composed of embedded small size and low cost acceleration and angular motion sensors.

Accelerometers were employed to measure the linear accelerations along all three axes (x,y and z) with respect to moving axes of the pebble (Body frame). Gyroscope measurements were used to measure the rotational changes of the body frame and calculate the accelerometer readings along the original reference frame. The 'Euler angle transformation concept' was adopted as the main working principle for these transformations. Further, a gravity compensation algorithm was developed to calculate the linear acceleration eliminating the gravity components.

After collecting the data all necessary processing was done in offline using MATLAB. Sensor was calibrated to identify the bias and other sensor related errors and measurements were corrected accordingly. Laboratory tests were carried out in a flume using this smart pebble and tests results showed that the smart pebble device and processing methods performed satisfactory when measuring the linear and rotational accelerations.

#### Summary

According to above studies low cost, widely available inertial measurements units (IMU) perform promisingly in a wide variety of disciplines to detect motions. With the rapid development of novel technologies, the performances of these sensors are further enhanced. Hence, implementing this technology is proven to be propitious in breakwater testings and it opens and paves the way to development of different instrumented breakwater armour units to study the rocking motions in a broader extent.

### 2.3.4. Forces and pressures on Core-Loc armour units in rubble mound breakwaters measured via instrumented smart units

[Eden \(2019\)](#)

In order to quantify the forces and pressures using an experimental approach, instrumented core-loc units were fabricated. These units were 3D printed using PLA plastic and have the ability to mount on the force transducers and six pressure sensors were embedded in the surface of each unit. The height of the unit is about 0.12m and was powered by Linux based Raspberry pi 3 computer hence a cable was used to interface with the Raspberry pi 3. Further, to avoid water penetration, the inner cavity was filled with silicon and surface was sealed by applying a thin layer of epoxy based 3D printing sealant.

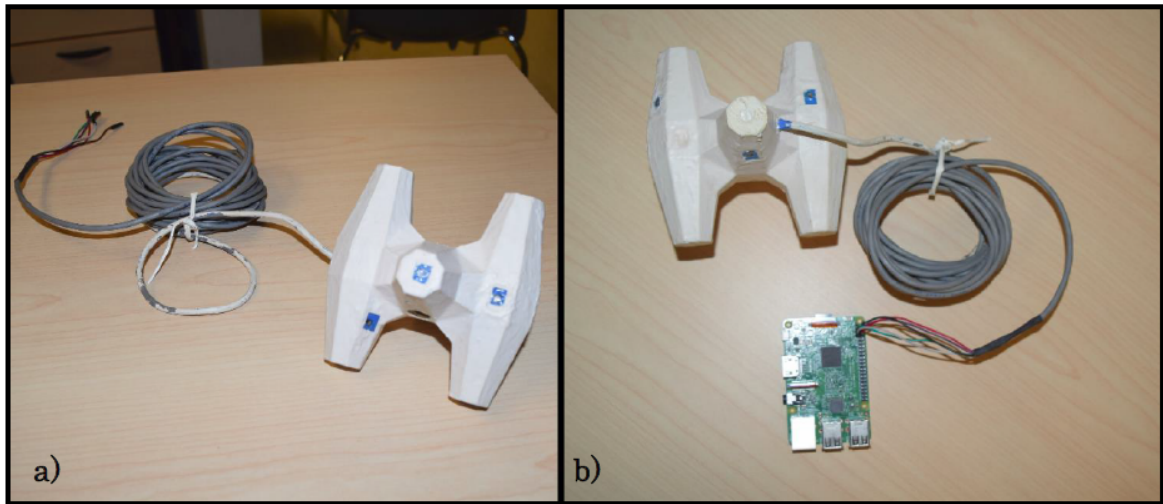


Figure 2.3: Instrumented 3D printed Core-Loc unit a) Front b) Back (Eden, 2019)

### Summary

This study also shows the new trend of implementing the smart units in coastal engineering researches and its potential development. Even though current research work was initiated prior to the publication of this thesis work, more or less the same approach was taken when preparing the instrumented single layer armour units (Xblocs).

# 3

## Experimental studies -Instrumented Xbloc Unit

In this chapter, construction of instrumented Xbloc units, hardware and software improvements and calibration and validation techniques are described in detail.

### 3.1. Instrumented units construction and development

The previous researches ([Arefin \(2017\)](#)) conducted by implementing the same technique showed that the technique is promising in detecting the rocking motion. Also the proposed technique can be adopted without any wires being connected to it, so that motions are not disturbed. But the only issue with the technique is its relative low sampling frequency. Therefore rocking motion can not be very accurately resolved in time with the relatively low data samples

If further improvements of sampling frequency to capture sufficient data to resolve the rocking motion in time is possible, this technique will open new paths for future researches in this field. Therefore, it was decided to use the same technique and try to improve the sampling frequency to get the maximum possible frequency and evaluate the effectiveness of the technique in detecting the rocking motion accurately.

#### 3.1.1. Model unit construction

To detect the rocking motion of Xblocs and quantify the impact velocity of them just before the collision with neighbouring units, an instrumented Xbloc unit was developed. Model units were designed according to the standard dimensions with Google sketch-up and 3D printed at Deltares (Figure 3.1). The size of the model unit was decided leaving enough space to embed the sensor and other small electronic devices ( $D=56.4\text{mm}$ ). Also the hollow units have enough space to house additional weights (lead pieces) that were used to correct the density of these printed model units. The Model unit was printed as two separate parts and then combined together after embedding all the instrumentation. Further, extra precautions were taken to avoid water penetration by using a synthetic resin as a sealant.

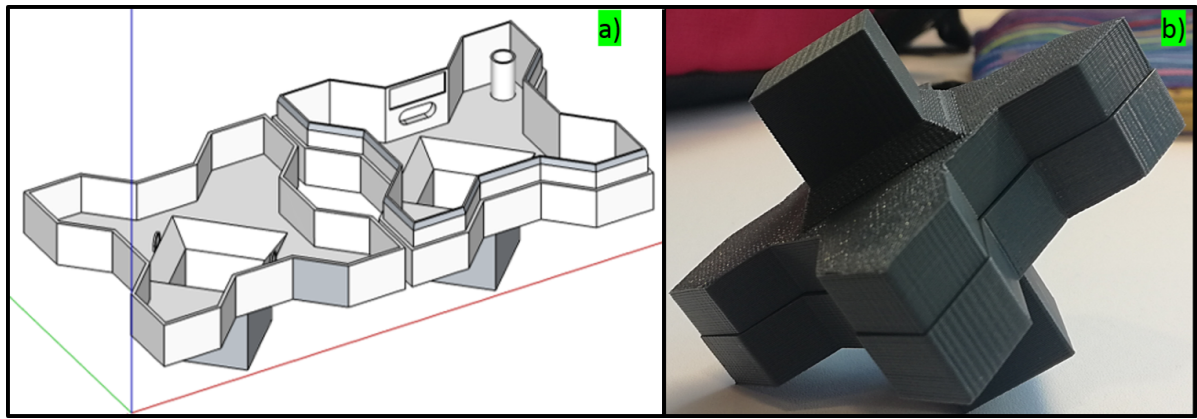


Figure 3.1: 3D printed Xbloc unit a) Design with Google Sketch-up b) After 3D printing

### 3.1.2. Instrumentation

A sensor that is capable of taking measurements was embedded in the printed model unit together with few other circuit boards such as processor board with a lithium battery, micro USB connection and SD card to store the data. Total size of this stack is about 2 cm x 2 cm x 2 cm. And total mass of the sensor is about 10 g. mass of the Few magnetic switches (reed switches) were used to turn the battery power and USB connection on and off. Soldering was done to make a small circuit between these electronic boards and magnetic switches. Therefore, this instrumented unit is capable of taking measurements stand alone. Also, longevity of the battery life is enough to perform the testings for about two hours and the unit can be recharged by connecting the USB cable without removing it from armour layer.

While taking the measurements, unit can be turned on using magnetic switch and then turned off after performing the test. Then the stored data can be retrieved with the USB cable.

#### Sensor

IMU sensor with nine degrees of freedom (9 DOF) including a 3D digital linear acceleration sensor (accelerometer), a 3D digital angular rate sensor (gyroscope), and a 3D digital magnetic sensor (compass) was used to take measurements. This sensor is based on the Arduino platform ([www.arduino.cc](http://www.arduino.cc) (2019)). This sensor can take measurements at a frequency of 100Hz approximately. For this study measurements from accelerometer and gyroscope were only recorded due to the limitations with storage capacity and the speed of the device.

### 3.1.3. Assembly and Fabrication

After printing the model unit all necessary instrumentation were embedded together with few lead pieces to get the correct density similar to the same size concrete model units. Figure 3.2 shows few important components required to make internal circuit and waterproofing.

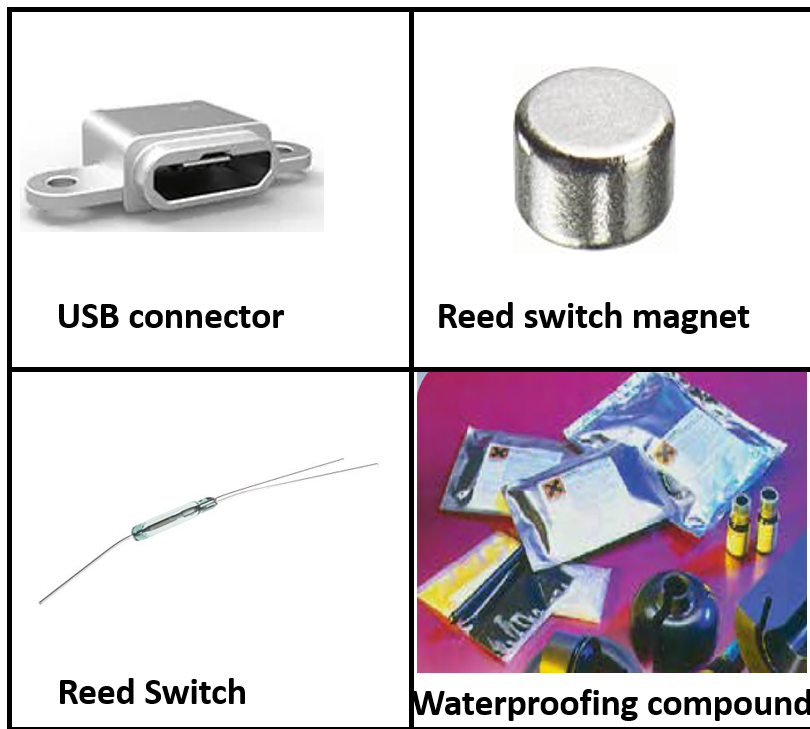


Figure 3.2: Main components required to make the circuit and waterproofing

Soldering and unit preparation

As explained in the section 3.1.2 to make the instrumented unit work some soldering works has to be performed. Internal circuit that is embedded inside the unit is shown in figure 3.3.

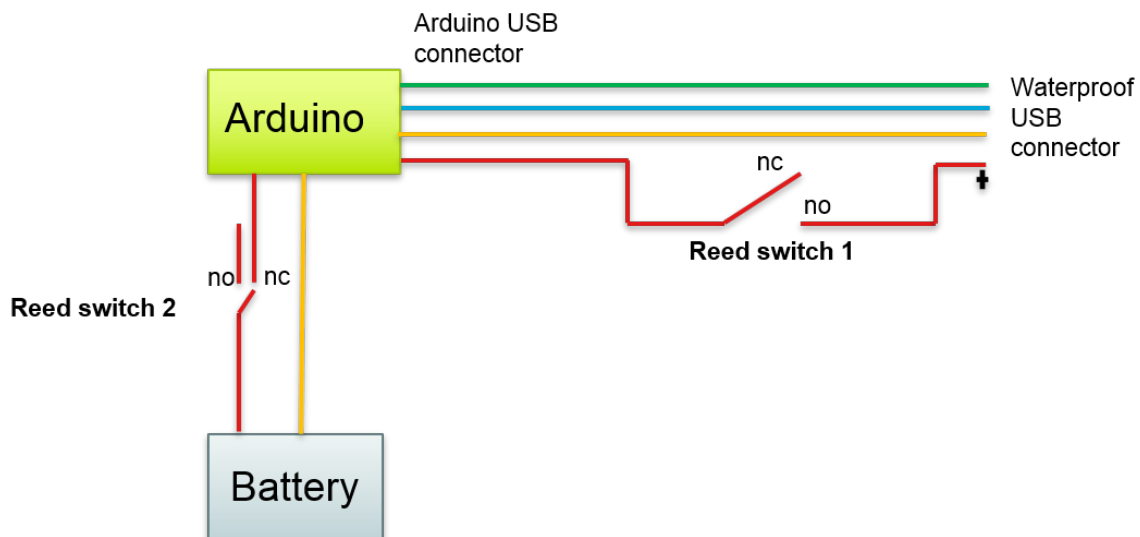


Figure 3.3: Internal circuit

As shown in the figure the internal circuit is very simple and requires soldering to get the connection between external waterproof USB connector and USB connector on the Arduino circuit board and connection with the battery. Soldering between USB connectors was very tricky due to the micro scale dimensions and therefore, very thin flexible wires are essential to do the soldering successfully. After soldering keeping the connection as it is without allowing it to damage until the assembly is also important. Hence, connections were covered with a non conductive resin that is capable of keeping the

soldering rigid and preventing the possibility of damage.

Two reed switches were inserted. One reed switch was connected to the positive end of the USB connections. This reed switch is in normally open position (no). Therefore, if one needs to connect the unit with a computer via a USB cable, a magnet should be placed on the switch to close the circuit. The other reed switch was connected between sensor and the battery. This switch is in normally close position (nc). Hence, to stop taking the measurements and save the battery life a magnet has to be placed on this switch to open the connection.

Figure 3.4 illustrates few intermediate steps towards the final development of the instrumented Xbloc unit. The picture one shows the connection after soldering at the one end of the USB connection. The other end of the wires were soldered to the external USB connector. The picture two shows completed sensor with all the connections.

The battery was also attached to the bottom of the sensor stack and rapped it tightly to avoid penetrating the waterproof compound through the circuit. Picture three shows both parts of the model unit with inserted lead pieces. The placement of the lead pieces are further described in the following section. Reed switch that is connected to the battery was placed in the cylindrical hole created in the design stage of the model unit and other reed switch was attached close to the USB connector. Tightly rapped sensor stack was placed at the middle and glued to the unit to avoid the tilting.

Before closing and sealing the unit it is important to check the connections again and make sure everything works fine. The final step shows the developed unit after injecting the water proof compound. To inject the compound, a small hole is placed at the bottom and resin was injected from bottom to top. Attention should be paid to avoid the air entrapment while injecting the resin.

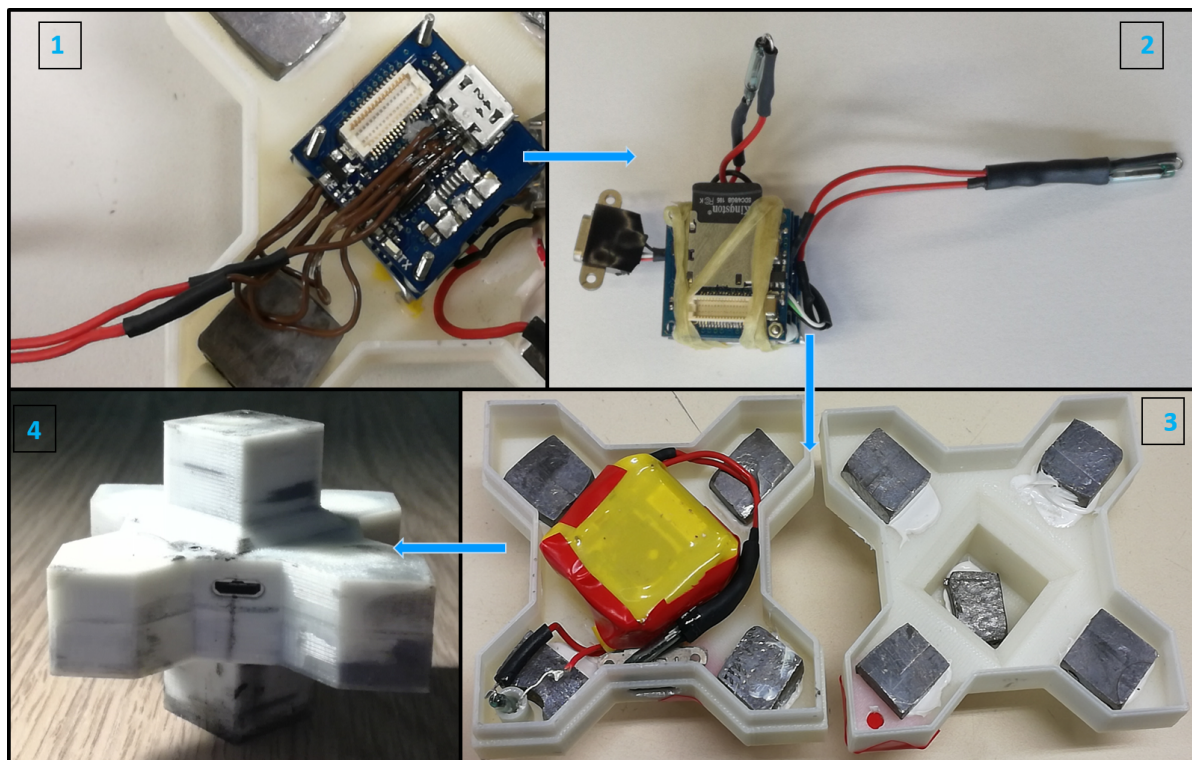


Figure 3.4: Development of the instrumented Xbloc unit

#### Density correction

As weight of the instrumented unit with the sensor and the resin alone is not enough to get the similar density of the concrete model units, extra weight had to be placed. As lead has relatively higher

density, it was chosen to place lead pieces inside the unit. To get the similar density it was decided to place 14g of lead pieces in all four legs and 12g of lead pieces in each nose of the unit. Available lead pieces were cut and reshaped to get the desirable weights.

Since the weights provided by the lead pieces are not equally distributed over the unit, the moment of inertia around any axis through the center would be different than concrete model units with same weight. Instrumented units with lower moment of inertia requires smaller force to get the same angular velocity compared to concrete model units. Hence, the distance required from the center to each lead piece was calculated to obtain the similar moment of inertia.

### Moment of Inertia

The instrumented unit should move in a way similar to the prototype block as rocking movement typically governed by rotation and hence moment of inertia should be represented well. The moment of inertia of the unit was calculated around the local Z axis (axis through the center of unit). As shown in the figure 3.5 for the simplicity, lead pieces placed distance  $r$  from the center were assumed as four masses of 14g per each and the masses placed at the center were considered as cubes of  $1.2 \times 1.2 \times 0.75 \text{ cm}^3$  when calculating the moment of inertia. Moment of inertia was calculated according to the equation 3.1.

$$I = \sum m_i r_i^2 + \sum m h^2 \quad (3.1)$$

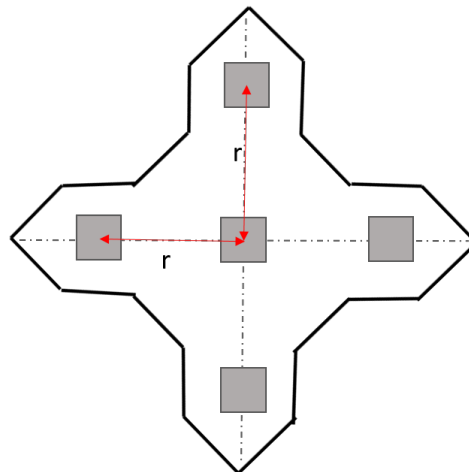


Figure 3.5: Positions of the lead pieces

Table 3.1: Summary of the calculation of Moment of Inertia

Element	Equation of I	Density/( $gcm^{-3}$ )	Moment of Inertia ( $gcm^2$ )
Concrete model unit	from Autocad	2.34	559.54
Model unit with resin	from Autocad	1.2	286.95
Masses at the center	$1/12m(a^2 + b^2)$	11	5.76
Masses on the Legs	$mr^2$	11	266.84 (Required)

Therefore, to get a moment of inertia similar to the concrete model units, the lead pieces on the legs should provide about  $267 \text{ gcm}^2$  of moment of inertia. Hence, the required distance  $r$  was calculated approximately as 22mm from the center of the unit. So that, the lead pieces were placed about 22 mm distance from the center when developing the instrumented model unit.

However, When the rotation happens around a point outside the body of the unit, the force needed to rotate the unit is same in both cases, as the point of action of the total weight of the body is acting at

the middle in both units and both concrete units and the instrumented units have same weights. When units are lying on a slope they are not likely to rotate around the center but around the support points and because of that, the different moment of inertia does not influence the damage that occurred to a very large extent [De Leau \(2017\)](#).

## 3.2. Hardware/Software improvements

In order to improve the performance of the developed Xbloc model unit some improvements were introduced in Hardware/Software settings.

### 3.2.1. Improving Sampling Frequency

Reduced recording speed of the data was one of the key issues encountered when store up the data in micro SD card with the initial arduino sketch. The initial arduino sketch available to read sensor data and write them to the SD card can achieve a maximum frequency of 25-30 Hz only with class four SD card. Hence, considerable amount of data taken by the sensor is not stored in the SD card. The main reason for this was caused by additional delay due to regular opening and closing of the SD after each set of readings. Therefore, some modifications were done in the programme to achieve the optimum sampling frequency minimizing the data loss. However, the lower writing speed of the class four SD card also affects problem of reduced recording speed.

Following methods were tried out to solve the issues with lower sampling frequency.

- Change the default Arduino SD library
- Use Char array to print data directly to the SD
- Write data to the SD as chunks and limit the opening and closing (or flushing) times of the SD
- Use higher class of SD card that has higher writing speed
- Use flash memory to store data instead of the SD card

#### Changing default Arduino SD library

The default Arduino SD library that allows for reading from and writing to SD is found as not efficient. Because it has set the SD to flush after every write (<http://forum.arduino.cc> (2019)). Therefore, more efficient 'SDFat' introduced by Bill Greiman (<https://github.com> (2019a)) was installed from Arduino Library Manager. Then the initial sketch was modified in a way it supports with the new SDFat library. This was resulted in an improved sampling frequency of 40 Hz with class four SD card.

#### Print data to the SD as Char arrays instead of numbers

As it is easy to print data to the SD card as Char array than a number ([HobbyTronics \(2019\)](#)) the modified sketch was further developed by printing them as Char arrays rather than numbers. This sketch resulted in even higher sampling frequency of almost 50Hz with class four SD card.

#### Writing data to the SD as chunks

Even though the proposed modifications could improve the sampling frequency, it still could not gain the maximum frequency of 100 Hz. Therefore, to limit the number of opening and closing times of the SD card, the data can be written as chunks than single readings. When the data are written to SD, the data are actually placed in a buffer. When the buffer is full, the data is written to SD. As SDFat library typically has 512 bytes buffer it was decided to close the SD only at once per ten readings (index=10). It is important to note that, in order to save the data physically to the SD card closing or flushing the SD is essential. Therefore, the closing time should be decided considering the allowable buffer limit. Otherwise, closing the SD after the allowable buffer limit may cause data loss.

However, with the class four SD card the time taken to open and close the SD gradually increases with the increasing data storage of the SD card. Most of the time during model testings, it was observed

that the armour unit stays in the static condition without any significant motion. Therefore it was decided to write the data to the SD card only when a significant movement is observed. From this way a large amount of data can be eliminated without writing to the SD. But at the same time, data taken at the static condition is important as it only accounts the gravitational acceleration, especially when processing the accelerometer data to find the linear accelerations while the unit is translating and rotating.

Therefore, using a higher class SD card that is capable of writing the data faster may also help to sort out the issue. Further, it was identified a common issue of occasional slowing down of the recording speed with all these sketches with class four SD card. It can be due to internal memory management of the SD card and better quality SD card may work better than lower class SD.

### Using a flash memory

The key advantage of using the flash memory is, it can reach frequencies up to 200 Hz when writing the data unlike the SD card. But on the other hand, this has smaller storage capacity (1 MB) compared with the SD card. The example arduino sketch available for the flash memory ([https://github.com \(2019b\)](https://github.com/2019b)) was modified to read the sensor data and store them to the flash memory. However, it was found that writing the data to the flash memory as numbers did not result in higher sampling rates as expected. But if one could try out to take sensor output in bytes before doing the conversion to the numbers and then write the data to the flash memory in bytes would be resulted in much more efficient data storage. Not only with flash memory, writing data to the SD with bytes would also be resulted in higher sampling frequencies. But this was not considered in the scope of this study as it was not that straight forward approach.

### 3.2.2. Performances with different classes of SD cards

As explained in the section 3.2.1 three different classes of micro SD cards were considered and performances of them were compared. Figure 3.6 illustrates the chosen classes of the micro SD cards; S4, V30 and V90.

Minimum Sequential Write Speed	Speed Class		
	Speed Class	UHS Speed Class	Video Speed Class (NEW)
90MB/sec			<b>V90</b>
60MB/sec			<b>V60</b>
30MB/sec		<b>U3</b>	<b>V30</b>
10MB/sec	<b>10</b>	<b>U1</b>	<b>V10</b>
6MB/sec	<b>6</b>		<b>V6</b>
4MB/sec	<b>4</b>		
2MB/sec	<b>2</b>		

Figure 3.6: Different classes of micro SD cards considered for the comparison and their writing speed limits

### Comparison of the performances of different classes of SD cards using different Arduino sketches

In this section performances of the each selected SD card class were evaluated and compared based on different ways of storing data in the SD card.

#### Initial Arduino Sketch

Firstly, how the different speed classes of micro SD cards affect the recording speed of the data was studied by recording data in each different SD card for 30 minutes period with the original Arduino sketch available.

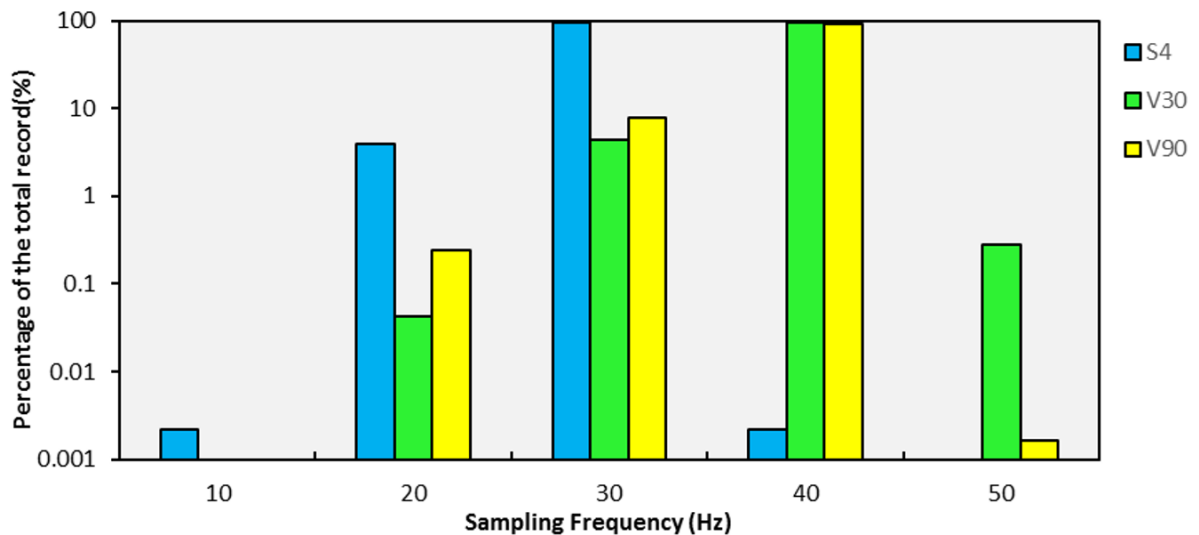


Figure 3.7: Comparison of sampling frequencies achieved by the different SD classes without any modification in original sketch

As shown in the figure 3.7 it can be clearly seen that lower class SD (Class 4 ) can only achieve a sampling frequency of 20-30 Hz in more than 90% of the considered time duration. Even without any modification to the initial sketch both V90 and V30 classes can achieve 30-40 Hz frequency in more than 90% of the time.

But the optimum frequency that can be achieved can not be maintained constant throughout the sampling duration. As shown in the figure 3.8, with increasing storage of the SD card, S4 type can go to 10-20Hz lower sampling frequency whereas class V30 and V90 can have 20-30 Hz reduced speed. But this reduced speeds occupy less than 10% of the total record. Other than that, some random slowing downs cause even lesser sampling frequencies than aforementioned frequencies. They are shown in the figure 3.7 with less than 0.5% of the total record. This gradual slowing down with time is illustrated clearly in figure 3.8.

Despite the fact that V90 being the highest class, performances of V30 class outweigh the performances of V90 class. This may due to the incapability of micro SD card adapter on the current circuit board, to get the full use of V90 class. Therefore, it was concluded that the V30 class is the most compatible type and hence, it performs better than other two types. Figure 3.9 also confirms this conclusion.

#### After modifying the sketch

Then performances were re-evaluated after modifying the initial Arduino sketch to achieve the maximum sampling frequency. According to the current modification, SD card closes only one time per ten readings which takes more time and rest of the time it can achieve maximum frequency of 100 Hz. Similar to the previous, data were written for 30 minutes period. As shown in the figure 3.9 class S4 has acquired data in 100 Hz frequency (time between two readings =10ms) for 70% of the total

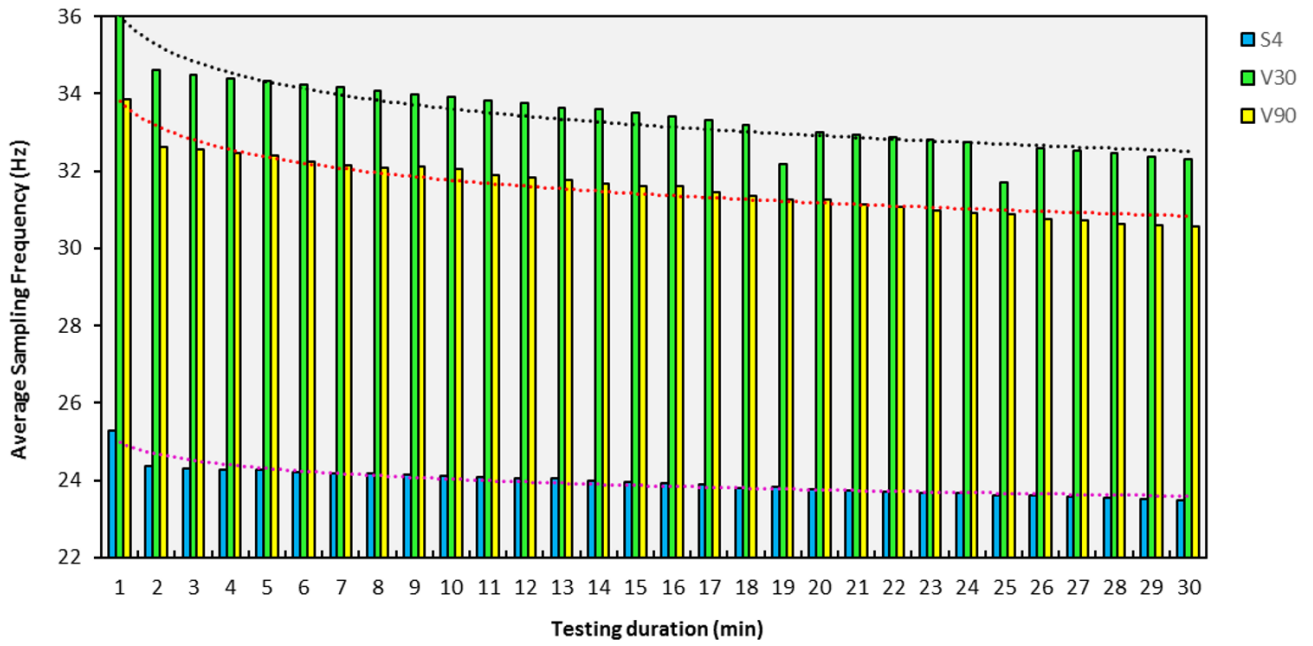


Figure 3.8: Average frequencies achieved without any modification and their slowing down with time

duration, whereas V90 class and V30 class acquired the same frequency for about 73% and 78% of the total duration respectively. However, S4 has the highest relative slowing down with time and the time taken to open and close the SD card has increased gradually. This may be due to high storage of the SD card with fast recording speed. The slowing down can be seen in other two classes as well but in V30 class the observed maximum time between two readings is between 40-50 ms and it occupies less than 0.01% of the total record.

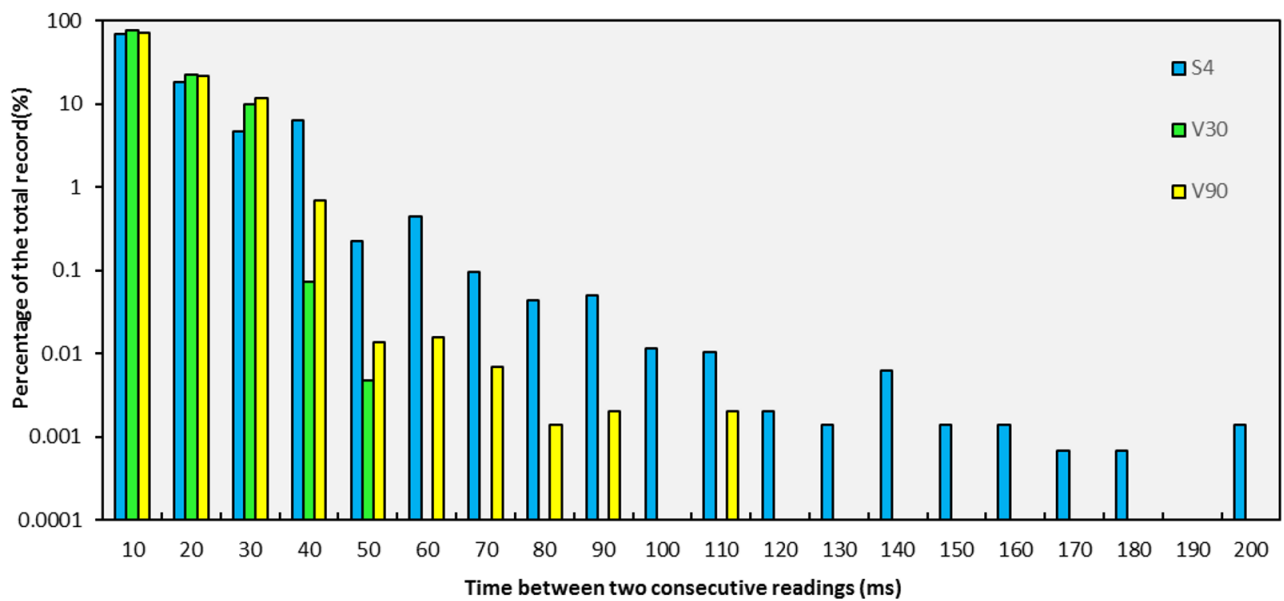


Figure 3.9: Comparison of time between two readings achieved by different classes after the modification

### 3.2.3. Comparison of the different techniques used to improve the data recording speed

In this section proposed techniques described in section 3.2.1 are compared by recording data for 30 minutes with V30 class micro SD card. The average sampling frequencies achieved from each method is illustrated in figure 3.10. Method 1 refers to the initial sketch, Method 2 refers to changing the Arduino SD library and data printing method and Method 3 refers to the method of writing data as chunks.

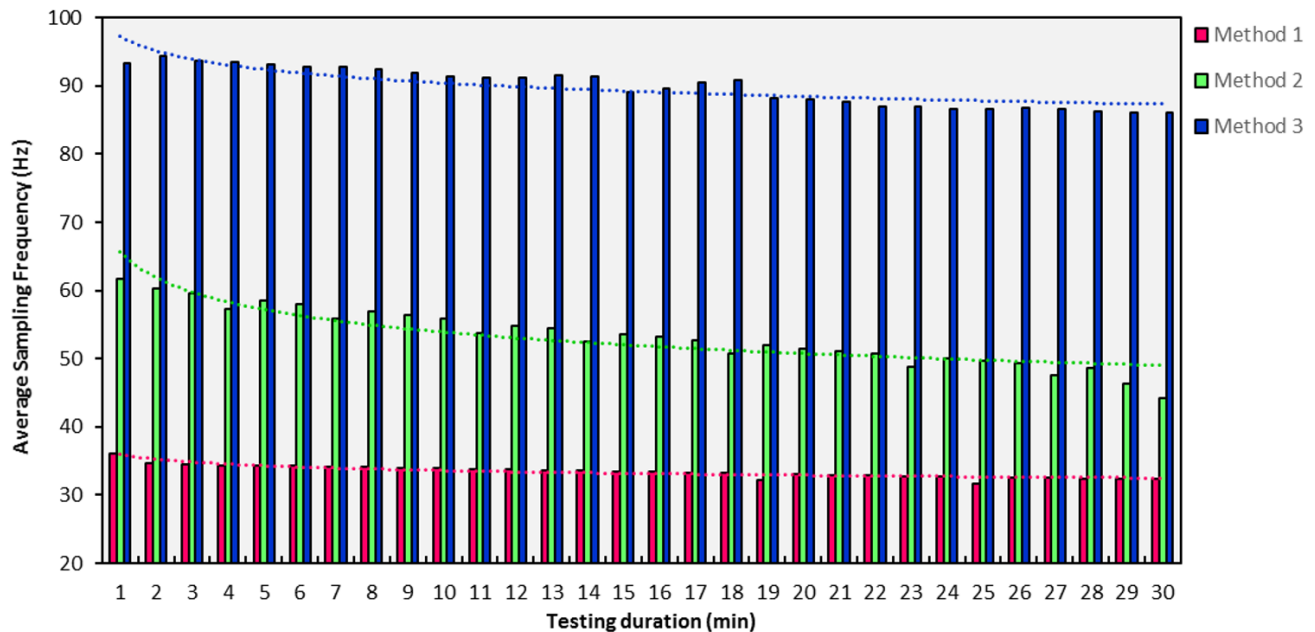


Figure 3.10: Comparison of different improvement techniques

It should be noted that the average frequency of method 3 is given as less than 100 Hz even at the beginning, because of the lower frequency achieved when closing and re opening the SD card in every 10 readings. The gradual slowing down of the frequency with time can also be observed clearly. After testing duration of 30 minutes the largest storage of the SD card can be expected in method 3 and because of this, the difference between initial average frequency and final average frequency is high for method 3 compared with method 1. This observation also inline with the conclusion of slowing down of the SD card with increasing storage.

To overcome this issue of slowing down, Method 3 was further modified to store the data when there is a movement only. More than 85% of the data can be eliminated by implementing this method. Apart from that, in order to process the accelerometer data, readings of the static condition were decided to record in every 0.5 seconds only.

## 3.3. Sensor Calibration and Validation

If the IMU sensor is placed static on a horizontal surface, it measures gravitational acceleration as a positive value. The data is given in  $g$ . Therefore, to get the acceleration in  $ms^{-2}$  the value obtained should be multiplied by gravitational acceleration of  $9.81 ms^{-2}$ . In the static condition the accelerometer measures a resultant acceleration equals to the gravitational acceleration irrespective to its orientation. But when it is accelerating it measures both linear acceleration and the influence of the gravity. Therefore to get the linear acceleration the influence of the gravity should be eliminated.

Gyroscope measures the angular velocity in  $rads^{-1}$ . Counterclockwise rotation around the each axes is measured as a positive value. The axis convention with respect to sensor local axes are shown in figure 3.11. Before taking the measurements it is important to check the accuracy of the sensor. Therefore, some measurements were taken when sensor was in the static condition and after rotating a known

angle.

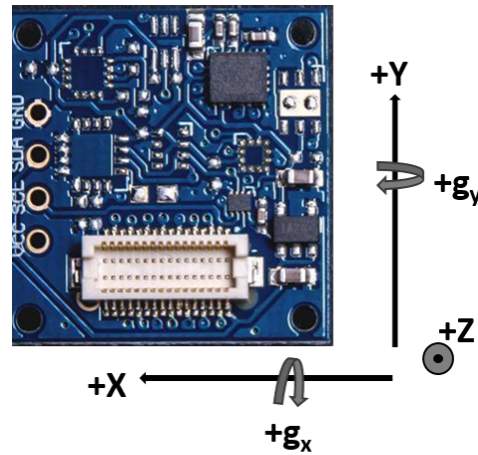


Figure 3.11: Axis convention of the sensor

### Static measurements

All the sensors were kept in the static condition for about an hour and checked the accuracy. Bias was determined by measuring the gravitational acceleration before and after rotating the sensor around a horizontal axis reversing the gravitational effect [Ferraris et al. \(1995\)](#). Bias was determined by averaging the two measurements. This was performed for all three axes separately. When the considered axis is gravity parallel and non parallel it shows more or less same value as bias, but at the same time considerable noise was observed. Different accelerometer axes showed different values for bias but, overall the average values varies between +/- 0.05g. In the static situation bias in the gyroscope is negligibly small.

Table 3.2: Bias of the acceleration measurements

Sensor	Bias-X (g)	Bias-Y (g)	Bias- Z(g)
Sensor 1	0.02	0.01	-0.02
Sensor 2	0.04	0.005	-0.055
Sensor 3	0.04	0	-0.025
Sensor 4	0.025	0.005	-0.035
Sensor 5	0.02	0.005	-0.002
Sensor 6	0.025	0.05	0
Sensor 7	0.02	0.01	0.025

### Rotating a known angle

To check the accuracy of the sensor in angle estimation six sensors were attached to a plate and rotated 90 degrees manually against a fixed reference block. Initially sensor Y axis is parallel to the gravity and after rotation it is perpendicular the the gravity. Then the acceleration measurements and gyroscope measurements were used to calculate the rotated angle using following formula ( equation 3.2 and equation 3.3). Where,  $\omega_y$  is angular velocity around Y direction,  $t$  is time taken for the rotation,  $\alpha_g$  is angle calculated from gyroscope measurements,  $\alpha_a$  is angle calculated from accelerometer measurements and  $a_x, a_y, a_z$  are acceleration measurements along x,y and z directions respectively.

$$\alpha_g = \int_0^t \omega_y dt \quad (3.2)$$

$$\alpha_a = \arctan\left(\frac{a_y}{\sqrt{a_z^2 + a_x^2}}\right) \quad (3.3)$$

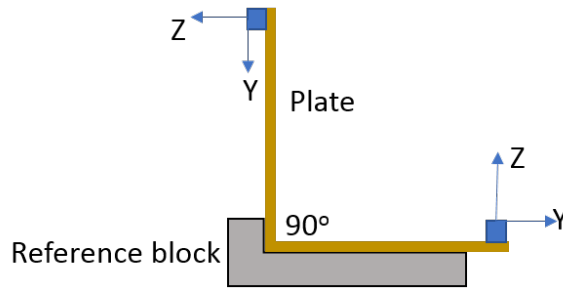


Figure 3.12: Rotation of 90 degrees

Angle was calculated by fusing both acceleration and gyroscope measurements as well (Section 3.3.1). As shown in figure 3.13 *acc* refers to the angle calculated from accelerometer data, *gyro* refers to the angle calculated from gyroscope data and *filtered* refers to angle obtained from sensor fusion. Overall, the sensors performed accurate enough in angle measurements. Acceleration measurements are quite noisy but accurate in long term. A small drift can be observed in the angle obtained from the integration of gyroscope measurements. However, filtered signal shows much more accurate value eliminating the drifting and noise. Calculated angle showed an average value of 88.6 degrees. During the manual rotation of the sensor, attention was paid to minimize the shaking but some deviations can be caused due to unintentional shaking movements occurred during the rotation.

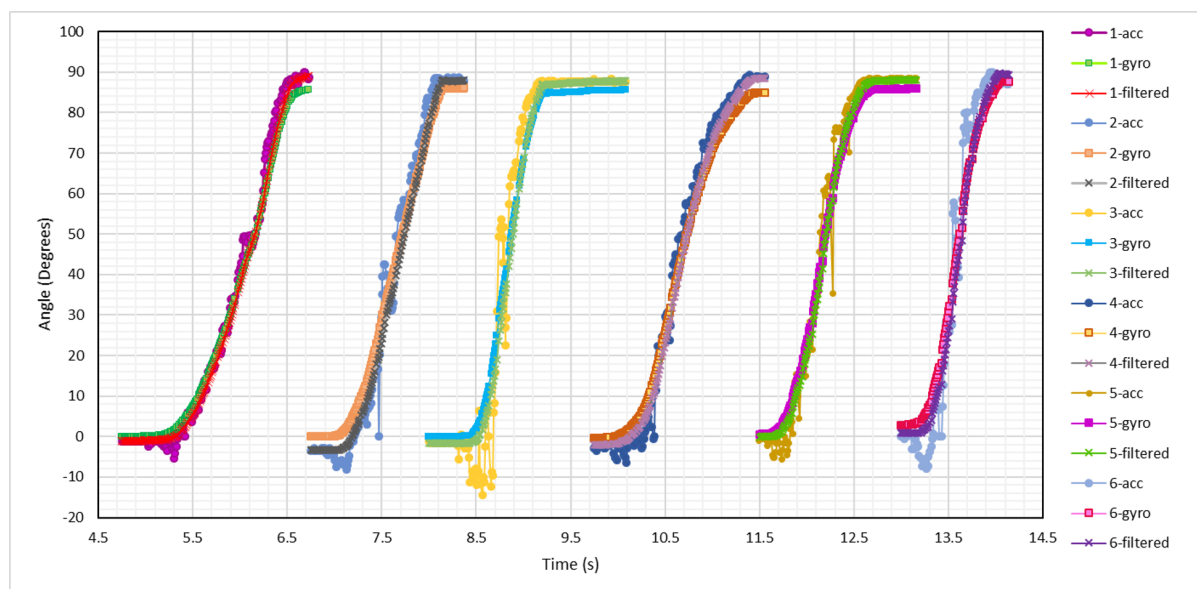


Figure 3.13: Change of angle with time for six sensors

### 3.3.1. Complementary filter

Generally accelerometer data are very noisy and can be influenced by external forces. Therefore it is hard to get accurate measurement for tilting angle in vibrating environment with accelerometer alone. But accelerometer data are stable and do not drift in long term.

Contrast to that, gyroscope measurements are more trustworthy in short term and are not susceptible for external forces. But in long term angular measurements data tend to drift due to accumulation of bias over time. Therefore sensor fusion is a known method to get more reliable estimation for the tilting angle accounting advantages of both gyroscope and accelerometer measurements.

Among various algorithms available for IMU sensor fusion, complementary filter technique uses relatively straightforward algorithm and it does not require complex computations. Hence, it is easy to

implement [Gui et al. \(2015\)](#). The basic principle of the complementary filter is illustrated in figure 3.14. The mathematical model for the complementary filter can be illustrated as equation 3.4.  $\theta_{angle}$  is the tilting angle (pitch or roll),  $\alpha$  is the filter coefficient (generally 0.98),  $\omega_{gyro}$  represents the angular velocity from the gyroscope, and  $a_{Acc}$  is the angle obtained through the data from accelerometer. The filter coefficient  $\alpha$  is determined by equation 3.5 where  $\tau$  is the time constant of the filter. Selection of the filter time constant relies on the experience and the coefficient of the filter depends on that choice.

$$\theta_{angle} = \alpha(\theta_{angle} + \omega_{gyro}dt) + (1 - \alpha)a_{Acc} \quad (3.4)$$

$$\alpha = \frac{\tau}{\tau + dt} \quad (3.5)$$

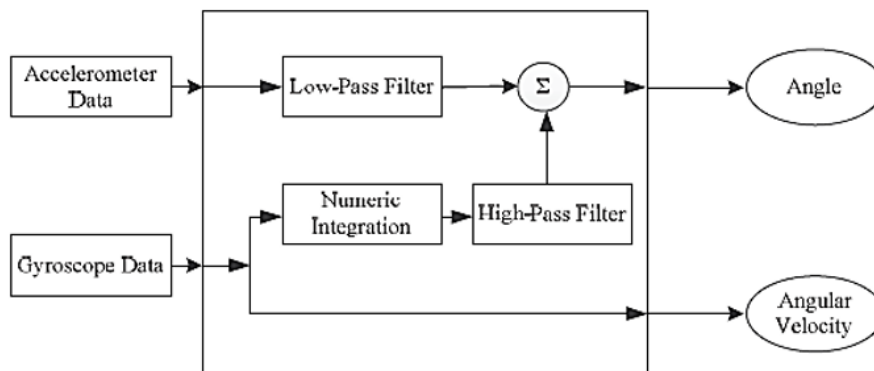


Figure 3.14: Complementary filter algorithm ([Gui et al., 2015](#))

# 4

## Experimental studies -Model Setup

To analyze the rocking behaviour of single layer armour units using the proposed technique, 2D physical model testings have been carried out with instrumented Xbloc units. In this chapter the preliminary steps towards the model testings including the scaling rules, selection of hydraulic conditions and the design of the cross section will be discussed.

### 4.1. Scaling Laws

Physical model testings are commonly used technique to get better insight into actual physical processes that are difficult to replicate through numerical modelling. The key requirement of the physical modelling is to ensure the model behaves same as the prototype condition. However, in a small size model scale effects can always present to some degree. Therefore it is important to minimize these scale effects according to the type of study by achieving the required similarities between the model and the prototype.

"To yield qualitatively and quantitatively useful results, physical model have to be geometrically, kinematically and dynamically similar to prototype conditions, dynamic similarity being the most important, followed by kinematic similarity" Kirkegaard et al. (2011). The forces that can affect a flow field are pressure, inertia, gravity, viscosity, elasticity, and surface tension. Hence to obtain dynamic similarity between the model and prototype when all of these forces act, all corresponding force ratios must be the same in model and prototype. But in the reality it is not possible to find a fluid that achieves the similarity between all these force ratios. Therefore, depending on the application the requirements to be fulfilled should be identified with respect to dominant forces acting on the system Dai & Kamel (1969).

For wave models, the relevant forces are the forces of gravity, friction and surface tension. For most of the small-scale coastal engineering models, however, the effects from friction and surface tension can often be neglected by ensuring the model is not too small and the model Reynolds number is in the same range as the prototype. Hence, Froude scaling can be applied assuming gravitational effects are dominant when waves interact with the structure. Therefore, for the realistic application of Froude similarity, the viscous, elastic and surface tension forces should be negligibly small. Usually in a real breakwater, flow through the layers and the core are fast enough to cause turbulent flow. Hence, to eliminate the viscosity effect, flow through the armour layers, under layers and the core should be high enough to cause turbulent flow instead of laminar in the model scale as well. Therefore, permeability of the materials use in the layers and the core is also important when it comes to the small scale model.

Another important scale effect is the friction. As the difference between the surface roughness of the model and the prototype can not be directly addressed, the friction forces may not be in similitude. But for the interlocking armour units, this effect is not crucial and by applying a paint or making model units in plastic, the surface roughness can be reduced in the model units. Following dimensionless

scaling ratios are usually considered in the wave modelling.

#### 4.1.1. Dimensionless Scaling

##### Froude Number

The Froude number (Equation 4.1), representing the ratio between inertia and gravitation. When the gravity force dominates, leading to the Froude similitude law, the Froude number in model and prototype should be the same.  $U$  is the flow velocity and  $L$  is the length scale.

$$Fr = \frac{U}{\sqrt{gL}} \quad (4.1)$$

##### Reynolds Number

As shown in the equation 4.2, Reynolds number represents the relation between inertia and viscous forces. When viscous forces are significantly dominant Reynolds similitude law should be applied. According to Dai & Kamel (1969), to maintain the turbulent flow in the model avoiding viscous scale effects  $Re > 3 \times 10^4$ . The flow velocity,  $U = \sqrt{gHs}$  in the armour layer Kirkegaard et al. (2011). The kinematic viscosity of water is  $\nu$  ( $1 \times 10^{-6} m^2 s^{-1}$ ) and  $d_n$  is the nominal diameter. However, if one applied the Froude similarity in wave modelling and in case of drag forces, as there are range of  $Re$  where drag coefficient is constant,  $Re$  doesn't need to be exactly equal in model and prototype.

$$Re = \frac{U d_n}{\nu} \quad (4.2)$$

##### Weber Number

The Weber number represents the ratio between inertia and surface tension (Equation 4.3). Surface tension is generally negligible in prototype condition and if wavelengths are much greater than 2 cm, wave periods  $> 0.35$  s, and water depths  $> 2$  cm Weber similitude can be neglected in small - scale models as well Kirkegaard et al. (2011). Otherwise the model will experience wave motion damping.

$$We = \frac{\rho_w U^2 L}{\sigma} \quad (4.3)$$

Moreover, these experiments were carried out assuming equal stability numbers (Equation 2.11) between the model and the prototype conditions according to the guidelines given by DMC (2003) and DMC (2011).

## 4.2. Test Programme

The main aim of the study is analyzing the rocking behaviour of single layer armour units with instrumented Xblocs units and evaluate the effectiveness of the technique to detect the rocking motion. Therefore, it is vital to select the test conditions and design the armoured slope in a way that acceptable rocking motion can be observed. Therefore as described in the following section, how the various phenomena affect the stability of armoured breakwater section were evaluated.

### 4.2.1. Phenomena that affect the stability of the armour layer

In this section both hydraulic and structural parameters that affect the stability will be discussed.

#### Breaker type

Wave breaking is an important phenomenon that influences the magnitudes of the forces experienced by the structure through wave structure interaction. The amount of run up and run down depend on the breaker type and accordingly the magnitudes of the destabilizing forces acting on the armour layer depend on that. The type of wave breaking on a slope can be determined by so called surf similarity parameter or Iribarren number ( $\zeta$ ). Iribarren number is basically a function of slope angle and wave steepness (Equation 4.4 and 4.5).

$$\zeta_{op} = \frac{\tan \alpha}{\sqrt{s_{op}}} \quad (4.4)$$

$$s_{op} = \frac{H_s}{L_{op}} \quad (4.5)$$

Figure 4.1 illustrates different breaker types. Steep waves on the very gentle slopes break by spilling water down the face of the wave. Spilling waves break for a longer time and there is little reflection of incident wave energy ( $\zeta_{op} < 0.4$ ). Plunging breakers ( $0.4 < \zeta_{op} < 2.3$ ) occur on steep slopes dissipating most of its energy at once in a violent impact. Because of this quick release of energy, the run-up and rundown velocities along the slope are relatively small even though the impact is violent.

In contrast, long waves on very steep slopes tend not to break. They usually surge rapidly up and down the slope with relatively high velocities where maximum down rush velocities occur just below the water level. This surging breaker ( $\zeta_{op} > 3.2$ ) reflects most of its energy and causes high destabilizing forces on the armour layer. The transition between plunging and surging breakers is known as collapsing breakers ( $2.3 < \zeta_{op} < 3.2$ ). Considering these facts it was decided to conduct the testings with  $\zeta_{op} = 3.2$  taking both surging and collapsing breakers into account as they can cause higher impact on rocking motion of armour layer.

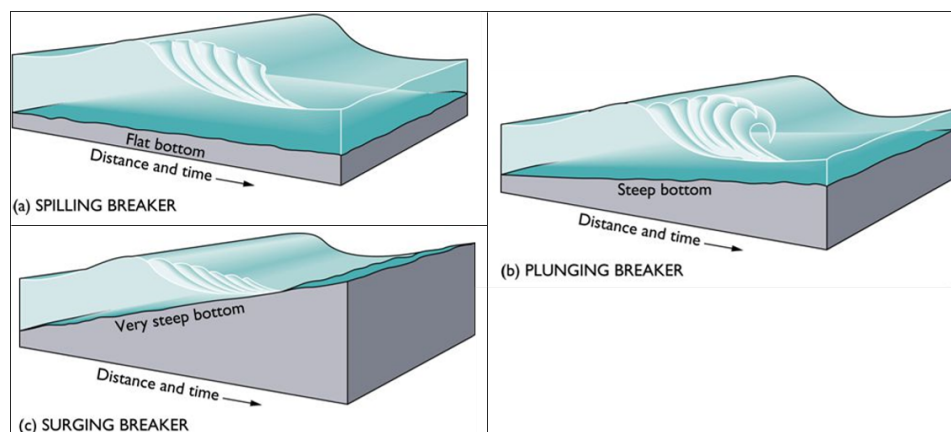


Figure 4.1: Breaker types

### Slope of the structure

Generally, Xbloccs are applied on an armour slope steepness of 3V:4H and 2V:3H. Xbloc being a randomly placed single layer armour unit type, gains the stability mostly from interlocking with its neighbouring units. However, on a steep slope interlocking is very effective and consequently the stability increases significantly. Therefore, to reduce the stability from interlocking for some extent slope of 2V:3H was applied.

### Permeability of the Core

A low core permeability causes higher flow velocities and large pressures in the armour layer and hence reduce the armour layer stability. The permeability of the core depends on the materials used and the distance at the water line between the armour layer and the impermeable layer DMC (2011). Largest destabilizing forces tend to occur during the down rush. To get the rocking motion with fairly larger Xbloc units, an impermeable core was applied reducing the stability of the structure.

### Relative freeboard

Larger relative free board usually results in increased number of rows which in turns increases the downward pressure on the bottom rows of Xbloccs and enhances the stability due to interlocking.

Therefore, on one hand minimizing the relative free board helps in reducing the stability of armour layer. But on the other hand, reducing the free board will cause significant overtopping which consequently reduce the down rush. Hence, selecting the freeboard is a trade off between these two factors.

### Packing density

A larger packing density increases the wave height which causes damage and the wave height which causes failure. Therefore, having more units per area increases the stability of the armour layer.

### Stability number

According to the model tests performed by DMC when developing the design formula for Xblocs (DMC (2003)), the start of damage value of  $H_s/\Delta D_n$  as observed in the tests is in average 3.5 (only randomly placed units considered) and varies between 3.25 and 3.85. Rocking starts approximately at  $H_s/\Delta D_n = 3.1$ . Start of failure is in average at 3.9 and varies between 3.61 and 4.31. This is further illustrates in figure 4.2.

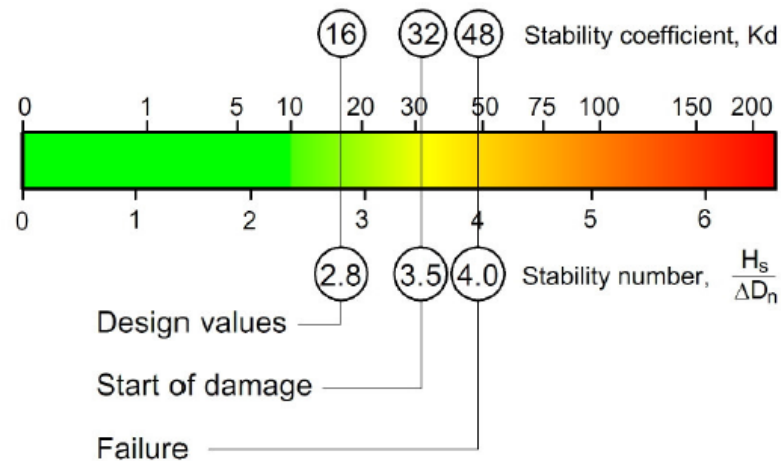


Figure 4.2: Design stability values (DMC, 2003)

Moreover, as shown in table 4.1 limiting wave conditions for design purposes can be defined (DMC (2003)). Where  $H_D$  is the significant design wave height.

Table 4.1: Limiting wave conditions for design purpose

Criteria	Effect on Xbloc slope
$1.0 * H_D$	Slope is completely stable
$> 1.1 * H_D$	Start of rocking
$> 1.25 * H_D$	Start of damage (1 or more units displaced)
$> 1.3 * H_D$	Continues damage (further units displaced)
$> 1.4 * H_D$	Start of progressive failure

### 4.2.2. Hydraulic test parameters

The hydraulic conditions were selected considering aforementioned phenomena to get sufficient movements with instrumented Xbloc units.

### Water Depth

Considering the flume restrictions and to have sufficient freeboard minimizing the number of rows above the water level, it was decided to carry out the experiments with constant water level of 0.5m.

### Wave conditions

It was decided to carry out the testings for two series with irregular waves. With the time restrictions, the slope will be rebuilt only one time after the first test series. The second series will be carried out considering the observations of first time series.

Further, as the armoured slope for testings was decided to build with impermeable core, aforementioned stability numbers given for the breakwater section with permeable core may overestimate the required wave conditions. Therefore, to avoid the risk of entire slope being washed out at once, the first test series will be carried out applying the correction factor for the impermeable core. The correction factor on unit weight for the impermeable core is two DMC (2011). But as the factor of two is given to ensure the stability, it may be conservative in this experiment and the advantage of getting more motions with impermeable core will be diminished. Therefore, it was decided to further increase the wave height progressively beyond the limit of rocking until sufficient movements are observed. The correction for the stability numbers ( $S$ ) was done using the following equation (Equation 4.6).  $D_n = 0.693D$  where  $D$  is the height of the unit and correction factor,  $C = 2$ .

$$D_n^3 = \left(\frac{H_s}{S\Delta}\right)^3 * C \quad (4.6)$$

Table 4.3 shows the wave conditions selected for the first test series. In accordance with table 4.1 and 4.2, input wave conditions were selected as Design wave height,  $H_D$  (With the correction for impermeable core),  $1.1H_D$ ,  $1.20H_D$ ,  $1.25H_D$  and  $1.35H_D$ . Constant wave steepness of 0.04 was considered considering  $\zeta = 3.2$  and slope of 2V:3H. Wave heights were calculated considering the density of fresh water ( $1000 \text{ kgm}^{-3}$ ) and density of model units ( $2341 \text{ kgm}^{-3}$ ). The Reynolds number ( section 4.1.1) calculated for the smallest wave height is  $4.2 \times 10^4$ . Hence, viscous scale effects can be neglected. Also, selected wave conditions are large enough to avoid surface tension effects.

Table 4.2: Correction for Stability numbers

Stability number Before correction	Wave height/(cm) Before correction	Stability number After correction	Wave height/(cm) After correction
2.77	14.52	2.20	11.52
3.10	16.25	2.46	12.90
3.50	18.34	2.78	14.56
3.90	20.44	3.10	16.22

Table 4.3: Selected Wave conditions- Series 1

Input $H_s$ /(cm)	Stability number	Wave steepness	Input $T_p$ /(s)	Water depth/(cm)
11.50	2.19	0.04	1.30	50
13.00	2.48	0.04	1.39	50
13.80	2.63	0.04	1.43	50
14.40	2.75	0.04	1.46	50
15.50	2.96	0.04	1.58	50

After performing the series 1, wave conditions for the series 2 were decided. As not much rocking was observed for long period series 2 was conducted considering the same wave steepness, but wave heights were further increased until the maximum limit that wave paddle can generate. Starting from the final wave condition of the first wave series, wave heights were further increased with about 1 cm

increment each time. Further details about the testing conditions can be found in following chapters. Table 4.4 shows the selected input wave conditions.

Table 4.4: Selected Wave conditions- Series 2

Input $H_s$ /(cm)	Stability number	Wave steepness	Input $T_p$ /(s)	Water depth/(cm)
15.50	2.96	0.04	1.58	50
16.50	3.15	0.04	1.63	50
17.50	3.34	0.04	1.67	50
18.00	2.43	0.04	1.70	50
19.00	3.63	0.04	1.74	50

### 4.3. Model layout

In this section main dimensions of the armoured slope and its individual components will be discussed.

#### 4.3.1. Main dimensions

As discussed in section 4.2.1, slope for placing the Xbloc units was prepared using a wooden base. This way the effect of impermeable core can be represented easily. The set up was kept as simple as possible, so that it can be easily installed inside the flume when required. The total height of the slope is 0.73m with a freeboard of 0.23m ( $1.2H_{smax}$ ). The figure 4.3 shows a sketch of the prepared slope with main dimensions.

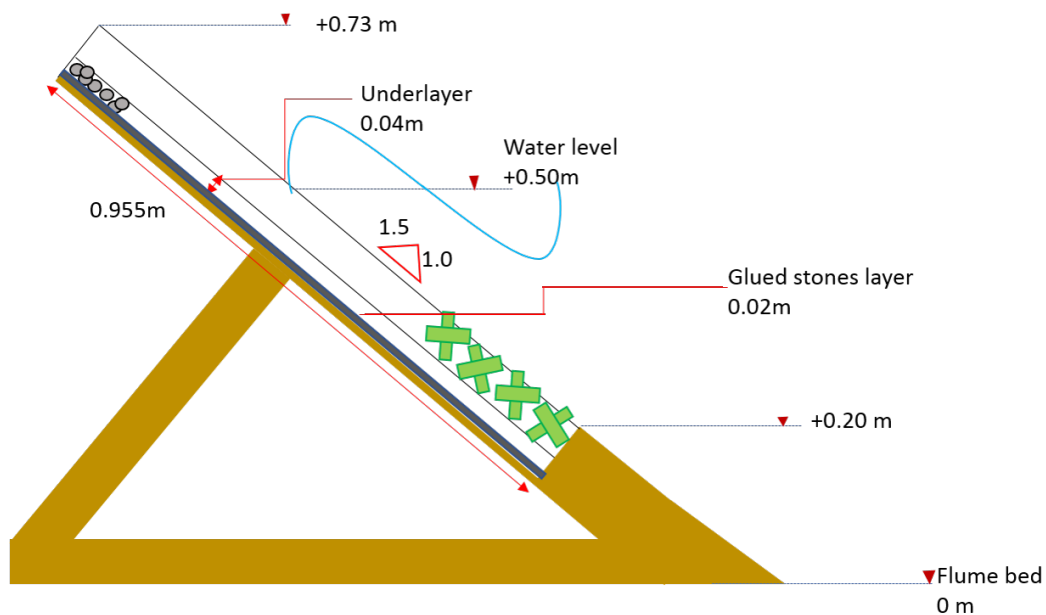


Figure 4.3: Slope dimensions

Xblocs were placed on a loosely placed under layer. Therefore, as shown in the figure 4.4 to increase the surface roughness of the smooth slope and place the underlayer on that, an additional layer of stones were glued to the wooden board which acts as an intermediate filter layer between the core and the underlayer. For this intermediate filter layer stones with 1cm diameter (Approximately the lower limit of the Underlayer stone size) were used and the thickness of the layer was 2cm.



Figure 4.4: Slope preparation a) Wooden slope b) After gluing the stone layer

#### 4.3.2. Armour layer

For the armour layer, Xblocs with height ( $D$ ) of 5.64cm ( $D_n = 3.9\text{cm}$ ) was selected. Because, it is the minimum available standard size that has enough space to accommodate all necessary electronics inside the instrumented unit.

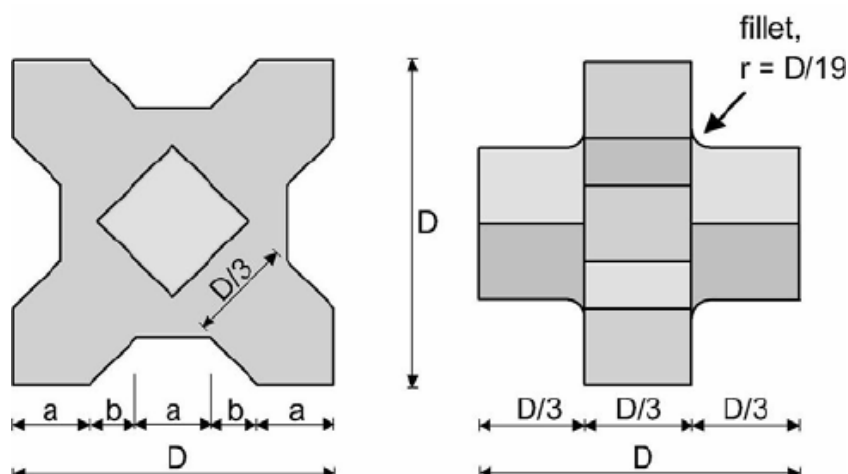


Figure 4.5: Geometry of the Xbloc

The density of the Xbloc model units are  $2.34\text{ gcm}^{-3}$ . Due to some practical issues and time restrictions, only two instrumented Xbloc units were able to prepare before start of the model testings. These instrumented Xbloc units were placed on the slope together with other model units. The first instrumented unit has the density of  $2.13\text{ gcm}^{-3}$  (about 9% lower density) and the second instrumented unit has the density of  $2.42\text{ gcm}^{-3}$  (about 3% higher density). The first instrumented unit was prepared inserting V90 class SD card and the second instrumented unit was prepared inserting V30 class SD card to record the data.

#### 4.3.3. Under layer

Generally Underlayer has two main functions. First function is to act as a filter layer to prevent core material being washed away through the armour layer. Second function is to provide surface for placement of the armour layer. DMC (2011) provide following guidelines for the selection of underlayer based on the weight of the Xblocs with regular concrete (Density= $2400\text{kgm}^{-3}$ ).

- The W85 of the underlayer grading shall be smaller or equal to  $W/7$ ,
- The W50 of the underlayer grading shall be between  $W/9$  and  $W/11$ ,

- The W15 of the underlayer grading shall be larger or equal to W/15,

Where,  $W$  is the weight of the Xbloc,  $W_{85}$  is the rock weight that is exceeded by 15% of the rocks in the underlayer,  $W_{50}$  is the rock weight that is exceeded by 50% of the rocks in the underlayer and  $W_{15}$  is the rock weight that is exceeded by 85% of the rocks in the underlayer.

However, in this study with instrumented Xblocs the weight of the model units can be slightly deviated from the actual model units. As the filter criteria is more important than the weight, the diameter ratios were calculated as follows from aforementioned weight ratios considering regular concrete of  $2400\text{kgm}^{-3}$  and rocks of  $2600\text{kgm}^{-3}$  density.

- $D_{nXbloc}/D_{85UL}=1.96,$
- $D_{nXbloc}/D_{50UL}=2.14\text{-}2.28,$
- $D_{nXbloc}/D_{15UL}=2.53,$

In which,  $D_{nXbloc}$  is the nominal diameter of Xbloc units,  $D_{85UL}$  is the 85% passing value of the underlayer material,  $D_{50UL}$  is the 50% passing value of the underlayer material, and  $D_{15UL}$  is the 15% passing value of the underlayer material.

According to the current size of the Xbloc model units, these criteria resulted in  $D_{85UL}=19.9\text{mm}$ ,  $D_{50UL}=18.3\text{mm}\text{-}17.1\text{mm}$  and  $D_{15UL}=15.4\text{mm}$ . To sieve these material the mesh size of the sieve should be about  $1.2 \times$  required diameter of the stones. Hence, the required sieve sizes are 23.8mm, 21.2mm and 18.5mm respectively. But with the available material and sieve sizes in the lab these requirements could not be able to fulfill exactly. Therefore, underlayer was prepared as a composition of 70% of 22mm sieve passing and 16mm sieve retained, 15% of 25mm sieve passing and 22mm sieve retained and 15% of 16mm sieve passing and 11mm sieve retained. Layer thickness is about 3.5cm ( $2D_{50UL}$ ). Figure 4.6 illustrates the prepared model section in the flume.

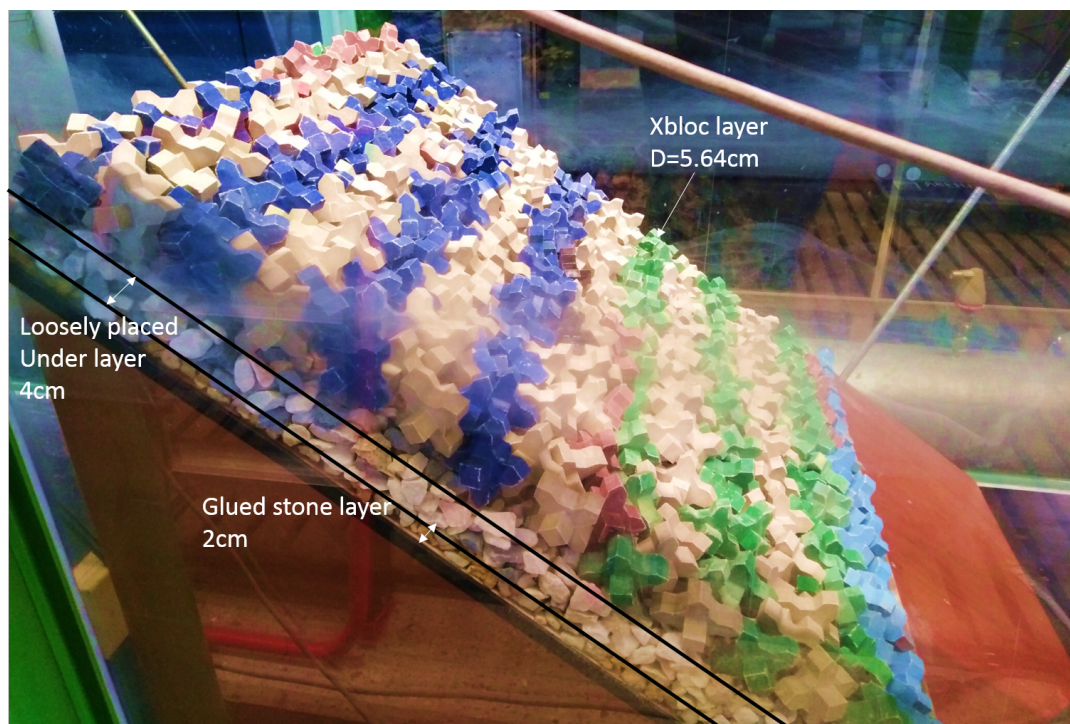


Figure 4.6: Model section

#### 4.3.4. Armour layer placement

The basic principles of Xbloc model units placing can be summarized as follows (DMC (2017)).

- Units are placed in a single layer and the orientations of the units should be random.
- Units are placed in diamond shape, staggered pattern. The horizontal grid distance between the center of gravity of two units in the same row is called  $D_x$  and  $D_x = 1.32 \cdot D$ . The upslope grid distance between two rows of Xbloc is called  $D_y$ . Along the slope of the structure  $D_y = 0.63 \cdot D$  (where  $D$  is the unit height). Please refer figure 4.7.
- Each unit must be in contact with the under layer and should be secured by two units in the above row.

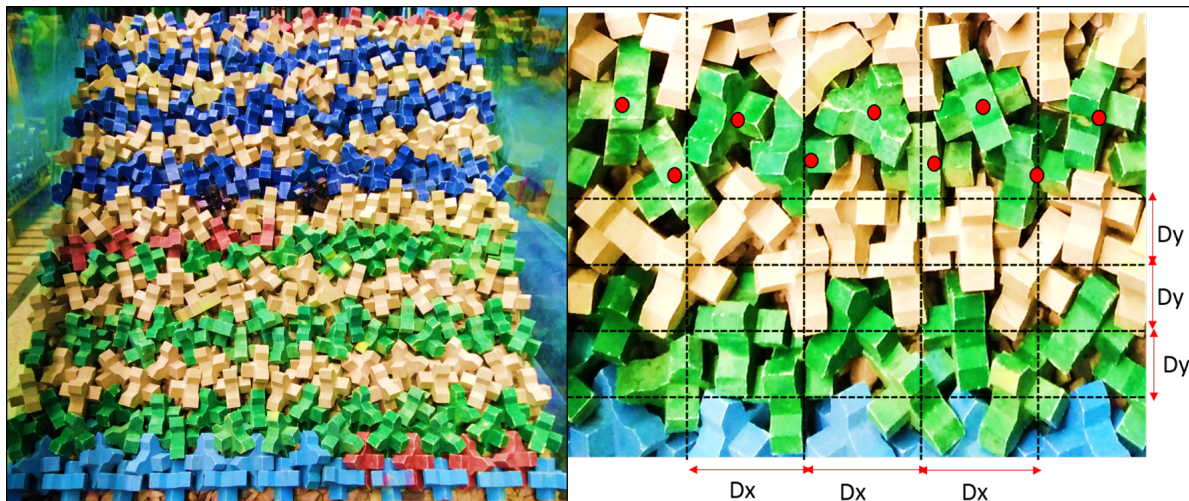


Figure 4.7: Placement of Armour layer

There are two options to place Xblocs on the slope.

- Starting with a Xbloc unit on either side of the flume against the side wall. The second row will contain one unit less.
- Starting with a Xbloc unit on one side of the flume against the side wall, The second row will start on the opposite side with a unit against the side wall. Each row consists of an equal amount of units.

Considering the size of the selected Xbloc model unit and the available flume width it was decided to choose the option one. Therefore starting from the first horizontal row, each odd row number (1,3,5...) contained 11 units and every even row number (2,4,6,..) contained 10 units.

In the very bottom row all the xblocs are regularly placed. Therefore, they have the same orientation, pointing one nose downward and supported by the wooden base and two other legs touching the underlayer. Two instrumented units are shown in black colour in figure 4.7. In total there were 27 horizontal rows in the model. Before placing the units actually in the model, placements were done few times to practise with the placement. Packing density was checked in several intermediate steps as well as after placing all the rows by measuring the center to center distance between the second row and the considered row.

#### Relative Packing Density

For hydraulic model experiments with Xbloc armour units DMC prescribes a packing density of  $1.20/D^2$ . Relative Packing Density (RPD) can be calculated from the ratio of this theoretical packing density and the actual packing density. It is recommended to maintain the packing density on the slope between 98% and 102% of the theoretical required packing density (DMC (2017)).

# 5

## Experimental studies -Model Testings

This chapter will provide details about model testings, observations and changes did while testing.

### 5.1. Test Facility

The 2D hydraulic model tests have been carried out in the wave flume of Water Lab in TU Delft. The flume has a length of 40 m, a width of 0.8 m and a height of 1.0 m. Waves are generated by the wave paddle which is at the one end of the flume, after sending the signal relevant to the required wave condition. The wave paddle has an active absorption system to absorb the wave energy of reflected wave and generate the right wave back into the flume. For the testings JONSWAP spectrum was used to interpret young sea state condition with irregular waves.

The structure was placed about 17m distance from the wave paddle location. Three wave gauges were placed 2m from the location of the structure. The spacing between the first and second gauge was 0.3 m and the spacing between first and third gauge was 0.7 m. Reflection analysis was performed to get the incident wave height separating from the reflected wave height. Incident wave conditions obtained after reflection analysis and details of the test conditions are included in appendix A.

### 5.2. Data Collection

As described in the previous chapter, two instrumented Xblocs were placed at the waterline. Before placing them on the slope the units were fully charged for 12 hours. Then the Arduino programme was uploaded to the units to collect the data in standalone mode. It was decided to upload the Arduino sketch which is capable of measuring the data at about 100 Hz frequency to capture all possible movements. To limit the number of data while unit is in the stationary position, Two threshold values were applied for both units.

For the accelerometer, initially applied threshold was; Absolute acceleration  $> 1.025g$  and for the gyroscope it was; Absolute angular velocity  $> 0.1 \text{ rad/s}$ . After the data retrieval of the first three tests in the second test series, the threshold values were decreased to  $1.01g$  and  $0.05 \text{ rad/s}$  for accelerometer and gyroscope respectively for the next three tests.

After performing the first test series, data were retrieved from the units. To collect and save the data another software package called Coolterm was used that acts as a bridge for Arduino and the processors. During the second series, data were retrieved for two times after the first three tests and then for the last three tests respectively.

### 5.3. Observations during the testings

#### 5.3.1. Test Series 1

For the test series 1 both units were placed at the waterline. The relative packing density of the Xbloc layer was 99.7% of the theoretical packing density. As the purpose of the study is to observe sufficient movements with fairly larger Xbloc units, instrumented units were placed with minimal interlocking with surrounding units increasing the possibility of rocking. The two units were placed in two different random orientations ( Figure 5.1).



Figure 5.1: Position of the instrumented units before starting the test series 1

The test series one was started with the smallest wave condition and continued with progressively increasing the wave height as given in table 4.3. After starting the test, no visible movements were noticed at the waterline but one unit at the flume side wall was clearly started rocking for few minutes and then stopped. Even with the smallest wave height slight settlement of underlayer was observed. Consequently, the spacing between rows above the waterline slightly increased (Figure 5.2). No rocking movements were visually observed with instrumented units as it was difficult to observe small rotations visually with its location on the slope and with the wave action.

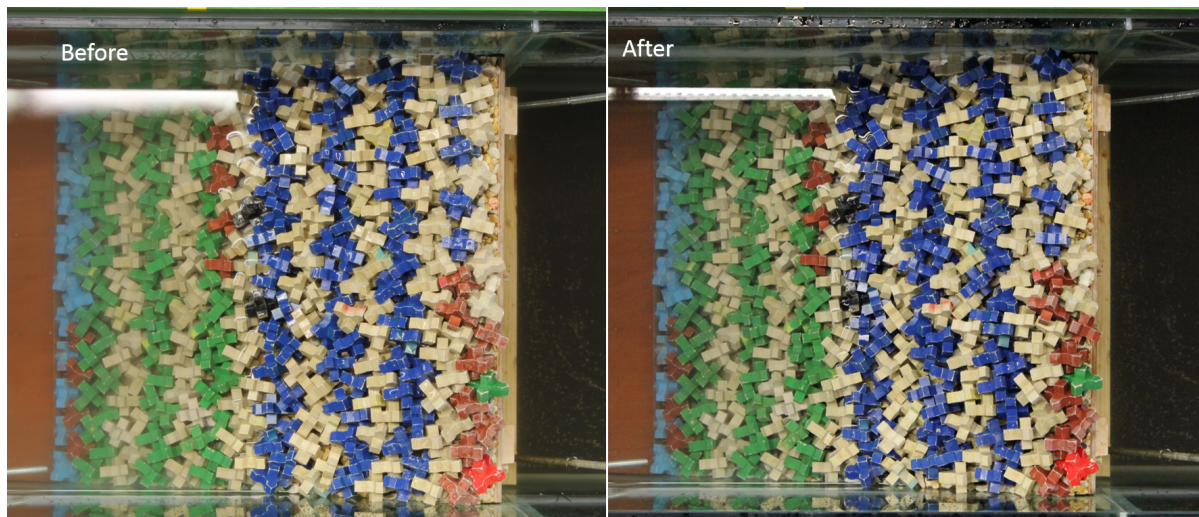


Figure 5.2: Before and After situation- test 1, series 1

During the second test a few motions were noticed with Unit 1 and no motions were visually observed with Unit 2. A progressive settlement of underlayer was observed. (All before and after images will be included in the Appendix). After test two, interlocking between the instrumented units and the surrounding units were checked. It was noticed that the Unit 1 still has the possibility of movements

whereas unit 2 was quite interlocked with surrounding units.

During the third test also a very few rocking movements were observed with unit 1 at the beginning but no movements were observed for long time at the latter part of the test. No movements were visually observed with the unit 2. At the end of the test three it was noted that both instrumented units were quite well interlocked with neighbouring units and settlement of the above rows also influenced the bottom rows to compact well.

It was realized with the current interlocking effect, the chance of getting rocking with instrumented units are very less even with the relative higher wave height in fourth test condition. But with the time restrictions it was not possible to build the slope again before perform the test four. As evaluating the feasibility of the technique in detecting the rocking is more important, the natural interlocking pattern around two instrumented units were disturbed and spacing around two instrumented units were slightly increased before starting the test four. As a result, with relatively higher wave height in test four some clear rocking movements were observed specially with unit 1.

During the final test, some clear rotations were observed in unit1 for few seconds at the beginning. After performing the first test series the slope was rebuilt.

### 5.3.2. Test Series 2

As not much rocking was observed during first test series specially with instrumented unit 2, the second test series was performed similar way with increased wave conditions (Table 4.4). In the test series 2 both units were placed at the waterline at the beginning. The relative packing density of the Xbloc layer was further reduced to 98.6% of the theoretical packing density. The two units were placed in two different random orientations.

During the first test in the testing series two, a clear settlement of the rows above the waterline occurred with the rapid rundown (Figure 5.3). One unit in the 10<sup>th</sup> row from the bottom was flipped out from the slope. But it was really difficult to observe any movements with the instrumented units with the high turbulence created with the wave - slope interaction.

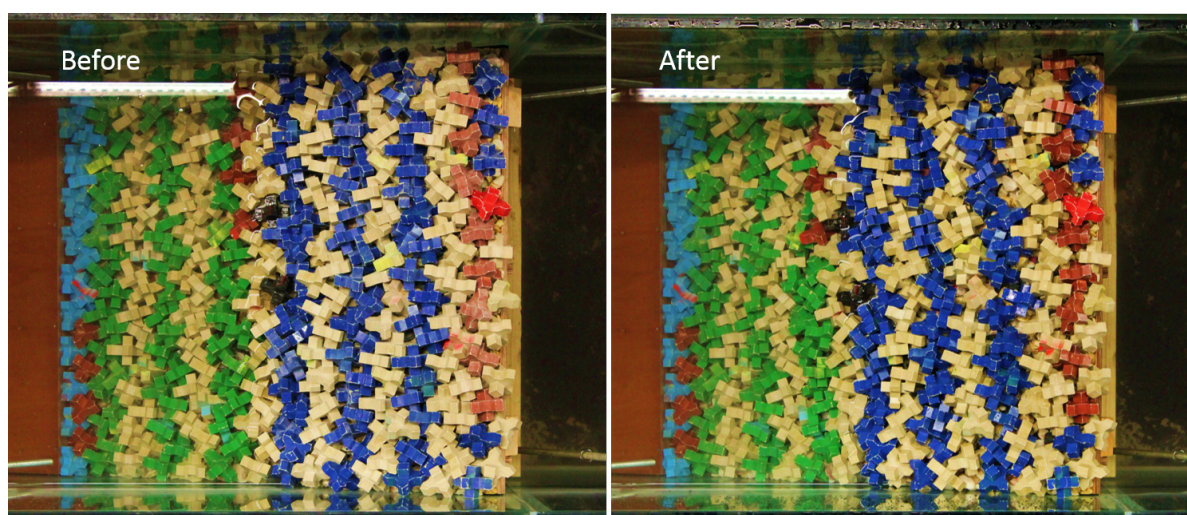


Figure 5.3: Before and After situation- test 1, series 2

Before start of the second test, Unit 2 was swapped with a unit in row number 22 (above the water line) as there was a clear space created around that unit with the settlement occurred during the previous test. During the test, one blue Xbloc unit from the very top row was displaced.

During the third test, three other units from the crest were flipped off. No visible rocking movements were observed. After the third test it was observed that Unit 1 is very well interlocked with neighbour-

ing units and possibility to movements are very less. Therefore, after the third test both units were removed from the slope and data were retrieved. After checking the recorded data, it was decided to further reduce the given threshold in Arduino as the recorded data were limited due to less rocking movements. Then, units were placed back on the slope in the same locations around the waterline (Unit 1) and above the water line (Unit 2). But around the unit 1 previous interlocking was reduced by taking off the unit and placing it back. Unit 2 was not interlocked well with surrounding units before removal and hence the interlocking was not disturbed.

During the test four a clear rocking of a unit just below the water level was observed. No clear rocking with the unit number 1 which is at the water level was observed. Another unit from crest was flipped off.

Before starting the next wave condition, the unit 1, which was at the water level was carefully swapped with the rocking unit just below the water level causing minimum disturbance to the surrounding units. Then the same wave condition was repeated again as the test number five.

During test five, some rocking was observed with the instrumented unit 1 which was placed just below the water level. During the test another two units were flipped off from the slope.

Then the final test, test six was performed without doing any changes to the locations of the instrumented units. The unit one started to rocking continuously under the waterline. Two other units from the crest was flipped off during the test. All together, 7 units from the crest row was displaced from the slope and three units were displaced from the lower positions of the slope.

# 6

## Data Processing and Analyzing

This chapter is focused on the analysis of rocking measurements with instrumented Xbloc units.

### 6.1. Possible movements

In three dimensional space a Xbloc unit has six degrees of freedom in total including translations along  $x,y,z$  and rotations around  $x,y$  and  $z$ . In general rotations are dominant in rocking motion.

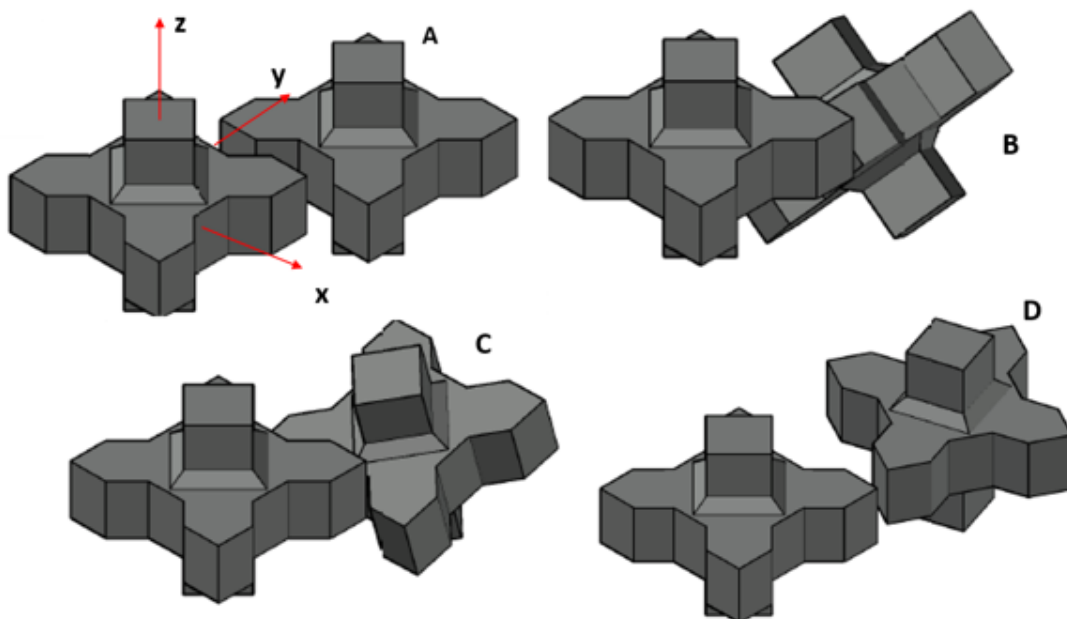


Figure 6.1: Rotational motion A)Initial position B)Rotation around y axis (pitch) C)Rotation around x axis (roll) D)Rotation around z axis (Yaw)

Figure 6.1 shows three rotations around each axis with respect to the local reference frame defined at the center of the unit. Figure 6.2 shows translation motion along y axis. Moreover, in reality motions can be due to both rotation and translations together.

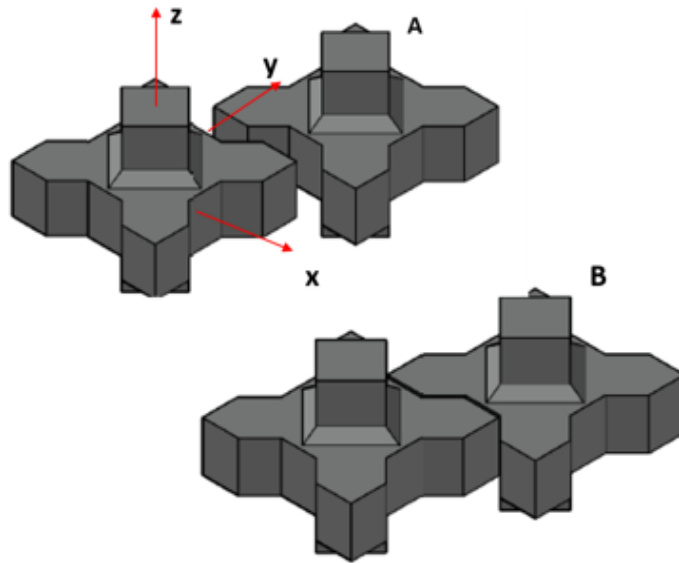


Figure 6.2: Translation motion A)Initial position B)Translation along Y axis

As shown in figure 3.4 the sensor is placed in the middle of the 3D printed xbloc unit and therefore, similarly a reference coordinate system can be defined at the center of the xbloc unit according to the local axes of the sensor that has been placed inside it. When the instrumented xbloc unit is placed on the horizontal plane the local axes can be defined as shown in the figure 6.3 (Please note that the axes shown in the figures are defined at the center of the unit and for the clear illustration axes are shown at the top and only represent the respective directions). Apart from that a global coordinate system can be defined along the structure slope where the units are placed on.

When instrumented Xbloc unit is placed stationary on the horizontal plane z axis measures the gravitational acceleration whereas x and y axis show zero accelerations. But when the xbloc unit is placed on the slope in a random orientation, the unit is already tilted and the measurement of gravity will be given either by one axis or as components of different axes.

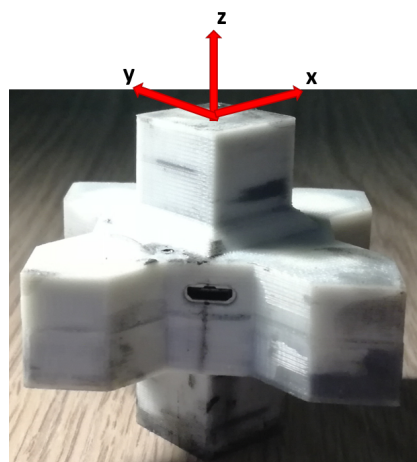


Figure 6.3: Local axes of instrumented Xbloc unit

## 6.2. Data Processing

The recorded data were processed using a Matlab script. The processing method will be discussed in the following sections. Initially, different threshold values were applied only to the gyroscope to process the obtained raw data. But, to process the data obtained from accelerometer no initial threshold was applied because, applying a threshold to raw accelerometer data can eliminate all the negative peaks from the calculation. Figure 6.4 and 6.5 show the resultant accelerometer and gyroscope data obtained from raw data. Two clear occasions can be identified with significant movements.

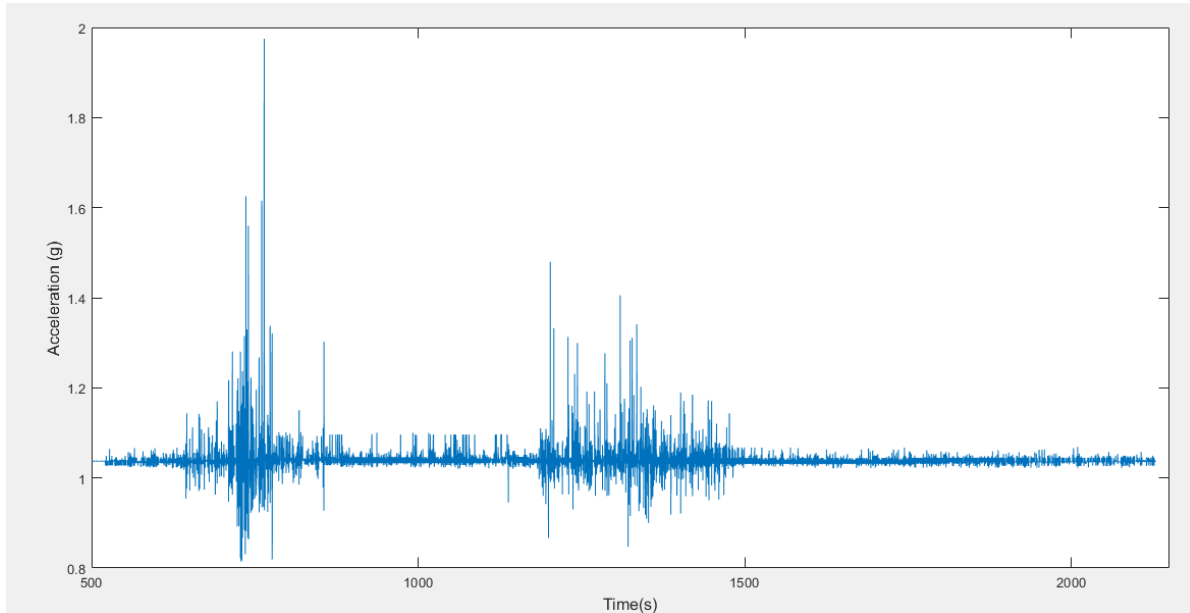


Figure 6.4: Raw accelerometer data (Resultant) of unit 1- $H_s/\Delta D_n = 2.03$ - series 1:1

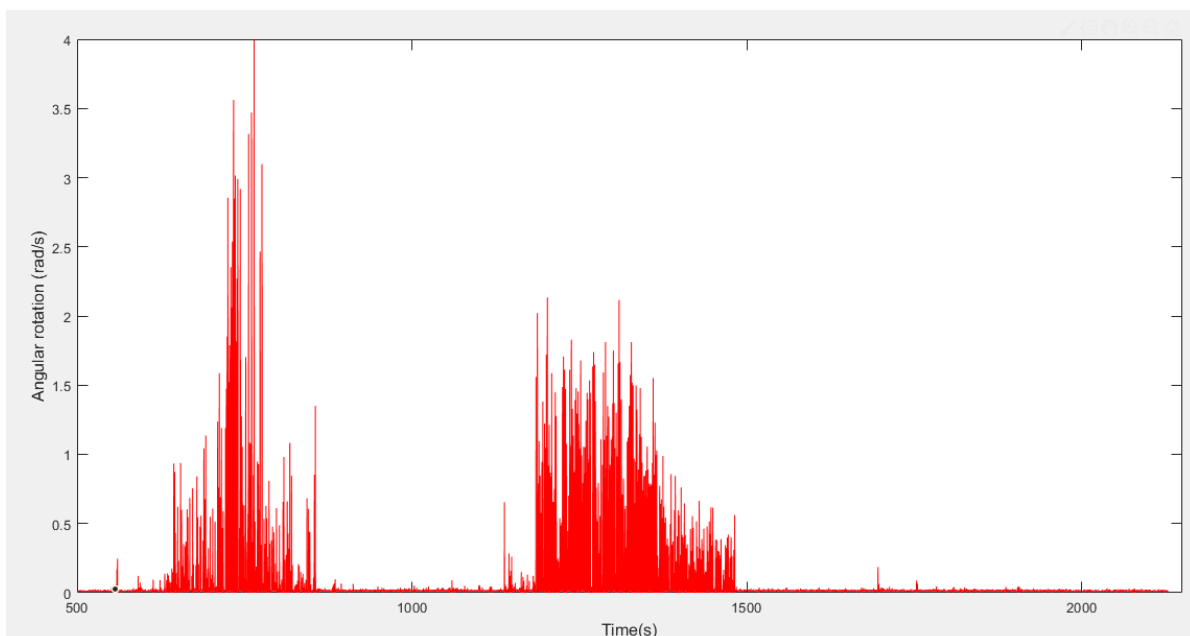


Figure 6.5: Raw gyroscope data (Resultant) of unit 1-  $H_s/\Delta D_n = 2.03$ - series 1:1

By further looking into the events with significant movements, some movements can be clearly identified with an time interval similar to the wave period (Figure 6.6).

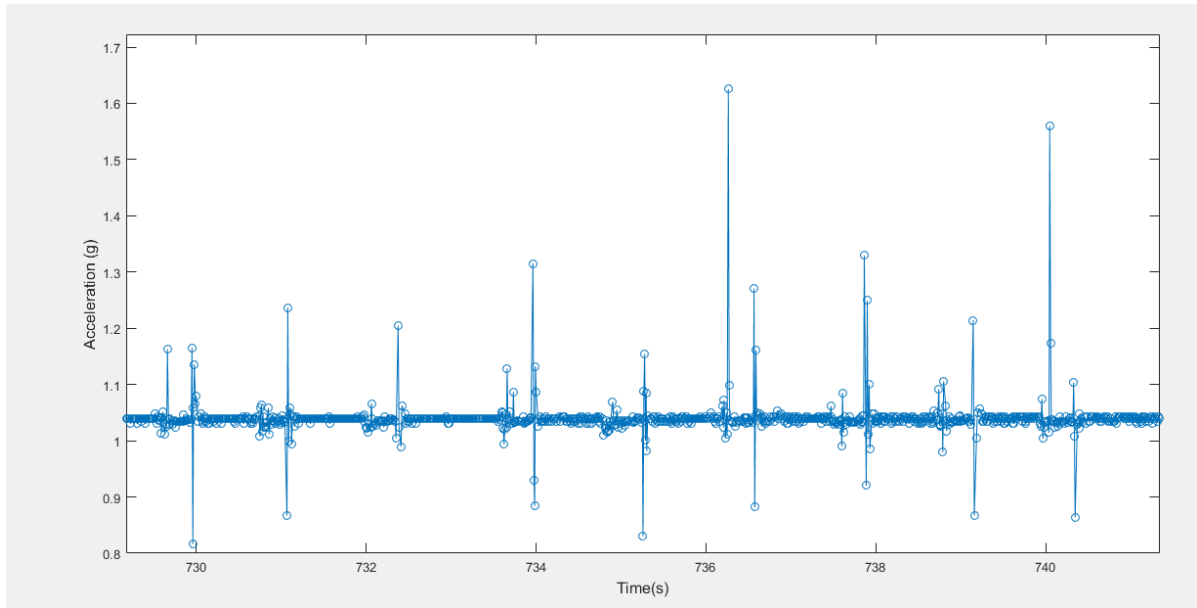


Figure 6.6: Variation of raw accelerometer data (Resultant) of unit 1- $H_s/\Delta D_n = 2.03$ - series 1:1

Further, in unit one, two close peaks for each rocking event can be identified in most of the recorded data. These peaks have the time difference about 0.3-0.5 seconds and visible in both accelerometer and gyroscope data. When closely look into the raw gyroscope data, it was identified that these peaks are related to upward and downward movement of the Xbloc unit. Therefore, when processing the data one event of movement is considered as a full rotation of the unit. Therefore, one event can include both upward rotation and downward rotation. Close comparison of few highest peaks in accelerometer and gyroscope data during a single event of impact can be seen in Figure 6.8 and 6.9.

Gyroscope measures the angular velocity measurements with respect to an inertial reference frame. With the measured angular velocities, gyroscopes can also be used in angular orientation estimation. Angular orientation can be defined as the position of the unit's local coordinate system relative to a initial reference coordinate system with the same origin.

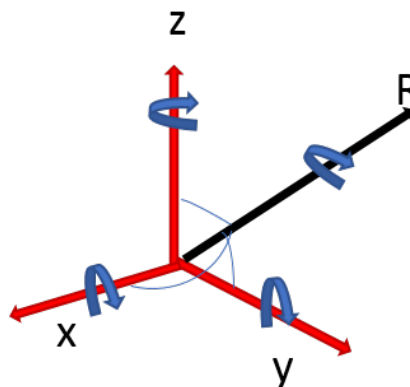


Figure 6.7: Rotation measured by the gyroscope

Three axis gyroscope angular velocity output represents the simultaneous rotations around axes of x, y and z. Therefore, the gyroscope represent a single rotation around a certain axis for a certain angle

(figure 6.7). This rotation and the resulting angular orientation can be uniquely represented using a rotation vector in which the vector aligned with the rotation axis and with the length equal to the rotation angle (Stančin & Tomažič (2011)).

In general as the rotations around x, y and z are simultaneous, they are not commutative. Therefore, rotations are not accurate to assumed as sequential rotations. Six possible sequences can be identified around three orthogonal rotations and six different angular orientations can be obtained. However, when the angles of the three simultaneous rotations are small, rotations become nearly commutative and the difference between the six aforementioned sequences become negligible (Stančin & Tomažič (2011)).

During the rocking motion the rotations around all three orthogonal x,y,z axes can be assumed as small and therefore rotations can be assumed as nearly commutative. Therefore, commonly used zyx sequence was used in the rotational transformation matrix calculation given in the section 6.2.1.

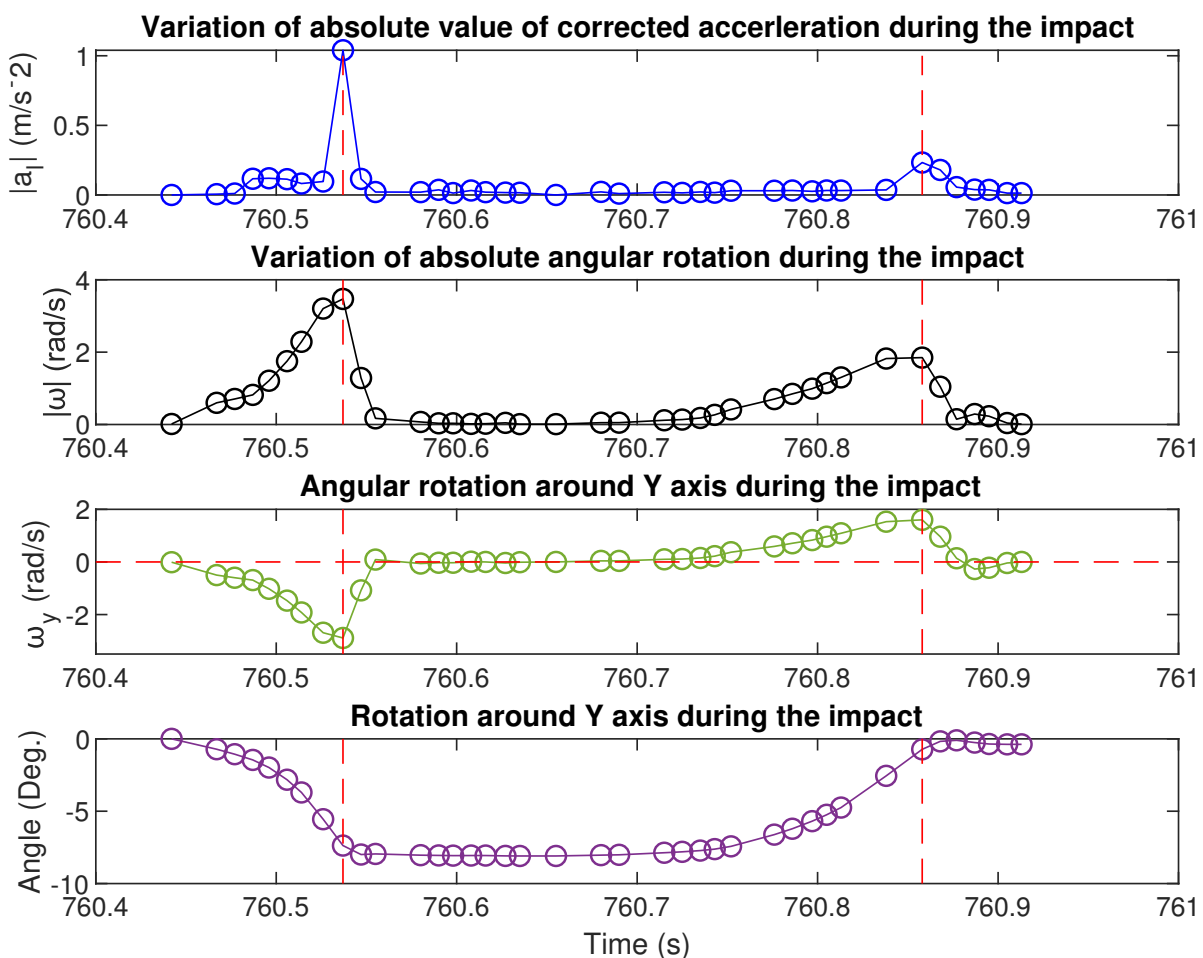


Figure 6.8: Behaviour of motion during the impact 1-unit 1-  $H_s/\Delta D_n = 2.03$ - series 1:1

In the figure 6.8 and 6.9 both upward and downward movements can be clearly identified within a single event of rotation. The corrected acceleration value refers to the linear acceleration data after removing the gravitational acceleration ( section 6.2.1). The peaks can be identified as the movement of collision and both accelerometer data and gyroscope data show the peaks at the same time. Dominant axis of rotation during the events were identified by observing the raw gyroscope data (The axis where the largest angular velocities can be observed) and the raw angular rotation values were plotted as shown in the figure. It can be observed that during the event the direction of the dominant rotation has changed according to the upward and downward rotation. Hence, upward and downward

movements can be distinguished with the sign of the dominant rotation direction. For this particular events the direction of rotation is clockwise (negative) for the upward movement and counterclockwise (positive) for the downward movement.

Also from the figure 6.8 and 6.9 it can be seen that the peak for the upward movement is relatively higher compared with the peak for the downward movement. Further, the magnitude of angle of rotation around the dominant axis of rotation is less than 10 degrees in these particular events. Also it can be observed that after the full rotation, the unit has come to its initial position. Therefore, it can be approximated that the angle of rotation is more or less same for the both upward and downward movement.

However, as mentioned in the section 6.2 the rotation around dominant axis does not represent the correct resulting orientation and its rotational axis resulted from the rotations around all three x, y, and z axes. Therefore, in order to calculate the correct angle of rotation during the upward and downward movements the resulting orientation from all three axes should be considered. But in this analysis it was not considered and only the rotational angle around the axis where highest angular velocities were observed was considered and referred as dominant axis of rotation. Nevertheless, angle calculation around this single axis clearly shows that after a complete rotation the unit returns to its original position.

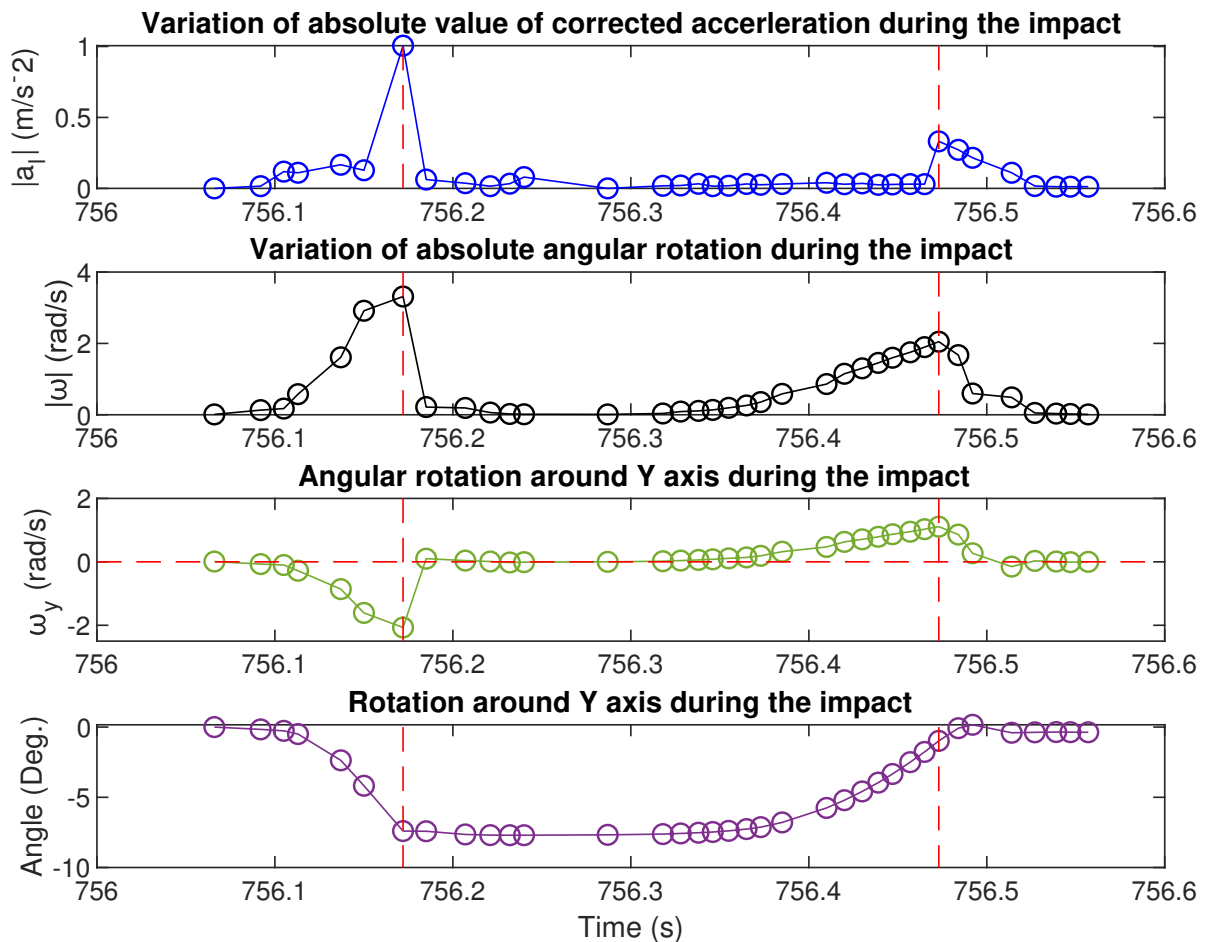


Figure 6.9: Behaviour of motion during the impact 2-unit 1-  $H_s/\Delta D_n = 2.03$ - series 1:1

The same analysis was performed considering four highest peaks from the test series 2 after placing the instrumented unit below the water level (appendix C). It was observed that, with relatively higher stability number the accelerometer data are quite noisy compared with the data obtained for the low-

est stability number. Also sometimes more than two peaks can be observed during one impact event. This may due to impact with several other surrounding units while rocking. The maximum rotational angle around the dominant axis was observed as around 10 degrees. Please note that this analysis was performed without interpolating the raw data. Therefore, sampling frequency is not constant. But around 100 Hz in average.

### 6.2.1. Impact Velocity Calculation

Impact velocities are calculated from two approaches.

- By taking the peaks of absolute angular velocity measurements
- By separating the gravity from each component of acceleration data and then by integration of linear accelerometer data

Following assumptions were made when calculating the impact velocity from gyroscope and the accelerometer.

- Number of collision is equal to the number of peaks in angular velocity signal and accelerometer signal
- Impact velocity is equal to tangential velocity of the rotating unit.
- Integration of gyroscope data for small time period (less than one second) does not result in significant drift

#### Data processing procedure

- Linear interpolation of raw data with 5ms intervals
- Identify the individual events with both upward and downward movements above a given threshold (both in raw accelerometer and gyroscope data)
- Correct the accelerometer data eliminating the gravitational acceleration within each individual event
- Assuming there is no linear acceleration before start of the event and after the event, linear acceleration data were corrected to make the linear acceleration zero after the event by removing the offset. [Brownjohn \(1999\)](#)
- Apply low pass filter to the linear accelerometer data [Brownjohn \(1999\)](#)
- Separate the events into upward and downward movements
- Calculate the resultant angular velocity and resultant linear acceleration for both upward and downward movements
- Get the maximum peak of the resultant gyroscope data for both upward and downward movements - Assumed as the impacts
- Identify the maximum peak value of resultant linear accelerometer data -Assumed as the impacts
- Identify the stationary location to start the integration of linear acceleration data based on the resultant angular velocity data.
- Integrate the accelerometer data for both upward and downward movements within each of the impacts using trapezoidal rule.

#### Identify the individual events with both upward and downward rotation

Before separate the upward and downward movements, firstly different events were identified. Assuming before and after the full rotation event there is no angular velocity (Resultant angular velocity  $\approx 0$ ) individual events with both upward and downward movements were separated. Then to identify the events with sufficient movements only, a threshold value was applied to the resultant angular velocity and events with maximum value above this threshold were selected in gyroscope data and respective data of the accelerometer were also extracted from raw accelerometer data.

### Separating Upward and downward movements

Generally, rocking unit moves upward direction of the slope with the wave run up and move backward again with the rundown. This kind of full rotation can be clearly observed in the recorded data with sufficient rocking movements. Therefore, this upward and downward movements were separated before determine the impact velocity. In figure 6.8 and 6.9 it can be clearly seen that the dominant axis of rotation has different sign convention during upward and downward movements. Hence, upward and downward rotations were separated using this sign. The identification of the rotational axis with relatively highest rotation and its change in sign with the motion was manually identified for each test and applied them in the matlab routing to separate the upward and downward movements.

### Impact velocity calculation directly from Gyroscope data

To get the impact velocity from the gyroscope data, the absolute value for the angular velocity is obtained from the three measured angular velocity components (Equation 2.8). Then the impact velocity is based on these peak angular velocities by assuming a pure rotational motion of the unit. For the calculation of tangential velocity (Equation 2.9), distance between the rotation point and the impact location,  $R$  was assumed as  $1/2$  of the height of the unit (Figure 6.10).

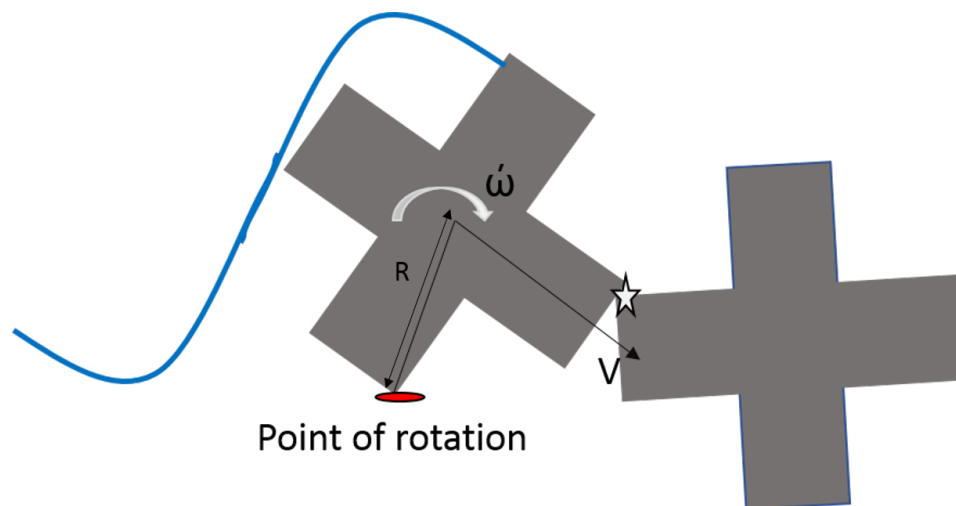


Figure 6.10: Simplified view of rocking event

### Impact velocity by integrating the accelerometer data

In reality there can be situations with both rotation and linear translation. Therefore getting the linear acceleration separated from the raw accelerometer data is important. But removing gravity from each component of accelerometer data is not straight forward approach, as accelerometer is also rotating while taking the measurements. Therefore the accelerometer data are recorded with respect to a sensor body frame. To remove the gravitational acceleration, the body reference frame should be transformed to the initial reference frame. In order to do this transformation, the rotational angle should be known. This can be obtained by integration of gyroscope data.

Initially, it was decided to calculate the pitch and roll angles (assuming yaw can be neglected) using the complementary filter. But after performing the testings, by having closer look in the gyroscope measurements some significant rotations were observed around the Z axis as well, because of the orientation of the unit placed on the slope. Therefore, complementary filter technique can not be used anymore as it does not give any information about the yaw angle.

Instead, rotational angles around all three axes were calculated by integration of the gyroscope data. As impact happens within very short duration it was assumed integration of gyroscope data during this short duration (only within the individual event ) will not cause any significant errors. Then the conversion of accelerometer measurements from body frame to inertial reference frame was done by

rotational matrix obtained from the Euler angle transformation.

Here the first stationary location of the unit just before the upward movement was assumed as the inertial reference frame. The initial gravitation acceleration values related to the stationary location was identified for the each individual impact events including both upward and downward rotation. The initial stationary location was identified using the resultant angular velocity data assuming it is approximately zero before start of the each individual event (see figure 6.8 and 6.9). The correction for the accelerometer data by removing the gravity component was performed for the each individual impact event separately.

Therefore the considered inertial reference frame is not constant for all the individual events as the initial reference frame was considered as the initial gravitation values at the start of the upward movement (stationary position where both linear acceleration and angular rotation is zero). The reason to adopt this approach is to limit the duration of integration of the gyroscope data to obtain the orientation within and after the impact. Because if one considered the inertial reference frame as gravitational data at the stationary position before starting of the test, the integration of gyroscope data has to be performed from the beginning to required moment to find the orientation with respect to the initial position and then rotational transformation matrix can be used to separate the linear acceleration. But integration of gyroscope data for long period may not result in accurate output as it would drift with time.

The work flow is illustrated in figure 6.11. Gravity compensation was done by using the equation 6.1, where  $a_I$  is the linear acceleration in initial reference frame,  $C_B^I$  is the rotational transformation matrix to body frame to initial reference frame,  $g_x, g_y, g_z$  are initial gravitational acceleration values in stationary position and  $a_m$  is the measured acceleration data in body frame Akeila et al. (2008). This model assumes that there are no cross-axis alignment, scale factor, or bias errors in the measurement. Then, after removing the gravity from all three  $x, y, z$  components of the accelerometer data, absolute linear acceleration was calculated. Thereafter, impact velocity was obtained from the integration of the absolute linear acceleration data until the peak.

$$a_I = C_B^I a_m + \begin{bmatrix} -g_x \\ -g_y \\ -g_z \end{bmatrix} \quad (6.1)$$

For the upward movement the integration of linear acceleration was started from the stationary position defined above. But for the downward movement it was difficult to identify a completely stationary position in between two rotations hence, integration was started from the timestamp related to the closest local minima of the resultant gyroscope signal relevant to downward movement (refer figure 6.8 and 6.9).

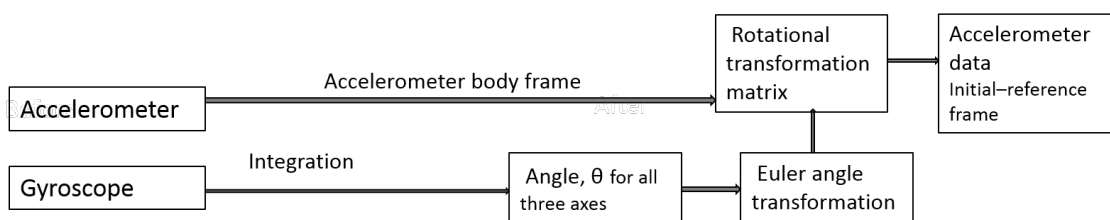


Figure 6.11: Processing accelerometer data based on Euler angle transformation

## 6.3. Results Analysis

### 6.3.1. Probability of exceedance of impact velocity

After finding the impact velocities from both ways, curves for probability of exceedance of impact velocity were made for both Units considering all test conditions with respect to number of waves,  $N$  (Equation 6.2). Impact velocities were calculated for both upward and downward movements. Then the characteristic impact velocity,  $V_{i2\%}$  was determined by taking the value of impact velocity that has

the exceedance probability of 2%.

$$P(v_i > v_{i,n}) = \frac{n}{N} \quad (6.2)$$

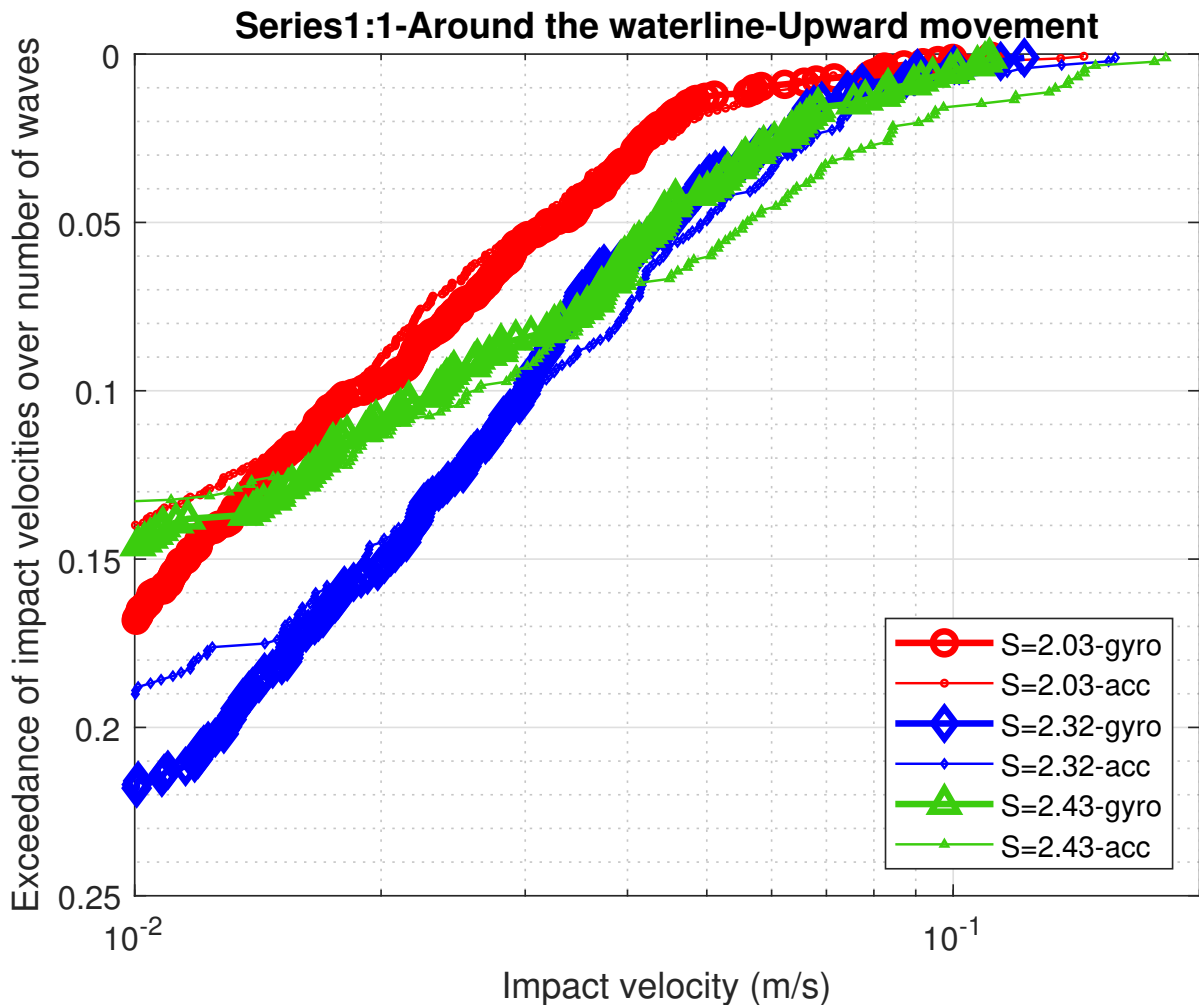


Figure 6.12: Exceedance probability in upward movement for Unit 1- series 1:1

### 6.3.2. Upward movement with run up

Exceedance probability for upward movement were plotted for both test series considering only the tests with significant motions. Refer figure 6.12 and 6.13.  $S$  refers to the stability number calculated according to the incident wave height (Appendix A).

As shown in figure, 6.12, 6.13 and appendix D accelerometer integration has resulted in higher impact velocities compared with velocity obtained from the gyroscope. In the test series 1, sufficient movements can be seen in all test conditions according to the recorded data in unit 1 even though it was hard to identify the motions while performing the testings. These observations are inline with the changes described in section 5.3. However, with the unit 2 no significant motions were observed during the test series 1 compared with unit 1.

After increasing the space around the waterline in test four (S1:2 T4) the highest impact velocities were observed (figure 6.12 and appendix D). However, in the fifth test (S1:2 T5) the movements were observed only at the beginning and when instrumented unit finds its stable position after few rotations, no more significant movements were observed. Also, despite of the higher stability number, the lower

impact velocities observed in the test five can also be due to considerable settlement of the above rows which resulted in increased pressure on the instrumented units.

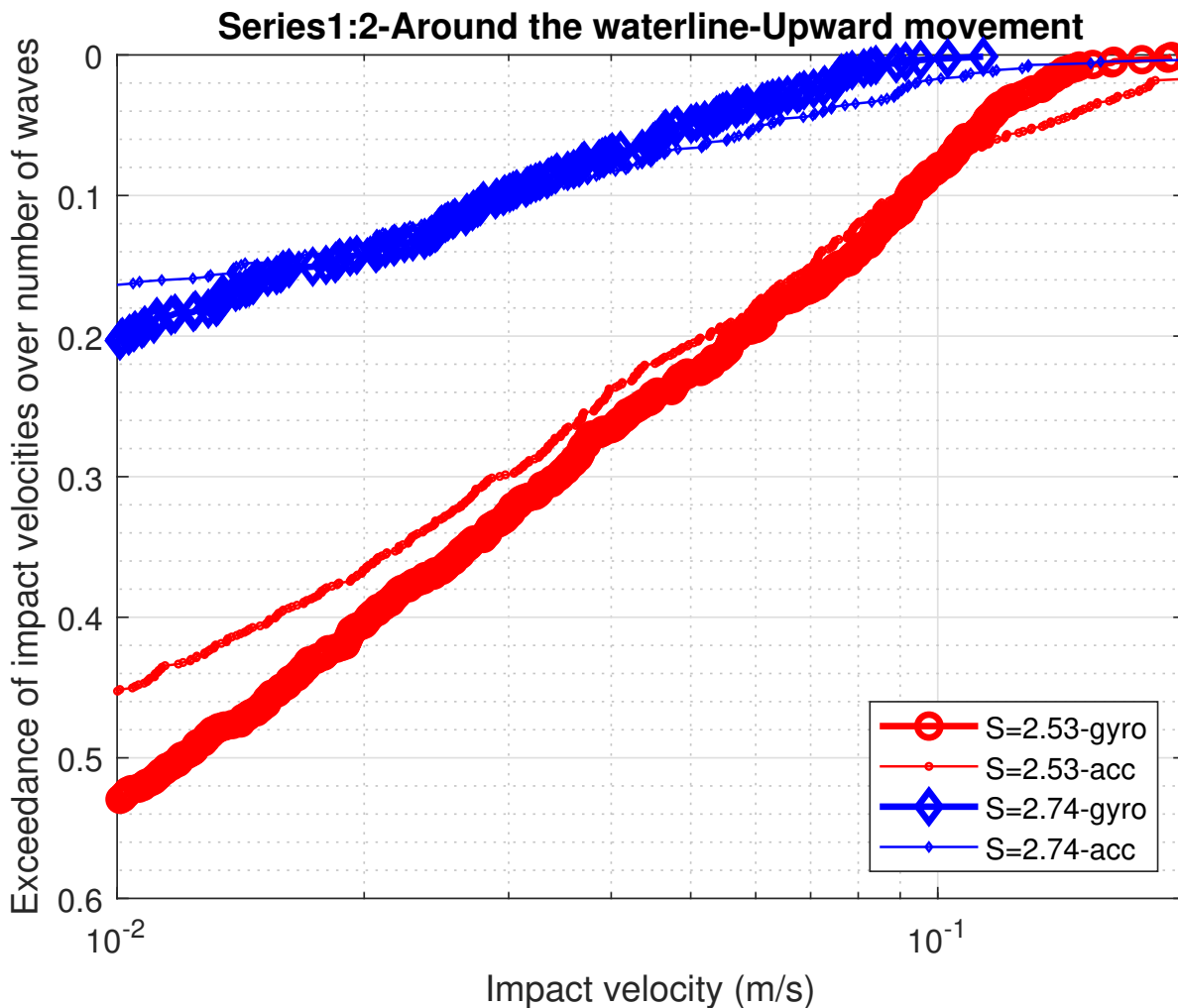


Figure 6.13: Exceedance probability in upward movement at waterline for Unit 1- series 1:2

The second test series was started with the highest wave condition of the first wave series and progressively increased the wave height. Because of the fairly larger wave height given at the start, and due to the lesser packing density a sudden settlement of the rows above the water level was clearly observed. Consequently, despite the higher stability numbers in the first three tests in the second test series, significant rocking movements could not be observed. As described in the section 5.3 after the third test, fourth test was performed after disturbing the natural interlocking pattern of the unit 1 which was placed at the water level. As a consequence, considerable change in number of movements and resulted impact velocities can be observed in figure 6.13. Therefore, it is clear that there is a significant influence on the rocking motion from first settlement of the armour units. The settlement of above rows can exert additional pressure on the below rows and can reduce the rocking in below rows. At the same time, the impact velocities caused by the settlement alone can have an influence on the breakage of armour units. Further research is recommended to use the proposed technique to evaluate the influence of the settlement on the breakage of armour units and to find the amount of settlement of armour units.

To identify the collision events with significant movement, a threshold value was applied based on the measurements obtained from the gyroscope. Only the events that have certain maximum resultant angular velocity were selected for further processing. For the unit 1, this threshold was kept as 0.35 rad/s in all the tests, except for first three tests of the second series. As observed movements

are very few, a less threshold value of 0.15 rad/s was applied in the first three tests of the second test series. For the unit 2, the threshold was kept as 0.15 rad/s in all the tests, except for last two tests of the first series. A threshold value of 0.35 rad/s was applied in the last two tests of the first series.

Further, the last two tests were performed in the second test series after changing the position of instrumented unit 1 from water line to location just below the waterline. Calculated characteristic impact velocities for units in upward movement are listed in table 6.1, 6.2 and 6.3.

Table 6.1: Characteristic Impact Velocity- Upward movement- Unit1-Series 1/2-at the waterline

Test number	Stability number	$V_{i2\%}$ from accelerometer (m/s)	$V_{i2\%}$ from gyroscope (m/s)
S1:1T1	2.03	0.0473	0.0447
S1:1T2	2.32	0.0728	0.0651
S1:1T3	2.43	0.0907	0.0650
S1:2T4	2.53	0.1818	0.1355
S1:2T5	2.74	0.0939	0.0749
S2:2T4	3.15	0.1491	0.0777

Table 6.2: Characteristic Impact Velocity-Upward movement- Unit1-Series 2- just below the waterline

Test number	Stability number	$V_{i2\%}$ from accelerometer (m/s)	$V_{i2\%}$ from gyroscope (m/s)
S2:3T5	3.15	0.1626	0.090
S2:3T6	3.27	0.1889	0.089

Table 6.3: Characteristic Impact Velocity-Upward movement- Unit2-Series 1/2

Test number	Stability number	$V_{i2\%}$ from accelerometer (m/s)	$V_{i2\%}$ from gyroscope (m/s)
S1:2T4	2.53	0.0570	0.0306
S2:3T5	3.15	0.0966	0.0665
S2:3T6	3.27	0.1109	0.0706

### 6.3.3. Downward movement with rundown

Similarly, exceedance probability for downward movements were plotted for both test series considering unit 1 and 2. Refer figure 6.14 and appendix D. Overall it can be observed that, impact velocities for the downward movement is lower compared with respective velocities obtained for the upward movement. But similar trends can be observed. Calculated characteristic impact velocities for unit 1 in downward movement are listed in table 6.4, 6.5 and 6.6.

Table 6.4: Characteristic Impact Velocity- downward movement- Unit1-Series 1/2-at the waterline

Test number	Stability number	$V_{i2\%}$ from accelerometer (m/s)	$V_{i2\%}$ from gyroscope (m/s)
S1:1T1	2.03	0.0382	0.0305
S1:1T2	2.32	0.0491	0.0360
S1:1T3	2.43	0.0585	0.0399
S1:2T4	2.53	0.1168	0.0907
S1:2T5	2.74	0.0458	0.0374
S2:2T4	3.15	0.0556	0.0394

Table 6.5: Characteristic Impact Velocity-downward movement- Unit1-Series 2- just below the waterline

Test number	Stability number	$V_{i2\%}$ from accelerometer (m/s)	$V_{i2\%}$ from gyroscope (m/s)
S2:3T5	3.15	0.1070	0.0719
S2:3T6	3.27	0.1156	0.0750

Table 6.6: Characteristic Impact Velocity-downward movement- Unit2-Series 1/2

Test number	Stability number	$V_{i2\%}$ from accelerometer (m/s)	$V_{i2\%}$ from gyroscope (m/s)
S1:2T4	2.53	0.0219	0.0197
S2:3T5	3.15	0.0713	0.0637
S2:3T6	3.27	0.0721	0.0608

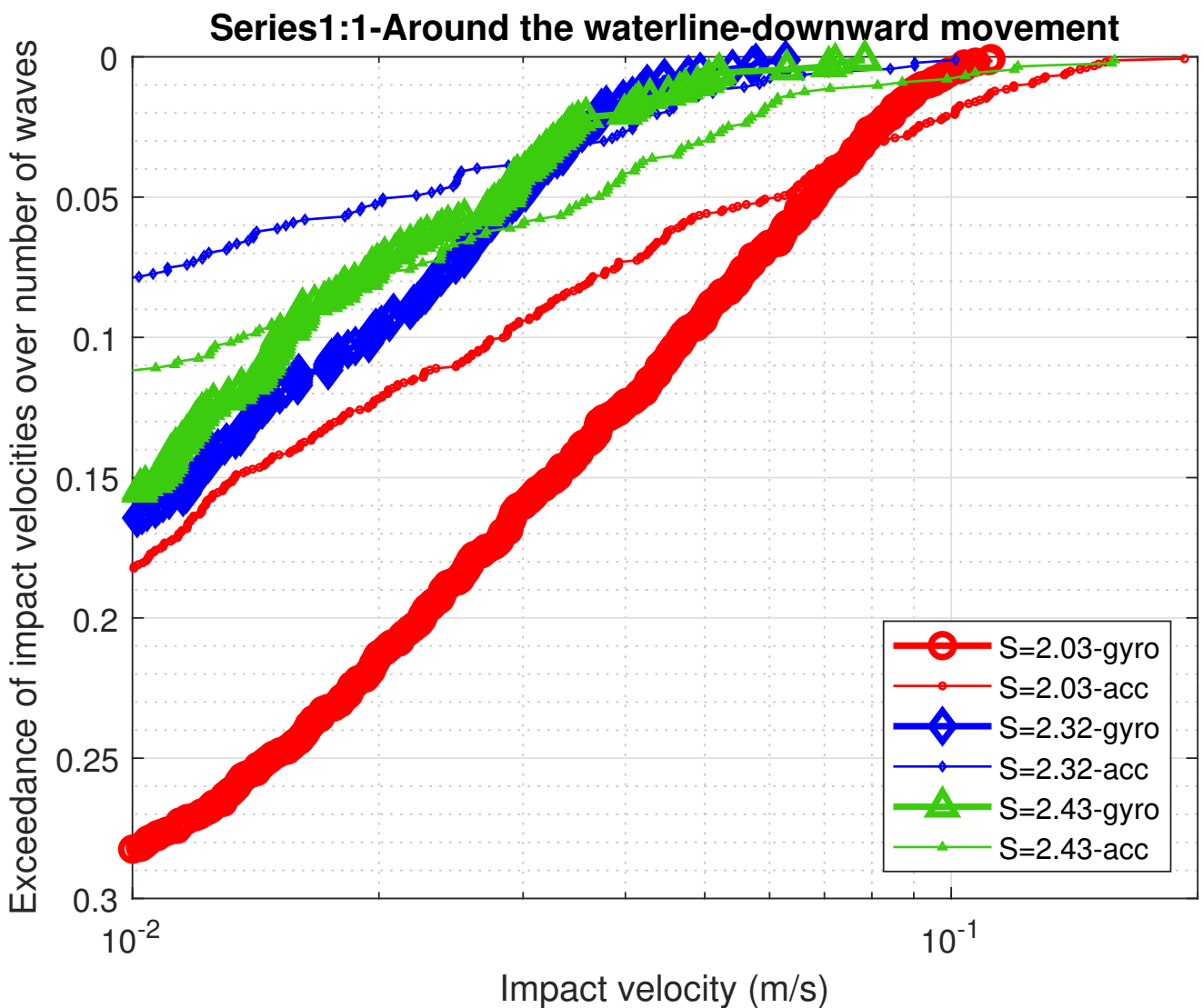


Figure 6.14: Exceedance probability in downward movement at the waterline for Unit 1- Test series 1:1

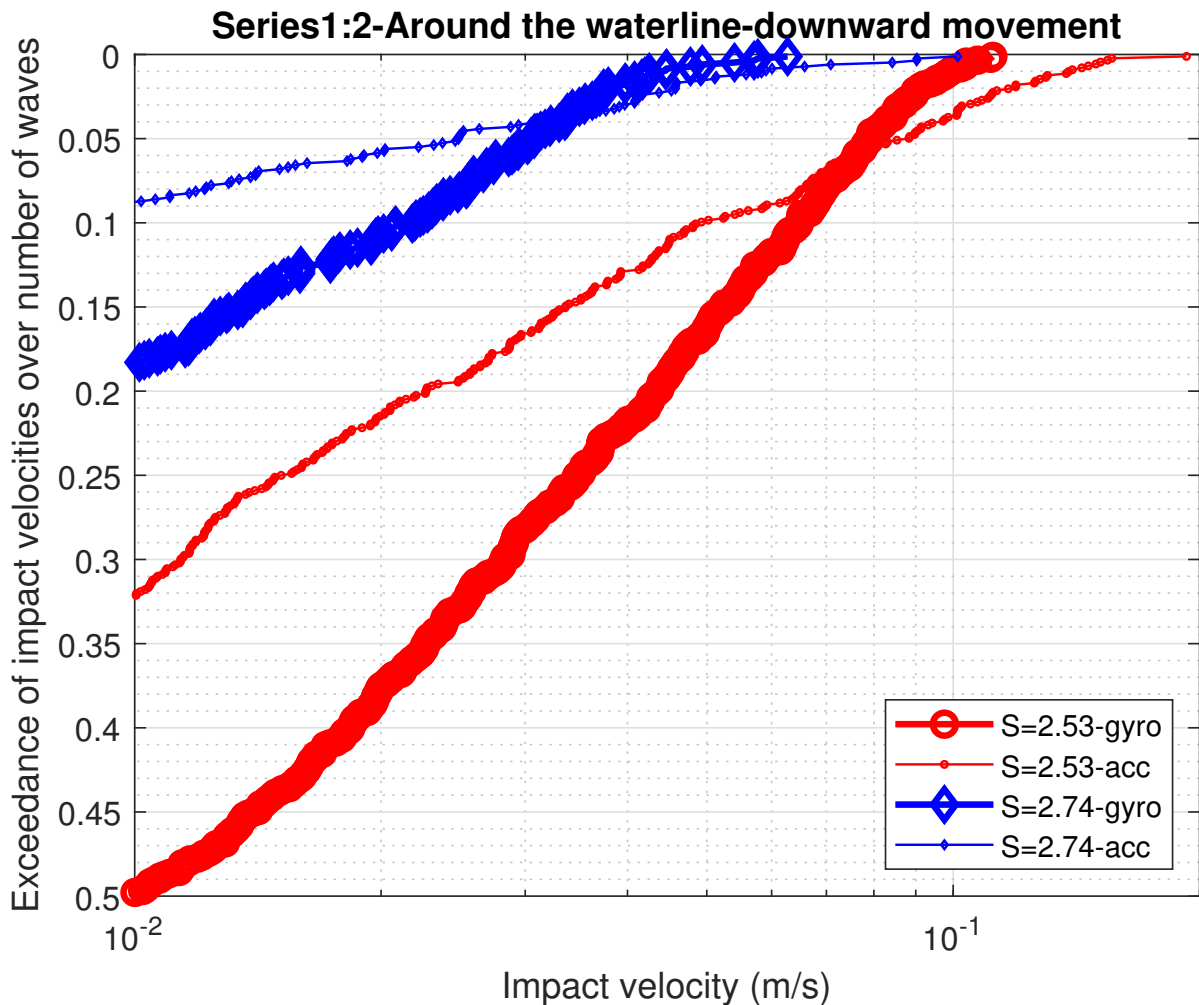


Figure 6.15: Exceedance probability in downward movement under the waterline for Unit 1- Test series 1:2

The figure 6.15 illustrates the impact velocities obtained for the downward movement just below the waterline. A comparison of upward and downward velocities is shown in figure 6.16, 6.17 and 6.18. Overall for both test series, an increase of the characteristic impact velocities can be observed with the stability number, but for the last test performed in the series 1 the trend is different. Even with the high stability number the impact velocity is low in that condition compared with the previous test condition. This may possibly caused by the increased stability due to interlocking, after unit finding its stable position. Further, gradual settlement of the rows above can also influence the amount of rocking.

By comparing test condition S1:2T4 for unit 1 and unit 2 (Table 6.2 and 6.3) it can be seen that there is a clear difference in characteristic impact velocities even at the same horizontal level (at the water level) of the slope. Therefore it is recommended to carry further research on this to find the dependence of the impact velocities on the horizontal position of the slope.

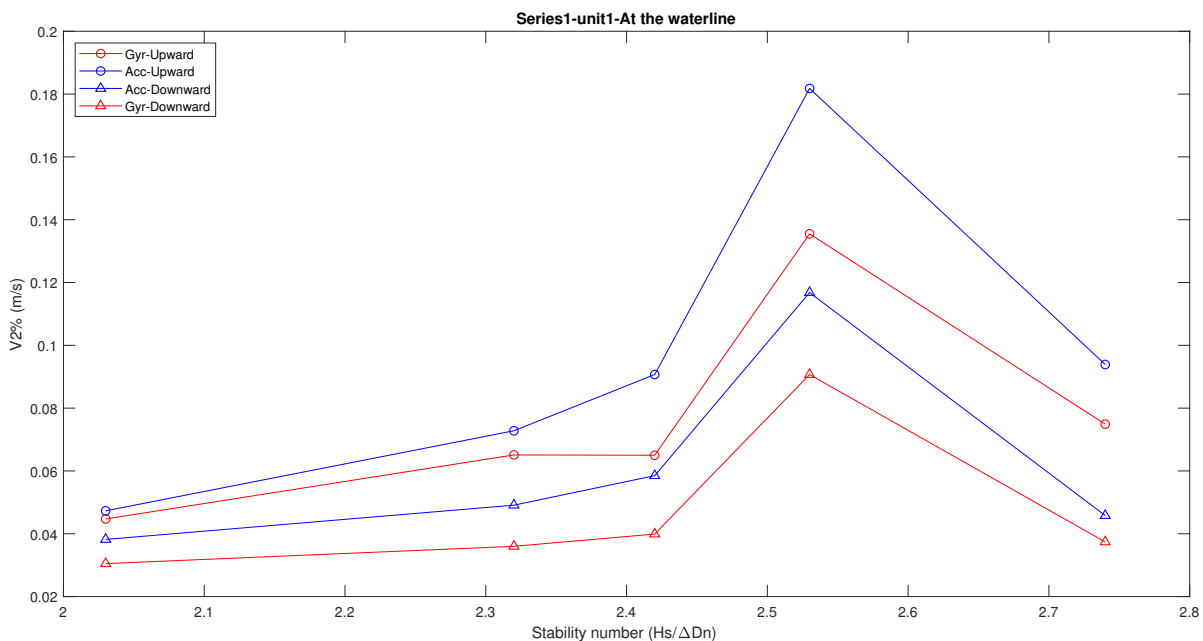


Figure 6.16: Comparison of characteristic impact velocities obtained at the waterline- Series 1

Moreover, the impact velocities resulted from the integration of the accelerometer data are larger than the impact velocities obtained from the peaks of the gyroscope data. This may be due to several uncertainties of the integration of accelerometer data. Also, significant motions were observed with unit 1 in which V90 class SD card was inserted (due to some practical issues with obtaining V30 class SD card when making the unit). Therefore, some random slowing downs can be observed with the data recorded with unit 1. Therefore, the impact velocities obtained from gyroscope are more trustworthy than the accelerometer. The possible reasons for the differences of impact velocities can be listed as follows.

- Random slowing down of the sampling frequency can result in data loss and this can influence in identification of the starting position of the movement. Correct identification of the starting position is important to start the integration of accelerometer data to find the impact velocity.
- Data loss due to random slowing down can also cause erroneous results in integration of gyroscope data.
- In this study, the accelerometer is not corrected for errors such as the misalignment error and cross axis effects. Correcting accelerometer data by taking all these errors would further increase the accuracy.
- As accelerometer data are too noisy, noise removal using more advanced filtering technique will result in higher accuracy.
- If the data are lost just before the start of the upward movement linear interpolation will result in the wrong interpretation for the start of the movement and can result in errors in integration.
- Having more than a single peak in accelerometer data during one rotation event can also result in overestimation of the impact velocity.
- Also the distance between rotation point and the impact location may be higher than the considered value for the calculation of the impact velocity from the gyroscope. (Further research is required)

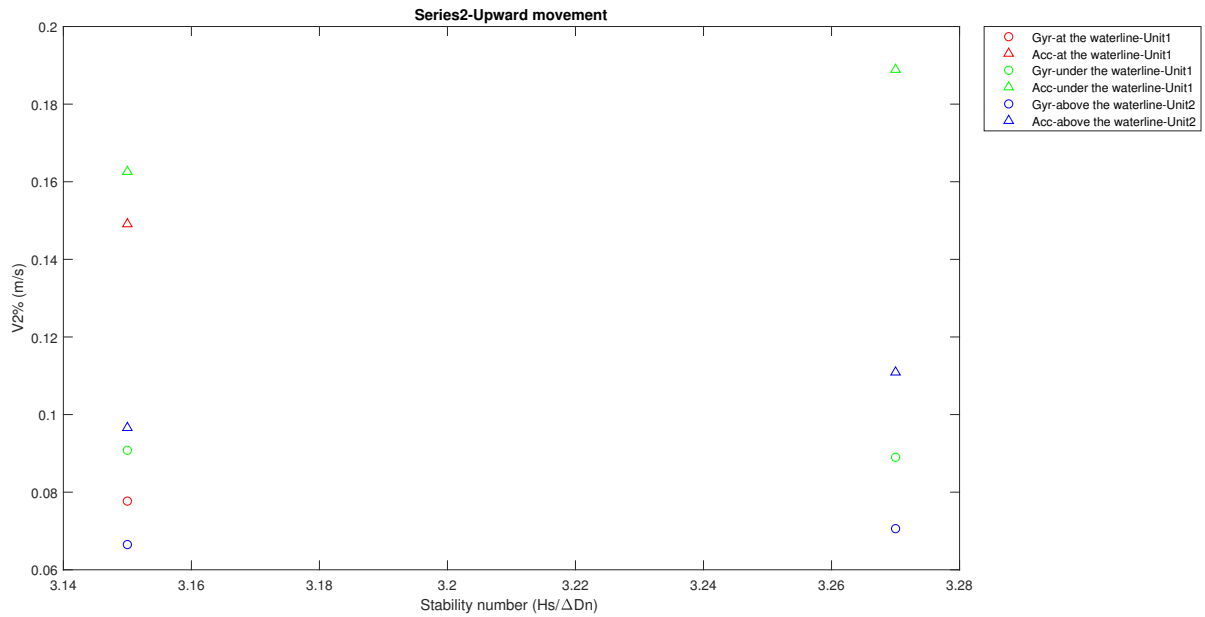


Figure 6.17: Comparison of characteristic impact velocities obtained at the waterline for upward movement -Test series2

By considering the observation from test series two (figure 6.17 and 6.18) it can be seen that the highest impact velocities are given after placing the unit below the water level. The impact velocities obtained for the unit which was placed above the water level has given lowest magnitude. Hence, it can be concluded that highest impact velocities can be obtained under the water level.

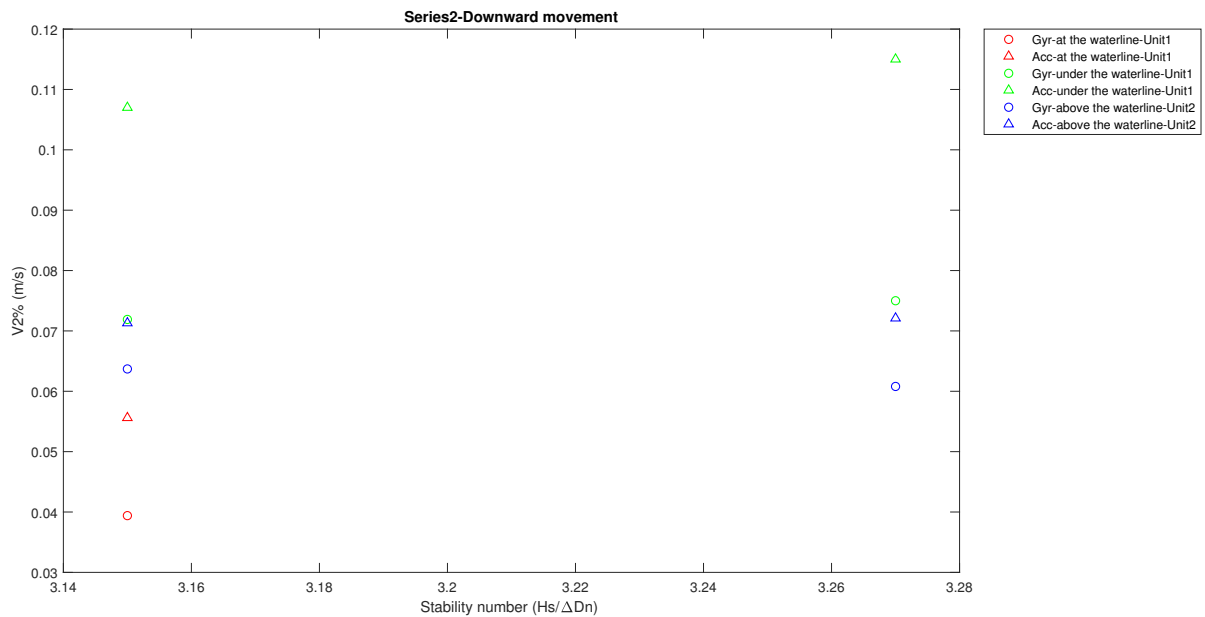


Figure 6.18: Comparison of characteristic impact velocities obtained at the waterline for downward movement- Test series 2

#### 6.3.4. Number of collisions

The number of collisions is presented in figure 6.19 in dimensionless manner. In the X axis the stability number is presented and in the Y axis the number of collision over number of waves are presented. The number of collisions were calculated based on the data obtained from the gyroscope considering both upward and downward movement as a one event.

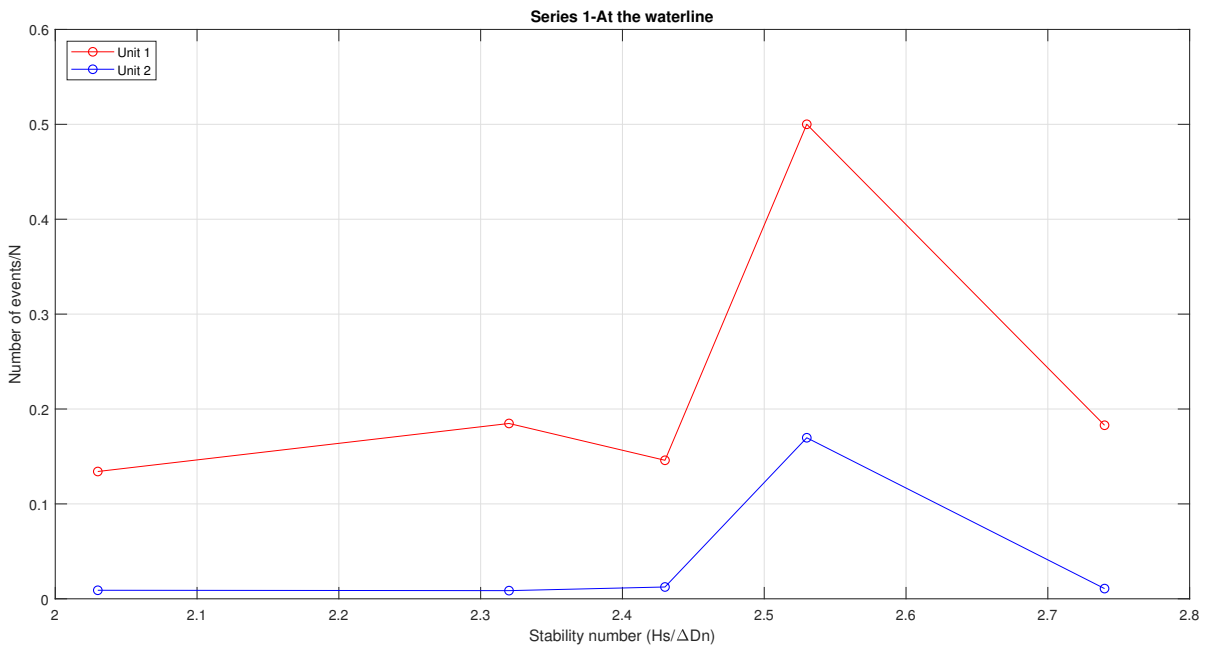


Figure 6.19: Comparison of number of collisions for test series 1

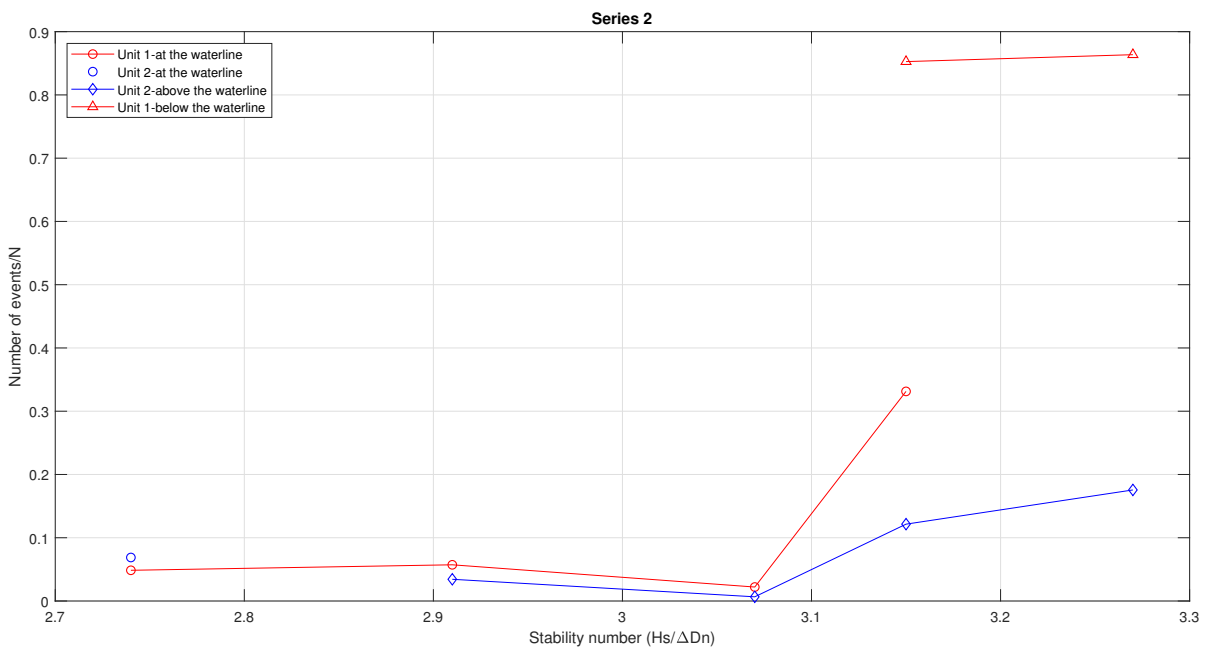


Figure 6.20: Comparison of number of collisions for test series 2

From figure 6.19 it can be observed that, several factors can affect the number of collisions and it does not rely on stability number only. In the test series 1, first two tests show some increase of number of collisions by increasing the stability number, but in the test three that trend can not be observed as before. Generally, after rocking for few minutes the units tend to find its stable position and no rocking can be observed after. A clear increase of the movements can be observed in both series in the test 4, after increasing the spacing around the waterline (figure 6.19 and 6.20). Therefore, it can be concluded that, both interlocking effect and the pressure of the rows above can influence the rocking motion of single layer armour units considerably.

Further, figure 6.19 illustrates that there is a clear difference in number of collisions in unit 1 and unit

2 even though they were placed on the same horizontal row. However, they have a similar trend.

Figure 6.20 shows comparison of number of collisions obtained for the test series two when the unit 1 is at the waterline and after placing it just below the waterline and when unit 2 is at the waterline and above the water line. A clear increase of the number of collisions can be observed just below the waterline. Also similar to the test series one, an increasing trend of number of collisions can be identified with unit 1 after increasing the spacing around waterline.

# 7

## Discussion and Conclusions

This study was performed to understand the rocking behaviour of the single layer armour units based on Xblocs, using the previously proposed novel stand alone measurement technique and to evaluate the effectiveness of the technique to detect the rocking motion of single layer armour units.

To fulfill the intended objectives, firstly a proper literature study was carried out. Secondly, the previously proposed state of the art measurement technique was further developed by increasing the sampling frequency from about 25 Hz to 100 Hz. Then, two instrumented Xbloc units were developed with embedded sensors and 2D physical model testings were performed. Finally, the data were analyzed and important conclusions were drawn. This chapter focuses on these conclusions.

### 7.1. Measurement and processing technique

The standalone method with no wire attached gives the unit full flexibility of movement during the experiment. Previously conducted researches with the same technique but with lower sampling frequency showed that technique is suitable to detect motions but further improvements might need to capture the full rotational motion. Because, with about 25 Hz sampling frequency, each peak value was given with just a single data point .

After performing the testings and collecting the data with 100 Hz frequency it was observed that the motions are well captured with the given sampling frequency and rocking event can be resolved in time with 5-10 data points. The data analysis of this study shows that now it is possible to interpret the complete rocking motion with both upward and downward movements clearly with the proposed technique. Also, it is verified that the proposed technique is very promising to detect the motions that are hard to observe visually while performing the model testings. Therefore it can be concluded that 100 Hz sampling frequency is enough to capture the motion just before the impact. Further, with the minimum error corrections for the sensors still the results are promising and has the same order of magnitude as previously conducted research of CUR70 (1989). As there are very limited studies on the behaviour of rocking motion of single layer armour units this research will be good starting point and paved the way to many opportunities of future researches.

### 7.2. Order of magnitude of Impact velocity

Comparing the characteristic impact velocities obtained for upward and downward movements, it can be concluded that both are in the similar order of magnitudes. But relatively higher velocities are observed with upward movement along the slope. This may due to reduction of downward flow velocity due to the friction. Also this is inline with the observations of the research by [Le \(2016\)](#). Also, it can be concluded that the magnitude of the characteristic impact velocity and number of collisions are not solely depend on the wave height or the stability number, as same order of magnitude of the impact

velocities and number of collisions can be observed with the smaller waves if the interlocking is less effective. Therefore it can be concluded for the single layer armour units, interlocking effect can significantly influence the magnitude of the impact velocity.

Further, it was observed during the testings, the first settlement can also significantly affect the amount of rocking. Mainly the settlement of top rows towards the bottom exert additional pressure on the below rows and hence stability due to interlocking increases consequently. Therefore, it can be concluded that the amount of settlement also influences the amount of rocking.

### 7.3. Difference with respect to unit position on the slope

By comparison of the test numbers S2:2 T4, S2:3 T5S2:3 T6 it can be concluded that the vertical position of the unit in the slope can influence the both impact velocity and the number of collision. After placing the unit just under the waterline, a clear increase in number of collisions can be observed. An increase of the characteristic impact velocity also observed. This is also inline with the observations from [Le \(2016\)](#) and [Arefin \(2017\)](#). However, after placing the units at the waterline, below the waterline and above the water line, the lowest impact velocities were observed with unit placed above the water line. Not only that but also after comparing the data of test S1:2 T4 it was observed that the horizontal position of the unit on the slope also affects the amount of rocking and magnitude of the impact velocity.

### 7.4. Number of collisions

During this research the number of collisions is analyzed for varying wave height, and position on the slope. Similar to the characteristic impact velocity, the stability number was found as not the only parameter that governs the number of collisions. Hence, it can be concluded that pressure from the upper rows and the interlocking effect has significant influence on number of collisions.

### 7.5. Amount of rotation during the rocking motion

By analyzing the angular velocity data around the axis where the largest impact velocities were recorded, it can be concluded that the rocking unit with significant motions comes to its original position after the full rotation. And the rotation around the aforementioned axis varies between 5 degrees to 10 degrees. Moreover, no pure translations were observed.

### 7.6. Impact velocity from gyroscope and the accelerometer

During the data analysis it was observed that angular velocity data from the gyroscope has a less noise level than the accelerometer. However, in most of the test conditions peaks of the acceleration signals were observed with peaks of the gyroscope. Therefore, from both observations impact velocity was calculated. But as the calculation of the impact velocity from the accelerometer requires integration and some error accumulation can be expected.

However, after correcting the measured accelerometer data and transforming it back to the initial reference frame, linear acceleration required to integration was obtained. After integration of the linear acceleration components, the obtained impact velocities have some higher values compared with the gyroscope measurements. But as these high values have lower probability, the characteristic impact velocities calculated from the both measurements are in more or less same order of magnitude, but still the values obtained from accelerometer integration have relatively higher characteristic impact velocity value compared with gyroscope.

Nevertheless, it is recommended to use the impact velocity given from the gyroscope because the higher value given from the accelerometer integration can be due to some error accumulations.

# 8

## Recommendations

This section presents the recommendations based on the work performed and the future opportunities will also be discussed.

### 8.1. Data Processing

#### 8.1.1. Frame of reference

In the current study linear acceleration data was calculated with respect to the initial frame of reference which was assumed as the orientation of the unit just before start of the upward movement. Instead in the future researches a global reference frame can be defined along the slope of the structure and orientation of the armour units can be estimated with respect to the global reference frame before start of the test and after the test. But this may require to integrate the angular velocity measurements for long time and suitable filtering techniques should be adopted to minimize the drifting errors.

#### 8.1.2. Rotation angle of the unit during the rocking

In this study maximum rotation angle and axis around which the unit rotates while rocking was obtained considering the axis with largest angular velocities only. But future researches can be performed to evaluate the resulting angle of rotation and dominant axis of rotation considering all three simultaneous rotations around the x,y, and z axes. Also upward and downward motions can be then separated using the sign convention of the resulting angular data.

#### 8.1.3. Corrections of the sensor

For the current study the sensor was not corrected for the cross axis effects and the misalignment error. Future researches can be done after accounting these corrections and applying advance filtering techniques.

#### 8.1.4. Minimizing the slowing down of the sensor

During the current research it was identified the random slowing downs can be minimized by using a class V30 sd card. Also further improvements can be achieved by using a processor with higher memory capacity (eg: Tinyzero), so that with the higher buffer limit more data can be collected and written to the sd card at once.

#### 8.1.5. Improving the method of integration of accelerometer data

The method adopted during this study to integrate the accelerometer data resulted in higher impact velocities. Hence, the method can be further improved to get more accurate value for the impact velocity calculation.

#### 8.1.6. Distance between point of rotation and location of impact

To calculate the impact velocity from gyroscope data distance between point of rotation and location of impact was assumed as half of the unit height. But further researches should be performed to validate

or update this.

## **8.2. Use of the proposed technique**

### **8.2.1. Impact velocity of single layer armour units**

In this research the main objective was determine the order of magnitude of the impact velocities while showing the effectiveness of the technique to detect the rocking motion. Hence, some changes were implemented during the testings in order to obtain the sufficient rocking motion with fairly large Xbloc units. Therefore, calculated impact velocities for some tests may represent the extreme end. Therefore, future research can be performed to determine the impact velocity, number of collisions, and its spacial and stochastic variation under the correct design conditions and without disturbing the natural interlocking pattern.

### **8.2.2. Synchronize the wave data with the measurements**

The current research was performed without synchronizing the wave data with rocking measurements. Future research can be done after synchronizing the wave data with the rocking measurements to identify the exact wave conditions that causes the motions.

### **8.2.3. Translation and settlement**

In this study no pure translation were observed. But further researches are recommended to verify the conclusion. Also the proposed technique can be effectively use in determining the amount of settlement and impact velocity caused by the settlement events in the future studies.



## Input and output wave conditions

Table A.1: Test conditions for unit 1-Day 1

Test number Day 1-Unit 1	Hs /(cm) input	Hs/(cm) output	Tp/(s) input	mean Tp/(s) output	Stability number	Unit Position
S1:1 T1	11.5	10.63	1.30	1.35	2.03	Water level
S1:1 T2	13.0	12.15	1.39	1.42	2.32	Water level
S1:1 T3	13.8	12.72	1.43	1.49	2.43	Water level
S1:2 T4	14.4	13.24	1.46	1.49	2.53	Water level
S1:2 T5	15.5	14.35	1.51	1.58	3.15	Water level

The different series (S1:1 and S1:2 ) refers to the situations before and after increasing the space around the unit.

Table A.2: Test conditions for unit 2-Day 1

Test number Day 1-Unit 2	Hs /(cm) input	Hs/(cm) output	Tp/(s) input	mean Tp/(s) output	Stability number	Unit Position
S1:1 T1	11.5	10.63	1.30	1.35	2.03	Water level
S1:1 T2	13.0	12.15	1.39	1.42	2.32	Water level
S1:1 T3	13.8	12.72	1.43	1.49	2.43	Water level
S1:2 T4	14.4	13.24	1.46	1.49	2.53	Water level
S1:2 T5	15.5	14.35	1.51	1.58	2.74	Water level

Table A.3: Test conditions for unit 1-Day 2

Test number Day 2-Unit 1	Hs /(cm) input	Hs/(cm) output	Tp/(s) input	mean Tp/(s) output	Stability number	Unit Position
S2:1 T1	15.5	14.35	1.51	1.58	2.74	Water level
S2:1 T2	16.5	15.25	1.63	1.62	2.91	Water level
S2:1 T3	17.5	16.12	1.67	1.72	3.07	Water level
S2:2 T4	18.0	16.54	1.70	1.72	3.15	Water level
S2:3 T5	18.0	16.54	1.70	1.72	3.15	under the Water level
S2:3 T6	19.0	17.13	1.74	1.78	3.27	under the Water level

Table A.4: Test conditions for unit 2-Day 2

Test number Day 2-Unit 1	Hs /(cm) input	Hs/(cm) output	Tp/(s) input	mean Tp/(s) output	Stability number	Unit Position
S2:1 T1	15.5	14.35	1.51	1.58	2.74	Water level
S2:2 T2	16.5	15.25	1.63	1.62	2.91	above the Water level
S2:2 T3	17.5	16.12	1.67	1.72	3.07	above the Water level
S2:3 T4	18.0	16.54	1.70	1.72	3.15	above the Water level
S2:3 T5	18.0	16.54	1.70	1.72	3.15	above the Water level
S2:3 T6	19.0	17.13	1.74	1.78	3.27	above the Water level

# B

## Photos taken during the model testing

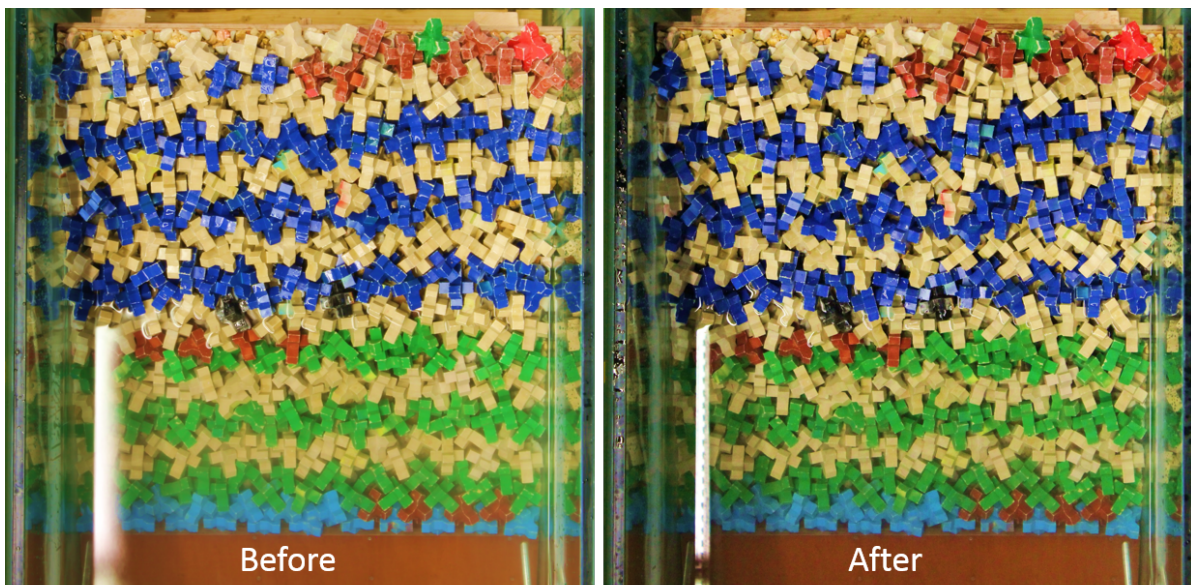


Figure B.1: Top view before and after the test  $H_s/\Delta D_n = 2.03$ - series 1:1

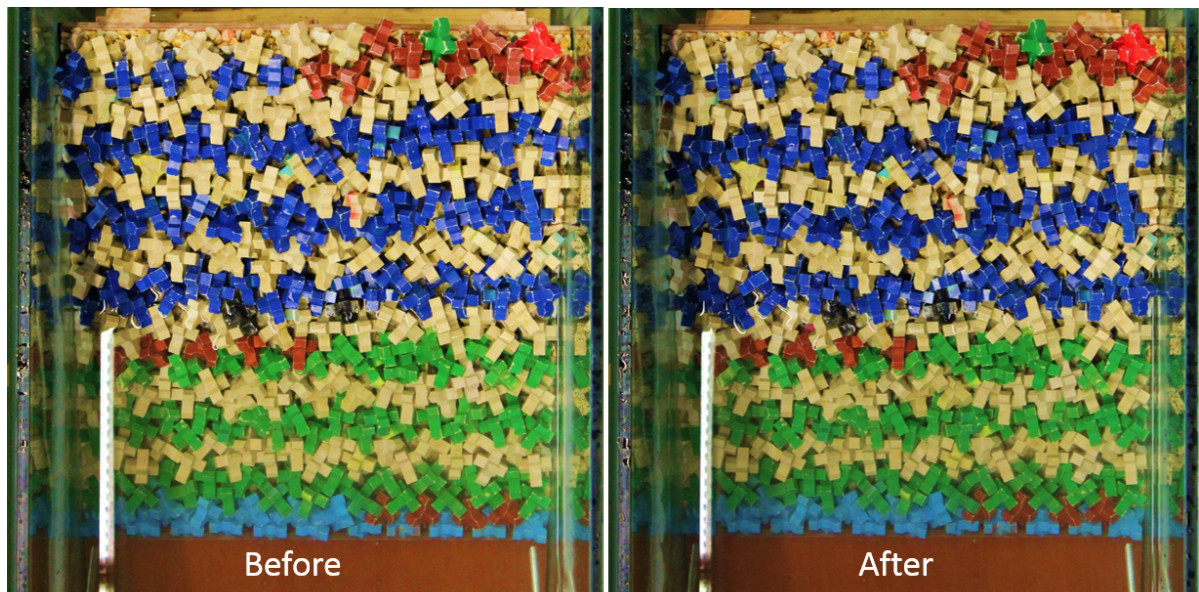


Figure B.2: Top view before and after the test  $H_s/\Delta D_n = 2.32$ - series 1:1

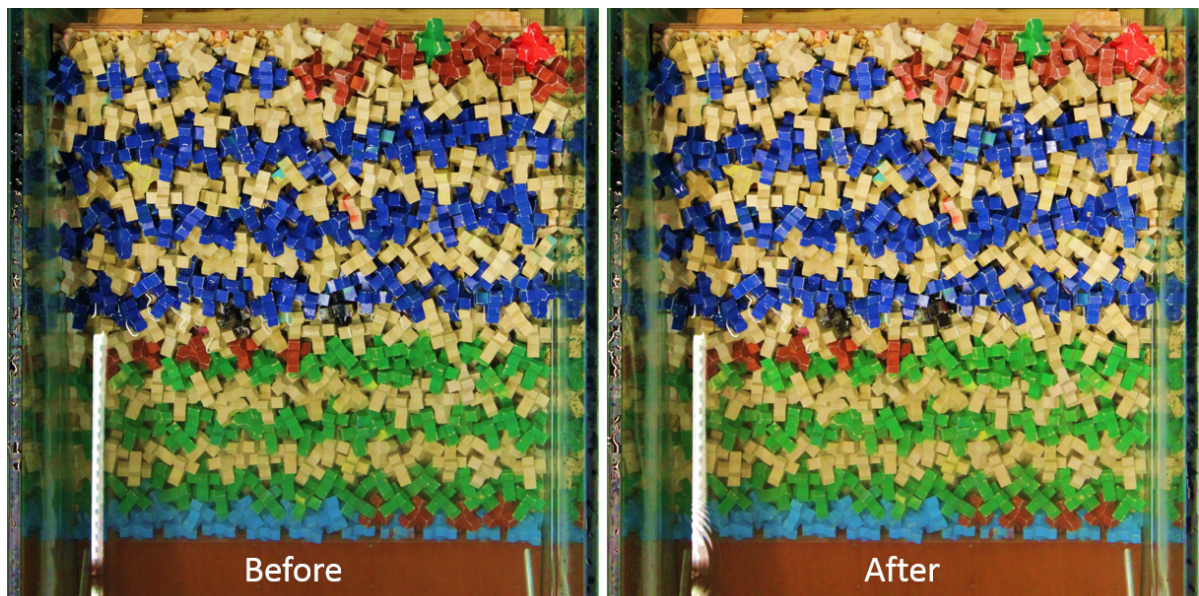


Figure B.3: Top view before and after the test  $H_s/\Delta D_n = 2.43$ - series 1:1

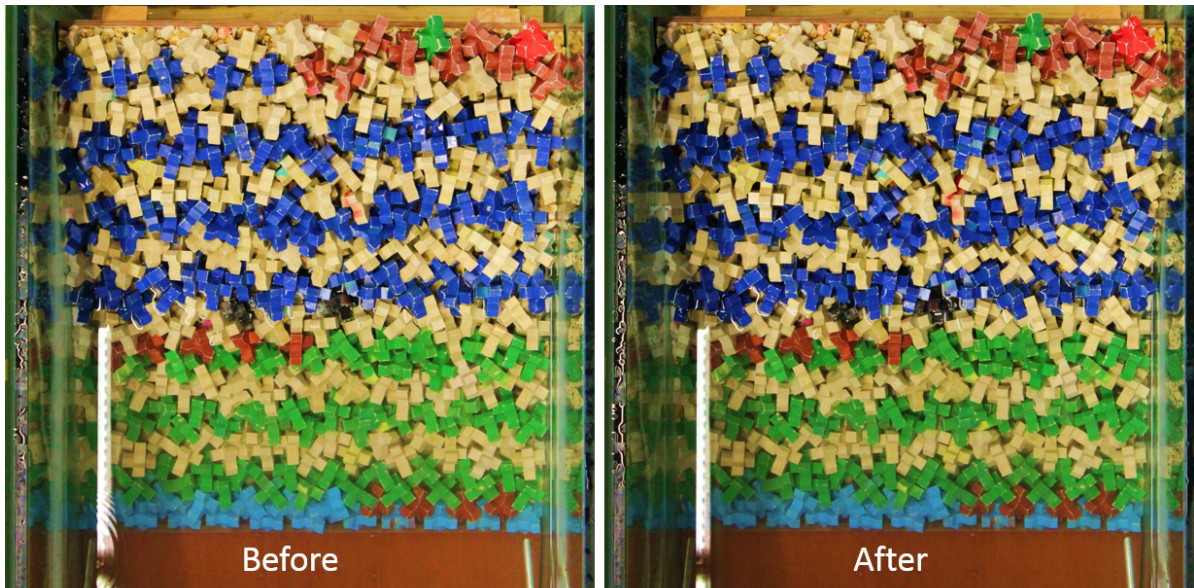


Figure B.4: Top view before and after the test  $H_s/\Delta D_n = 2.53$ - series 1:2

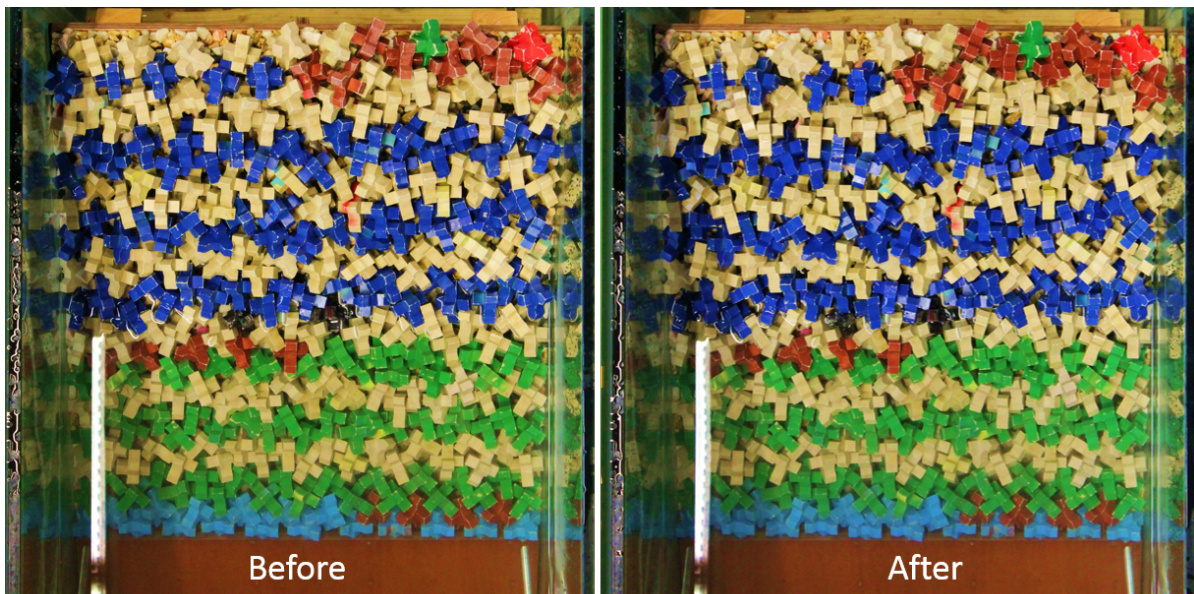


Figure B.5: Top view before and after the test  $H_s/\Delta D_n = 2.74$ - series 1:2

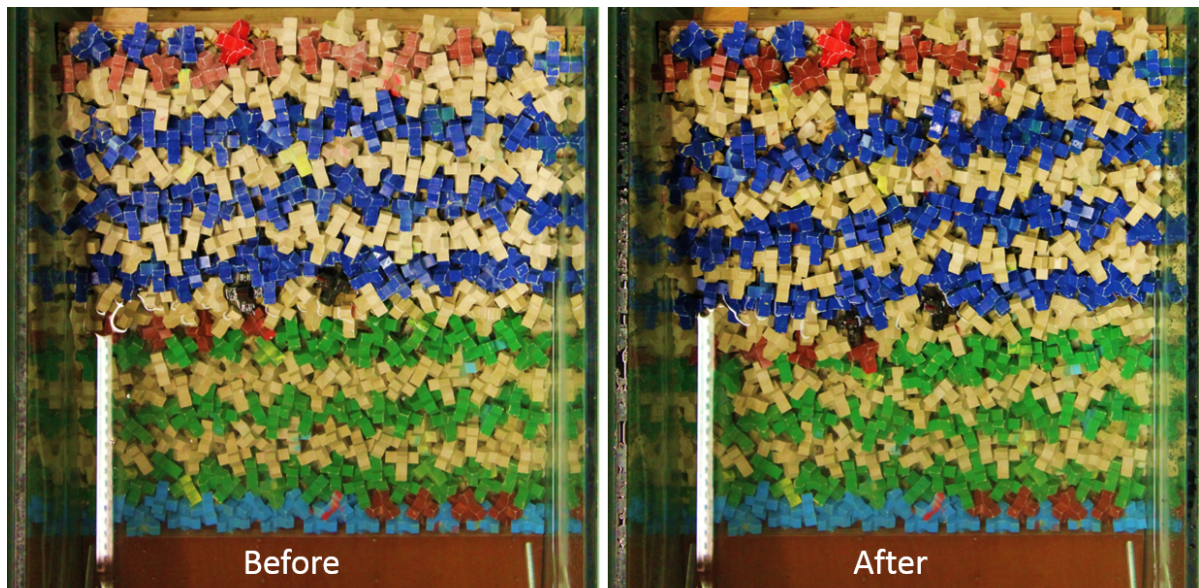


Figure B.6: Top view before and after the test  $H_s/\Delta D_n = 2.74$ - series 2:1

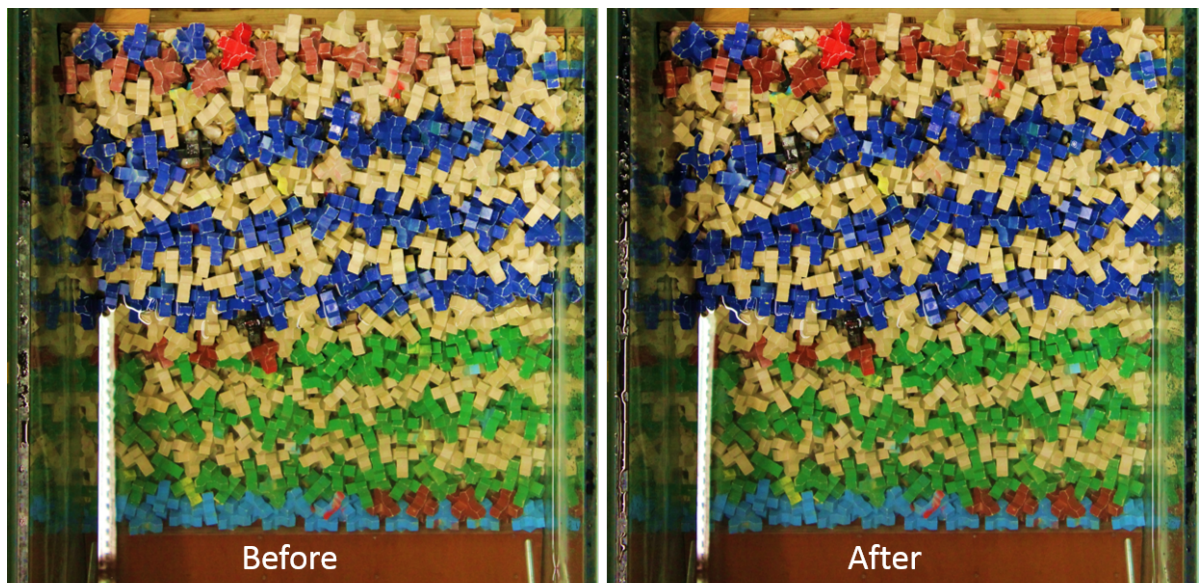


Figure B.7: Top view before and after the test  $H_s/\Delta D_n = 2.91$ - series 2:1/2

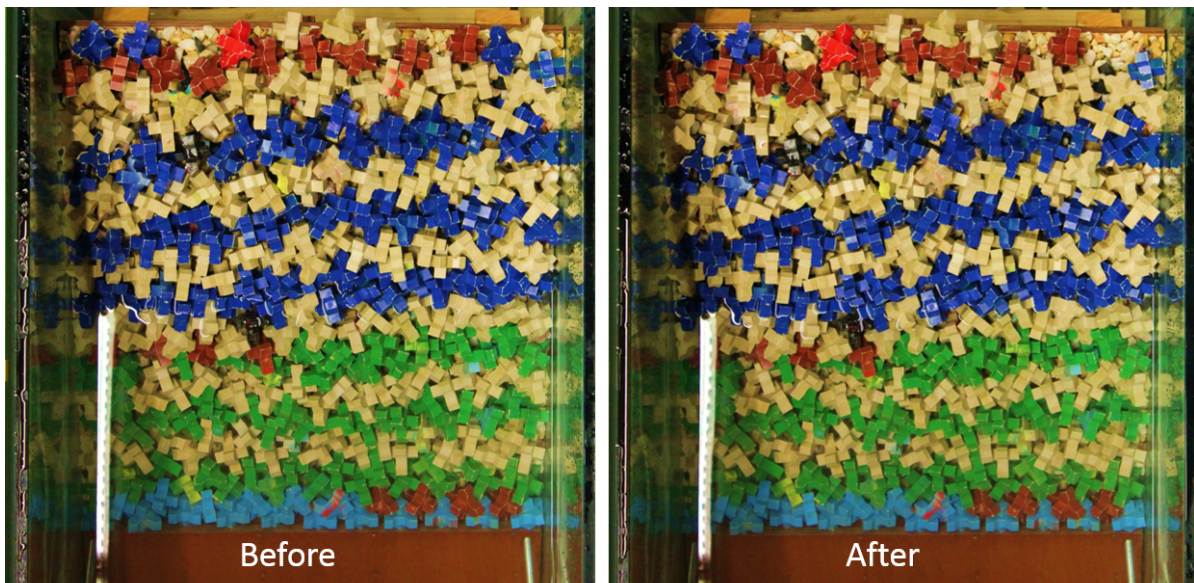


Figure B.8: Top view before and after the test  $H_s/\Delta D_n = 3.07$ - series 2:1/2

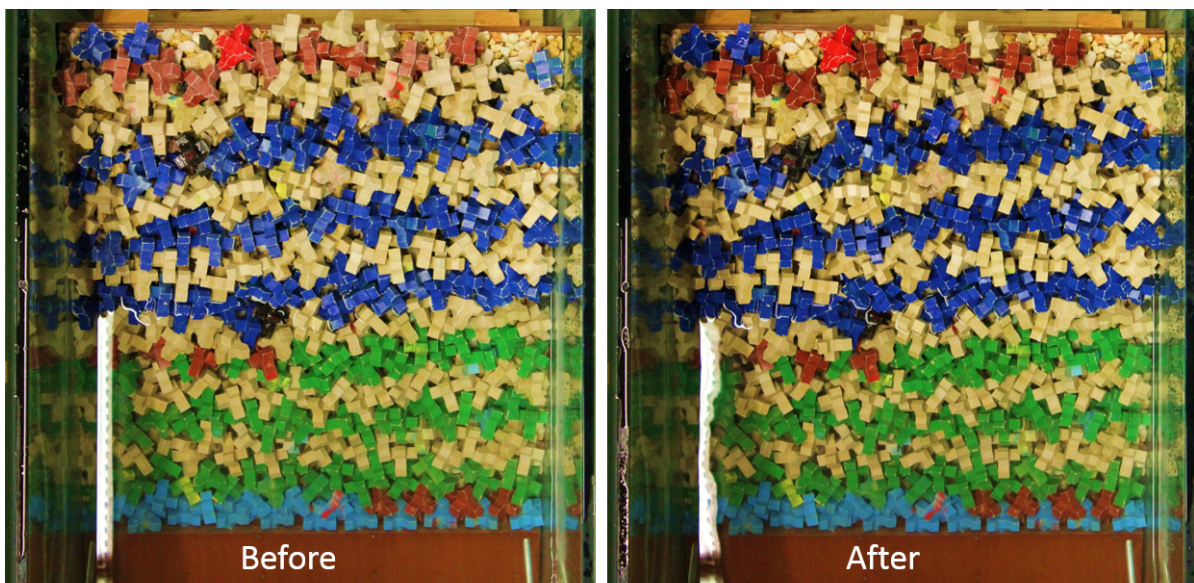


Figure B.9: Top view before and after the test  $H_s/\Delta D_n = 3.15$ - series 2:2/3

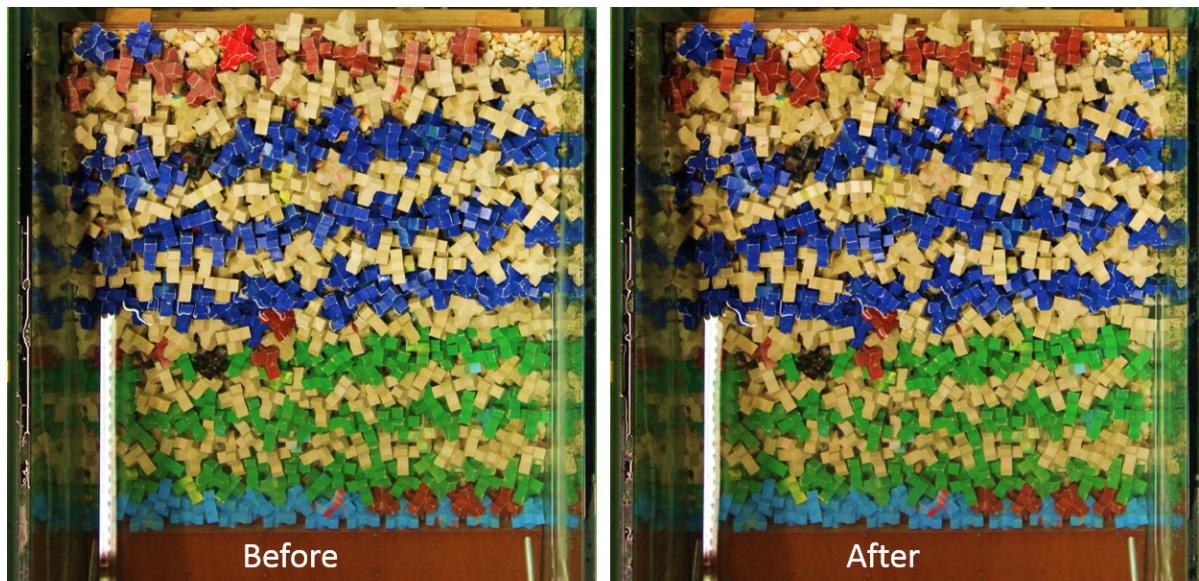


Figure B.10: Top view before and after the test  $H_s/\Delta D_n = 3.15$ - series 2:3

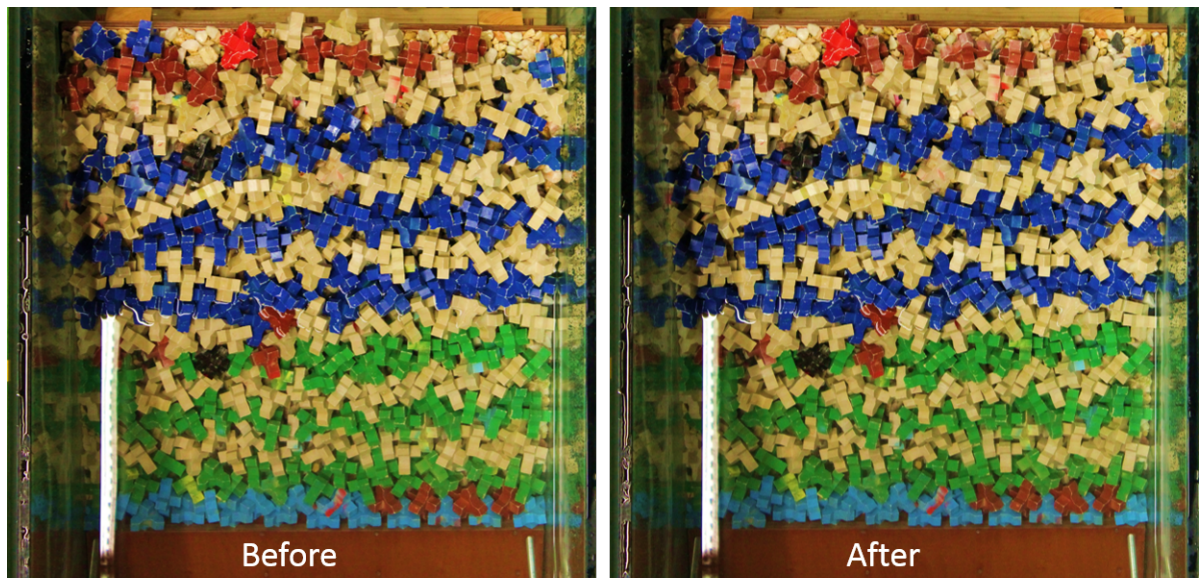


Figure B.11: Top view before and after the test  $H_s/\Delta D_n = 3.27$ - series 2:3



# Analyzing the data during the impact

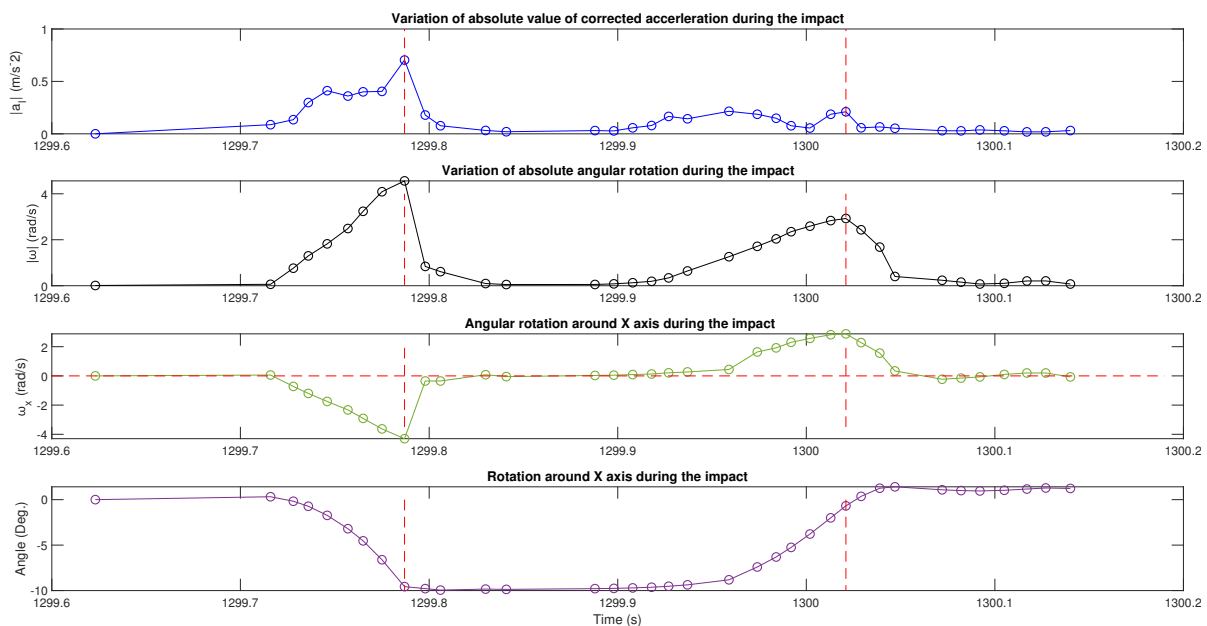


Figure C.1: Behaviour of motion during the impact 3-unit 1-  $H_s/\Delta D_n = 3.15$ - series 2:3

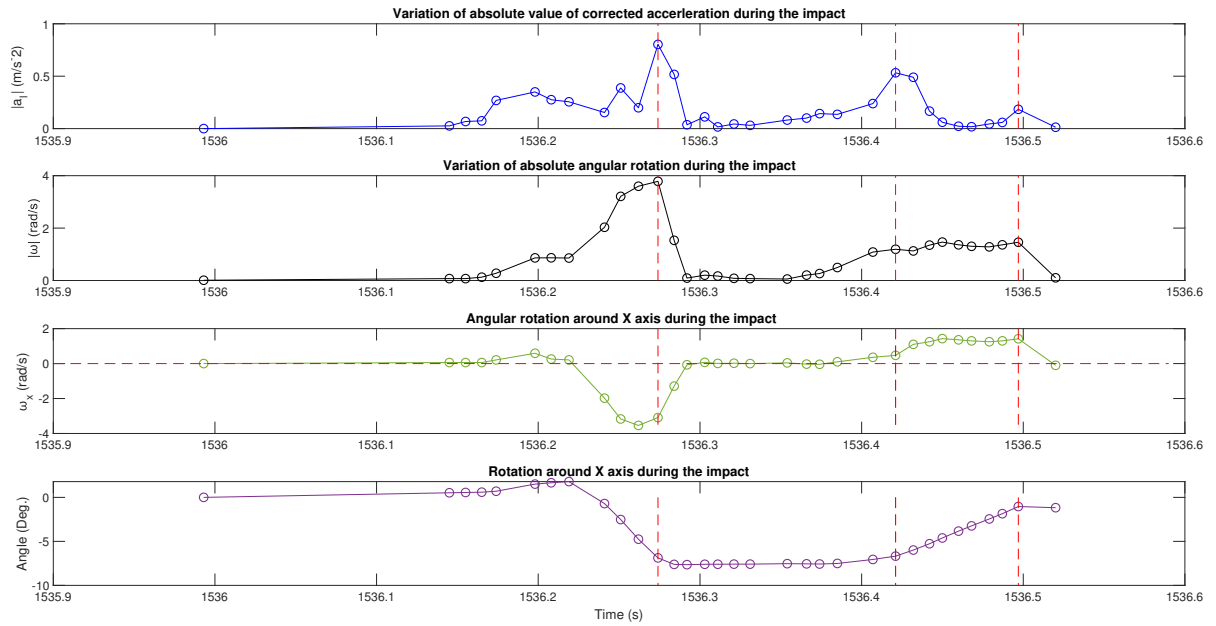


Figure C.2: Behaviour of motion during the impact 2-unit 1-  $H_s/\Delta D_n = 3.15$ - series 2:3

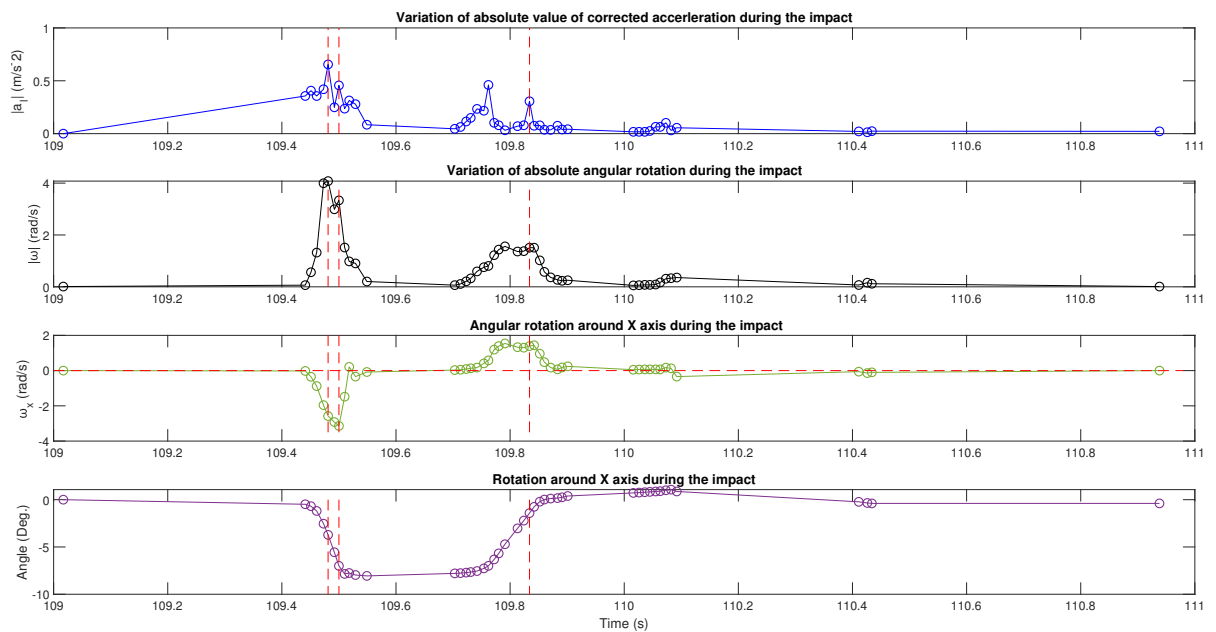


Figure C.3: Behaviour of motion during the impact 1-unit 1-  $H_s/\Delta D_n = 3.15$ - series 2:3

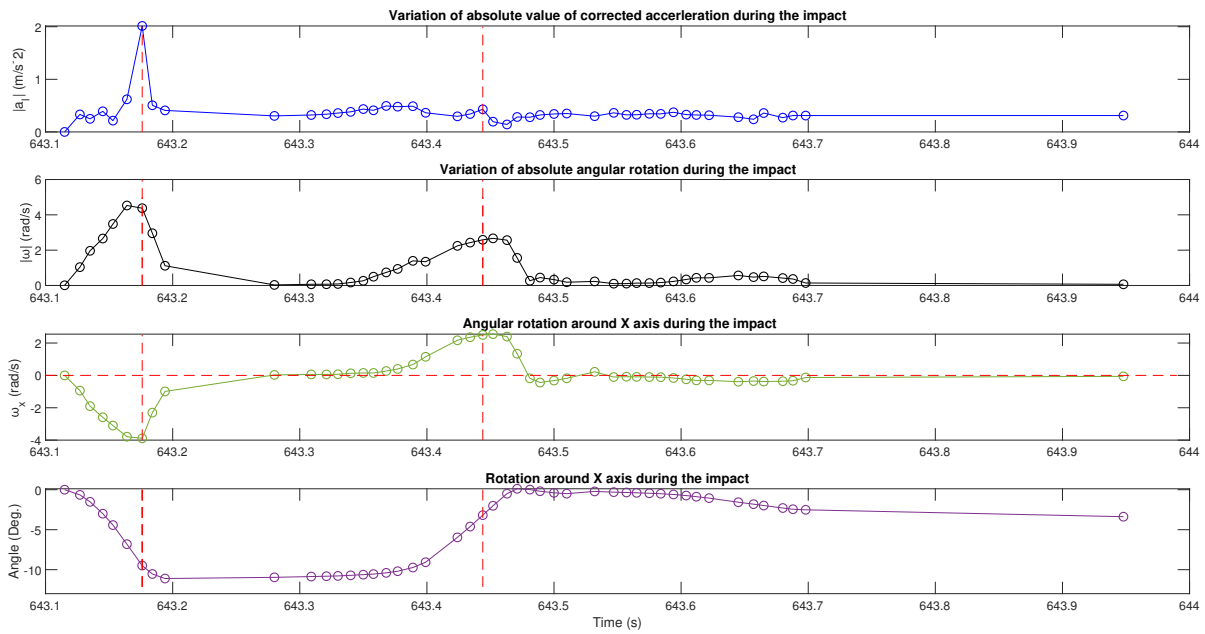


Figure C.4: Behaviour of motion during the impact 1-unit 1-  $H_s/\Delta D_n = 3.27$ - series 2:3

# D

## Probability of exceedance of impact velocities before collision

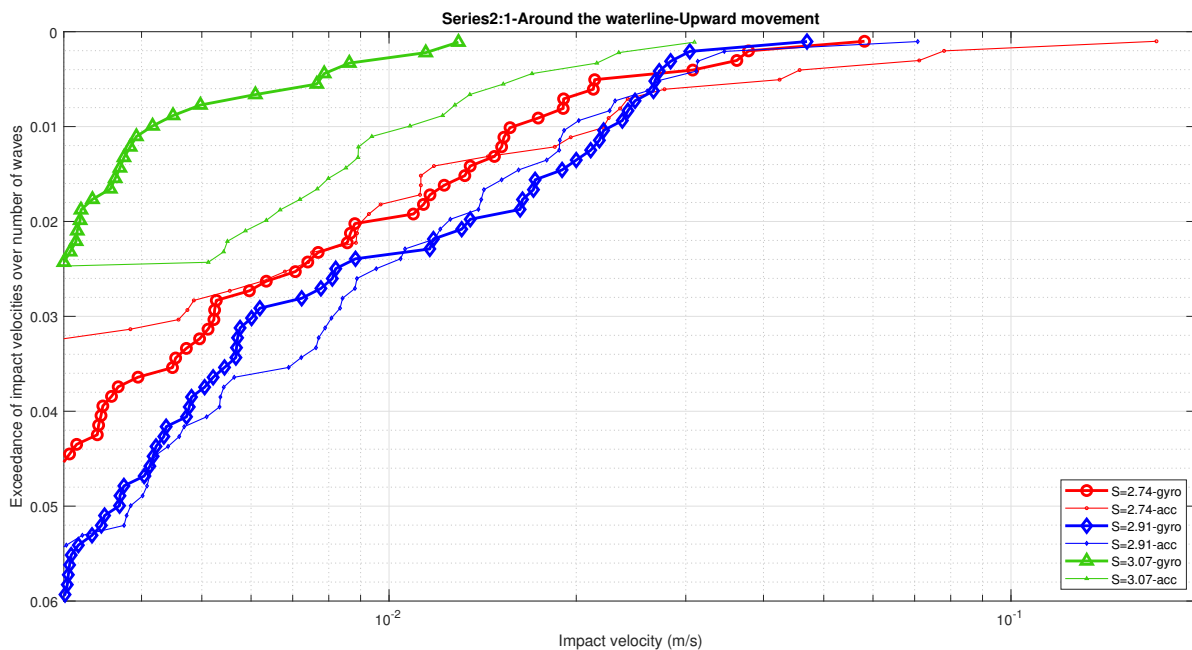


Figure D.1: Exceedance probability in upward movement at waterline for Unit 1- series 2:1

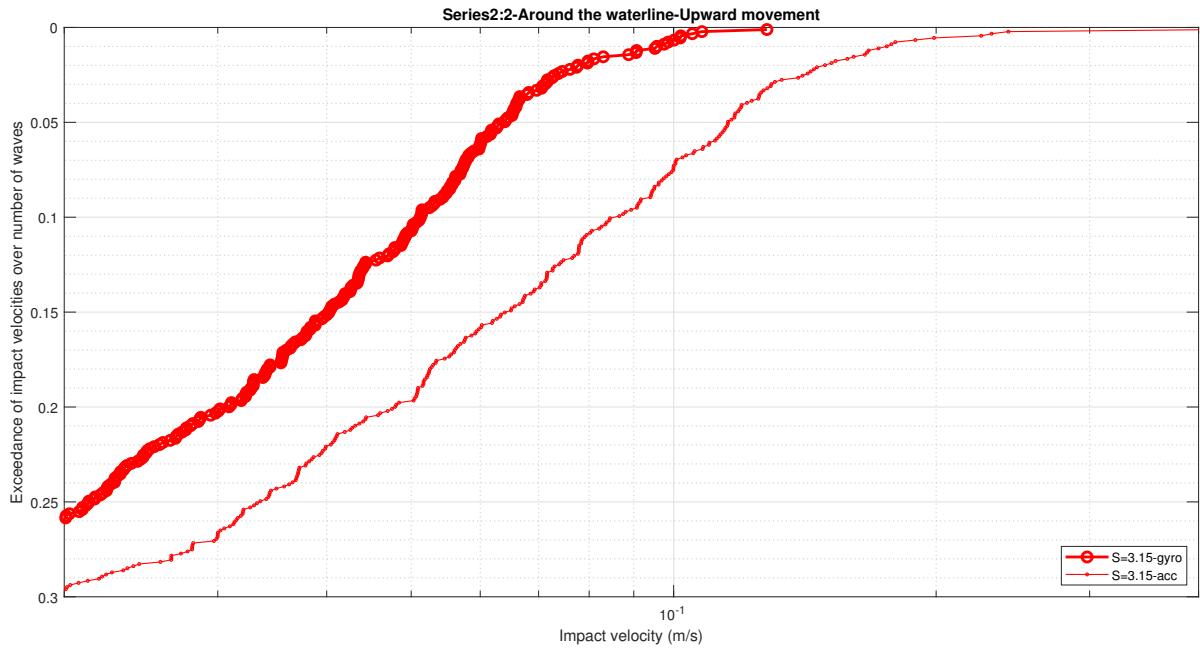


Figure D.2: Exceedance probability in upward movement at waterline for Unit 1- series 2:2

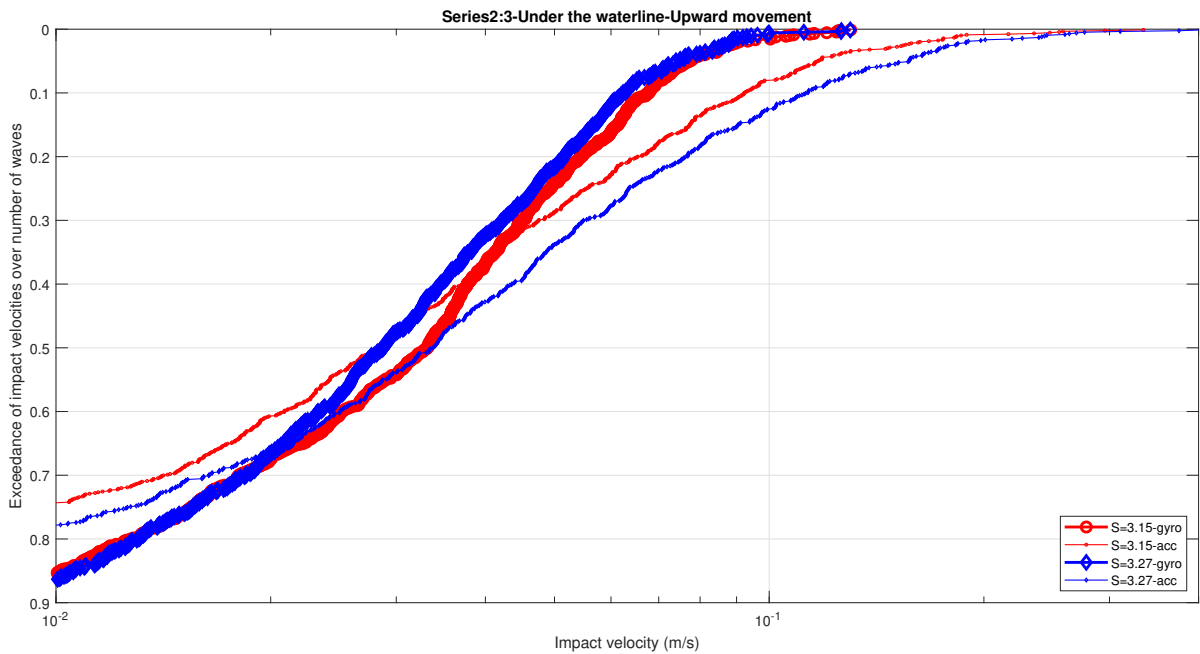


Figure D.3: Exceedance probability in upward movement under the waterline for Unit 1- series 2:3

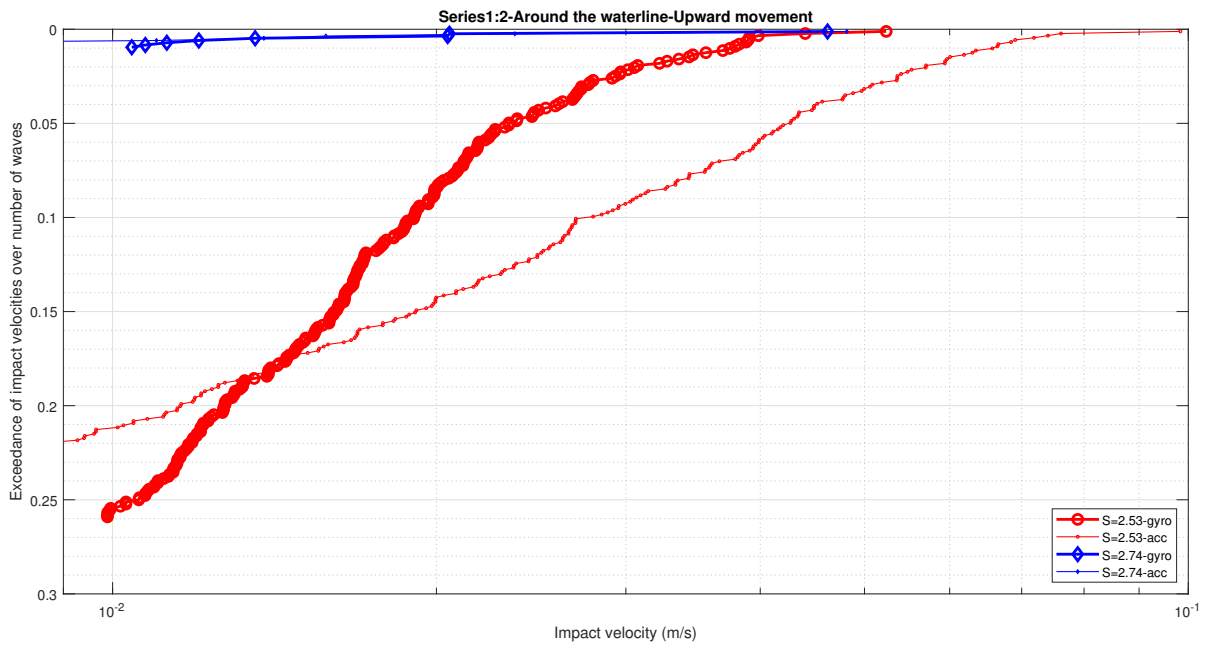


Figure D.4: Exceedance probability in upward movement at waterline for Unit 2- series 1:2

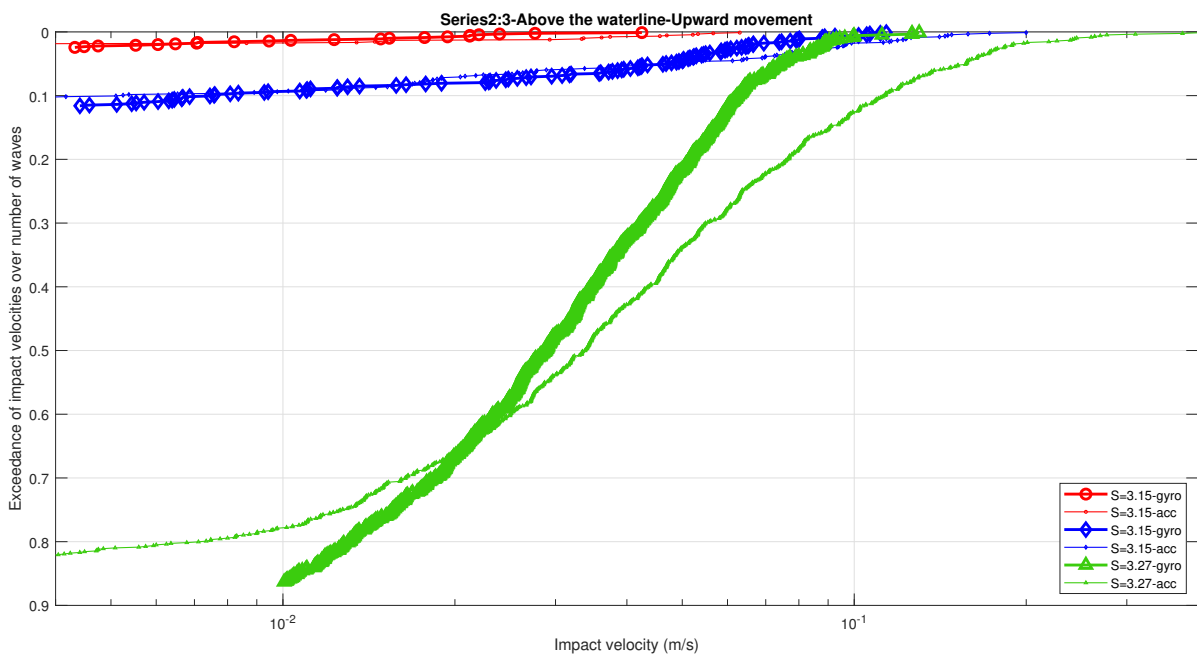


Figure D.5: Exceedance probability in upward movement above the waterline for Unit 2- series 2:3

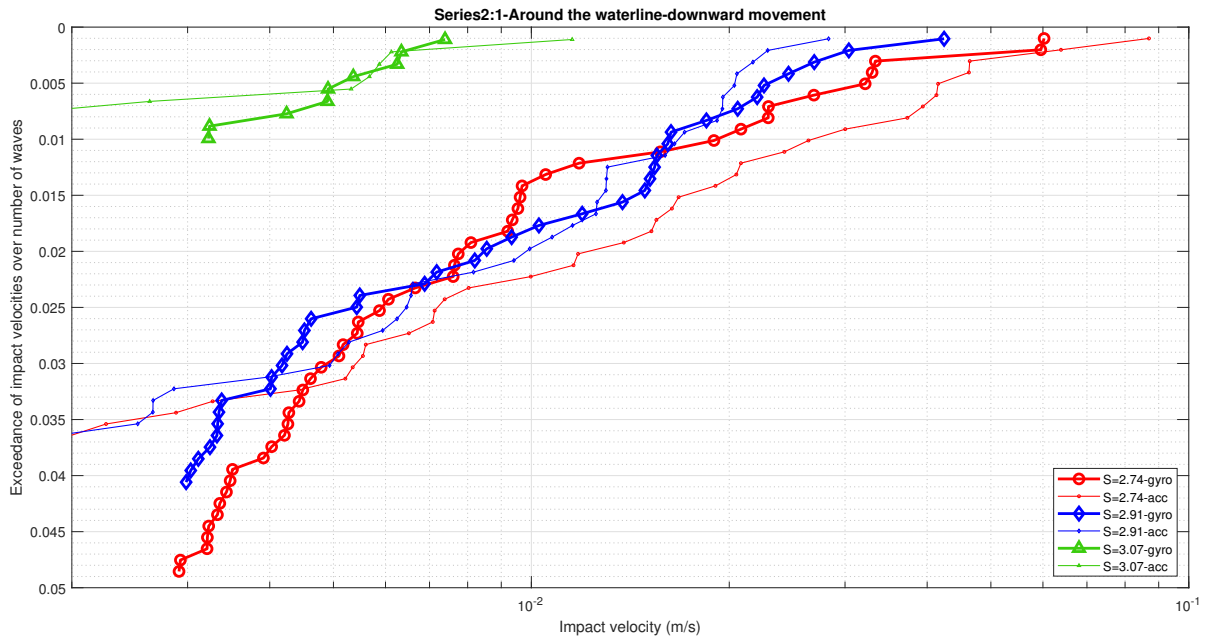


Figure D.6: Exceedance probability in downward movement at waterline for Unit 1- series 2:1

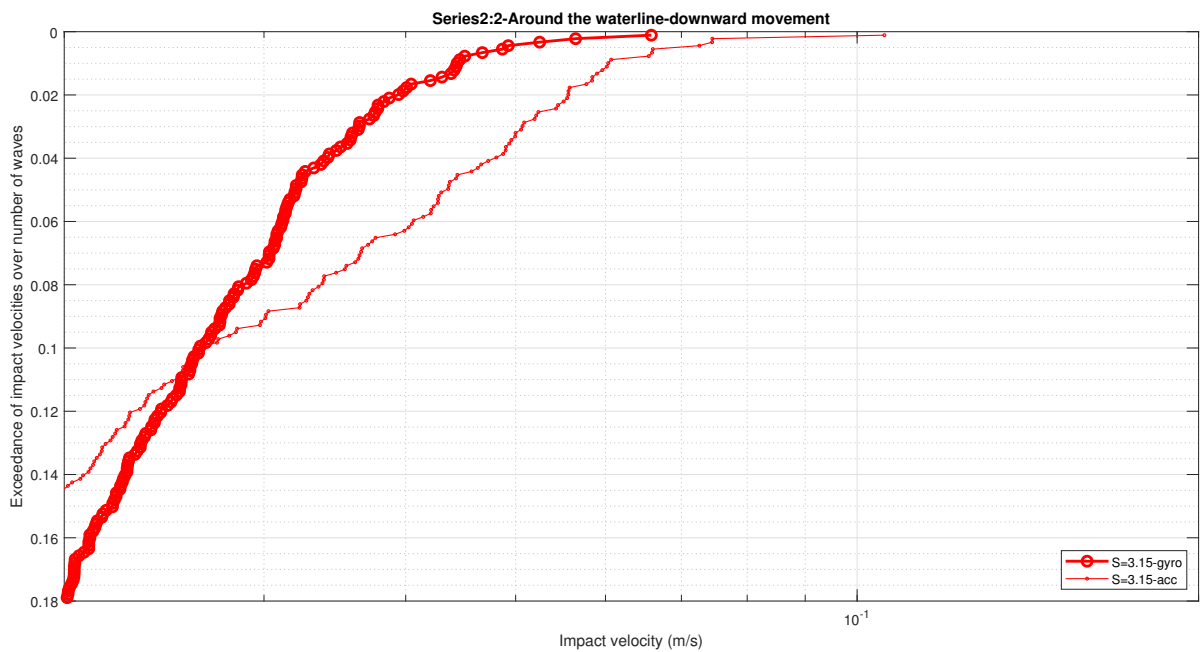


Figure D.7: Exceedance probability in downward movement at waterline for Unit 1- series 2:2

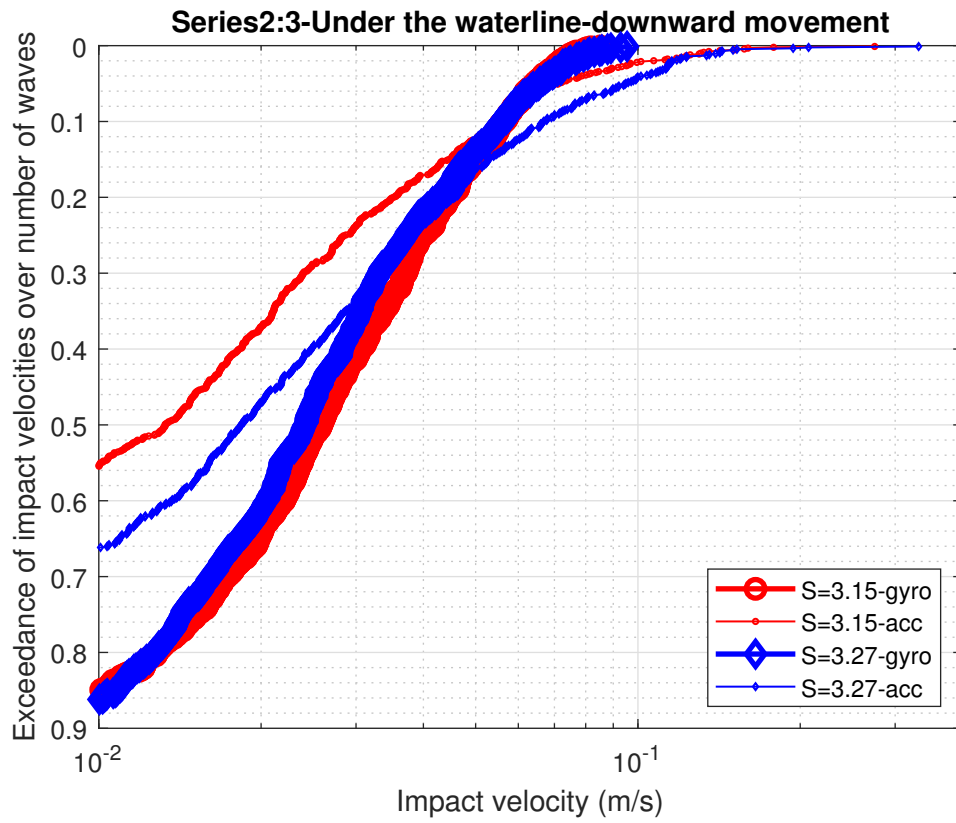


Figure D.8: Exceedance probability in downward movement under the waterline for Unit 1- series 2:3

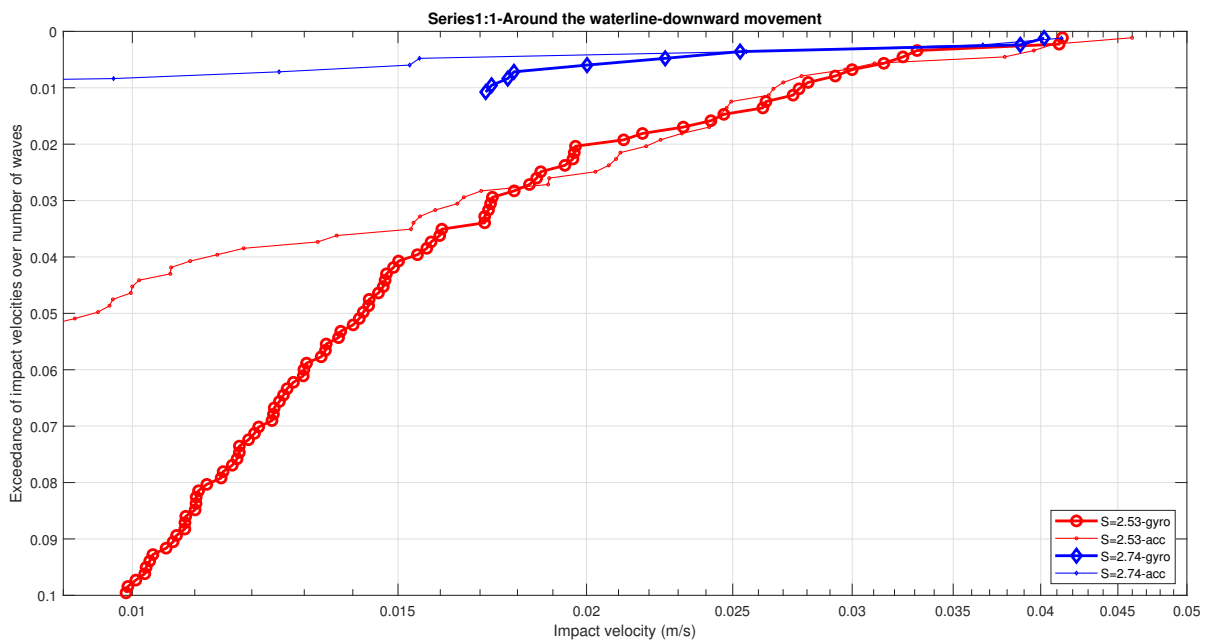


Figure D.9: Exceedance probability in downward movement at waterline for Unit 2- series 1:2

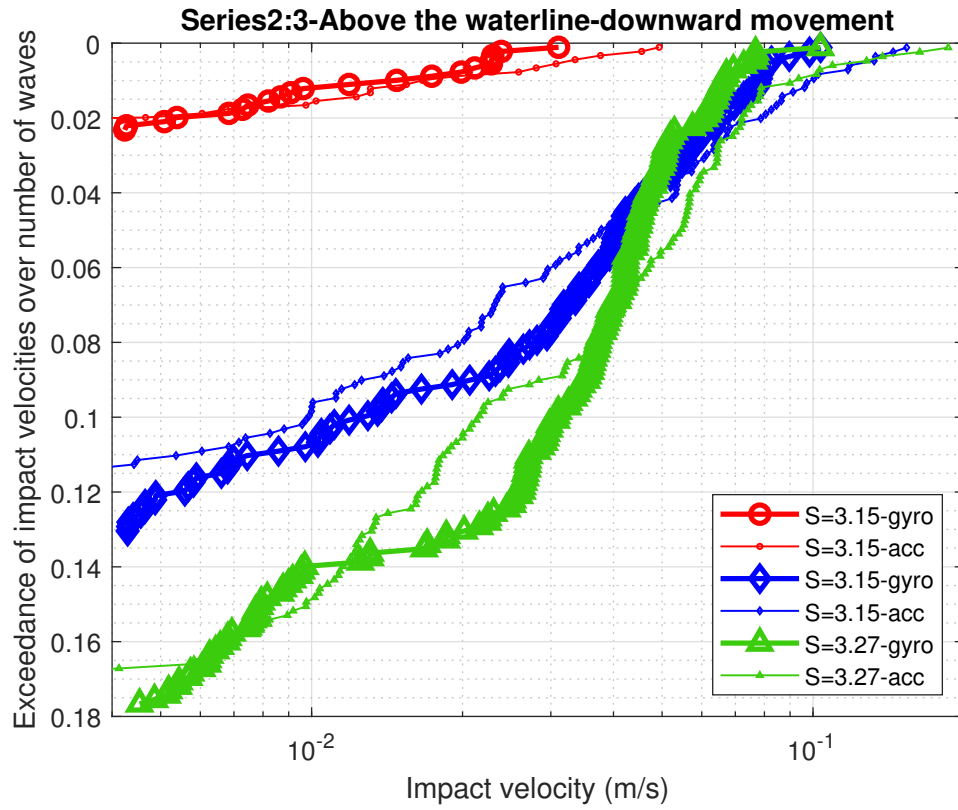


Figure D.10: Exceedance probability in downward movement above the waterline for Unit 2- series 2:3

# List of Figures

1.1	Typical cross section of a rubble mound breakwater (Verhagen et al., 2008)	1
1.2	Different types of armour units (Reedijk & Muttray, 2009)	2
1.3	Xbloc placement on a breakwater	2
2.1	Schematic representation of the time variations of acceleration $a$ and angular velocity $\omega$ during rocking and collision, starting at vertical solid line (Hofland et al., 2018)	9
2.2	Change in angle over time due to falling test of eight sensors (Arefin, 2017)	10
2.3	Instrumented 3D printed Core-Loc unit a) Front b) Back (Eden, 2019)	14
3.1	3D printed Xbloc unit a) Design with Google Sketch-up b) After 3D printing	16
3.2	Main components required to make the circuit and waterproofing	17
3.3	Internal circuit	17
3.4	Development of the instrumented Xbloc unit	18
3.5	Positions of the lead pieces	19
3.6	Different classes of micro SD cards considered for the comparison and their writing speed limits	21
3.7	Comparison of sampling frequencies achieved by the different SD classes without any modification in original sketch	22
3.8	Average frequencies achieved without any modification and their slowing down with time	23
3.9	Comparison of time between two readings achieved by different classes after the modification	23
3.10	Comparison of different improvement techniques	24
3.11	Axis convention of the sensor	25
3.12	Rotation of 90 degrees	26
3.13	Change of angle with time for six sensors	26
3.14	Complementary filter algorithm (Gui et al., 2015)	27
4.1	Breaker types	31
4.2	Design stability values (DMC, 2003)	32
4.3	Slope dimensions	34
4.4	Slope preparation a) Wooden slope b) After gluing the stone layer	35
4.5	Geometry of the Xbloc	35
4.6	Model section	36
4.7	Placement of Armour layer	37
5.1	Position of the instrumented units before starting the test series 1	40
5.2	Before and After situation- test 1, series 1	40
5.3	Before and After situation- test 1, series 2	41
6.1	Rotational motion A)Initial position B)Rotation around y axis (pitch) C)Rotation around x axis (roll) D)Rotation around z axis (Yaw)	43
6.2	Translation motion A)Initial position B)Translation along Y axis	44
6.3	Local axes of instrumented Xbloc unit	44
6.4	Raw accelerometer data (Resultant) of unit 1- $H_s/\Delta D_n = 2.03$ - series 1:1	45
6.5	Raw gyroscope data (Resultant) of unit 1- $H_s/\Delta D_n = 2.03$ - series 1:1	45
6.6	Variation of raw accelerometer data (Resultant) of unit 1- $H_s/\Delta D_n = 2.03$ - series 1:1	46
6.7	Rotation measured by the gyroscope	46
6.8	Behaviour of motion during the impact 1-unit 1- $H_s/\Delta D_n = 2.03$ - series 1:1	47
6.9	Behaviour of motion during the impact 2-unit 1- $H_s/\Delta D_n = 2.03$ - series 1:1	48

6.10 Simplified view of rocking event . . . . .	50
6.11 Processing accelerometer data based on Euler angle transformation . . . . .	51
6.12 Exceedance probability in upward movement for Unit 1- series 1:1 . . . . .	52
6.13 Exceedance probability in upward movement at waterline for Unit 1- series 1:2 . . . . .	53
6.14 Exceedance probability in downward movement at the waterline for Unit 1- Test series 1:1 . . . . .	55
6.15 Exceedance probability in downward movement under the waterline for Unit 1- Test series 1:2 . . . . .	56
6.16 Comparison of characteristic impact velocities obtained at the waterline- Series 1 . . . . .	57
6.17 Comparison of characteristic impact velocities obtained at the waterline for upward movement -Test series2 . . . . .	58
6.18 Comparison of characteristic impact velocities obtained at the waterline for downward movement- Test series 2 . . . . .	58
6.19 Comparison of number of collisions for test series 1 . . . . .	59
6.20 Comparison of number of collisions for test series 2 . . . . .	59
B.1 Top view before and after the test $H_s/\Delta D_n = 2.03$ - series 1:1 . . . . .	67
B.2 Top view before and after the test $H_s/\Delta D_n = 2.32$ - series 1:1 . . . . .	68
B.3 Top view before and after the test $H_s/\Delta D_n = 2.43$ - series 1:1 . . . . .	68
B.4 Top view before and after the test $H_s/\Delta D_n = 2.53$ - series 1:2 . . . . .	69
B.5 Top view before and after the test $H_s/\Delta D_n = 2.74$ - series 1:2 . . . . .	69
B.6 Top view before and after the test $H_s/\Delta D_n = 2.74$ - series 2:1 . . . . .	70
B.7 Top view before and after the test $H_s/\Delta D_n = 2.91$ - series 2:1/2 . . . . .	70
B.8 Top view before and after the test $H_s/\Delta D_n = 3.07$ - series 2:1/2 . . . . .	71
B.9 Top view before and after the test $H_s/\Delta D_n = 3.15$ - series 2:2/3 . . . . .	71
B.10 Top view before and after the test $H_s/\Delta D_n = 3.15$ - series 2:3 . . . . .	72
B.11 Top view before and after the test $H_s/\Delta D_n = 3.27$ - series 2:3 . . . . .	72
C.1 Behaviour of motion during the impact 3-unit 1- $H_s/\Delta D_n = 3.15$ - series 2:3 . . . . .	73
C.2 Behaviour of motion during the impact 2-unit 1- $H_s/\Delta D_n = 3.15$ - series 2:3 . . . . .	74
C.3 Behaviour of motion during the impact 1-unit 1- $H_s/\Delta D_n = 3.15$ - series 2:3 . . . . .	74
C.4 Behaviour of motion during the impact 1-unit 1- $H_s/\Delta D_n = 3.27$ - series 2:3 . . . . .	75
D.1 Exceedance probability in upward movement at waterline for Unit 1- series 2:1 . . . . .	77
D.2 Exceedance probability in upward movement at waterline for Unit 1- series 2:2 . . . . .	78
D.3 Exceedance probability in upward movement under the waterline for Unit 1- series 2:3 . . . . .	78
D.4 Exceedance probability in upward movement at waterline for Unit 2- series 1:2 . . . . .	79
D.5 Exceedance probability in upward movement above the waterline for Unit 2- series 2:3 . . . . .	79
D.6 Exceedance probability in downward movement at waterline for Unit 1- series 2:1 . . . . .	80
D.7 Exceedance probability in downward movement at waterline for Unit 1- series 2:2 . . . . .	80
D.8 Exceedance probability in downward movement under the waterline for Unit 1- series 2:3 . . . . .	81
D.9 Exceedance probability in downward movement at waterline for Unit 2- series 1:2 . . . . .	81
D.10 Exceedance probability in downward movement above the waterline for Unit 2- series 2:3 . . . . .	82

# List of Tables

3.1	Summary of the calculation of Moment of Inertia . . . . .	19
3.2	Bias of the acceleration measurements . . . . .	25
4.1	Limiting wave conditions for design purpose . . . . .	32
4.2	Correction for Stability numbers . . . . .	33
4.3	Selected Wave conditions- Series 1 . . . . .	33
4.4	Selected Wave conditions- Series 2 . . . . .	34
6.1	Characteristic Impact Velocity- Upward movement- Unit1-Series 1/2-at the waterline . .	54
6.2	Characteristic Impact Velocity-Upward movement- Unit1-Series 2- just below the waterline	54
6.3	Characteristic Impact Velocity-Upward movement- Unit2-Series 1/2 . . . . .	54
6.4	Characteristic Impact Velocity- downward movement- Unit1-Series 1/2-at the waterline	54
6.5	Characteristic Impact Velocity-downward movement- Unit1-Series 2- just below the wa- terline . . . . .	55
6.6	Characteristic Impact Velocity-downward movement- Unit2-Series 1/2 . . . . .	55
A.1	Test conditions for unit 1-Day 1 . . . . .	65
A.2	Test conditions for unit 2-Day 1 . . . . .	65
A.3	Test conditions for unit 1-Day 2 . . . . .	65
A.4	Test conditions for unit 2-Day 2 . . . . .	66

# Bibliography

- Akeila, E., Salcic, Z., & Swain, A. (2008). Direct gravity estimation and compensation in strapdown ins applications.
- Akeila, E., Salcic, Z., & Swain, A. (2010). Smart pebble for monitoring riverbed sediment transport. *IEEE Sensors Journal*, 10-11, 1705-1717. doi: 10.1109/JSEN.2010.2046726
- Arefin, S. S. (2017). *Rocking revisited 2, measurement on rocking of cubes in a double layer on a breakwater* (Unpublished master's thesis). Delft University of Technology, Delft, The Netherlands.
- Brownjohn, J. M. W. (1999). *Double integrated response of accelerometer data* (Tech. Rep.). Matlab code.
- Dai, Y. B., & Kamel, A. M. (1969). *Scale effect tests for rubble-mound breakwaters: Hydraulic model investigation* (Tech. Rep.). US Army EngineerWaterways Experiment Station.
- De Leau, J. (2017). *Laboratory experiments on the stability of concrete cubes; a comparison of testing methodologies* (Unpublished master's thesis). Delft University of Technology, Delft, The Netherlands.
- DMC. (2003). *Xbloc armour unit development,hydraulic performance of xbloc armour units - 2-d model tests at wl delft* (Tech. Rep.). Delta Marine Consultants.
- DMC. (2011). *Guidelines for xbloc concept designs* (Tech. Rep.). Delta Marine Consultants.
- DMC. (2017). *Instruction xbloc model testing, revision d* (Tech. Rep.). Delta Marine Consultants.
- Eden, D. (2019). *Forces and pressures on core-loc armour units in rubble mound breakwaters measured via instrumented smart units* (Unpublished master's thesis). University of Ottawa, Ottawa, Canada.
- Ferraris, F., Grimaldi, U., & Parvis, M. (1995). Procedure for effortless in-field calibration of three-axis rate gyros and accelerometers. *Sensors and Materials*, 7, 311-330.
- Goseberg, N., Stolle, J., & Nistor, I. (2016). Inertial forces on shipping containers from a broken tsunami bore. In *Proc. 6th international conference on the application of physical modelling in coastal and port engineering and science*. Ottawa, Canada: Coastlab16.
- Gronz, O., Hiller, P. H., Wirtz, S., Becker, K., Iserloh, T., Aberle, J., & Casper, M. C. (2015, April). Smartstones: a small e-compass, accelerometer and gyroscope embedded in stones. In *Egu general assembly conference abstracts* (Vol. 17, p. 12214).
- Gui, P., Tang, L., & Mukhopadhyay, S. (2015). Mems based imu for tilting measurement: Comparison of complementary and kalman filter based data fusion. In *2015 ieee 10th conference on industrial electronics and applications (iciea)*. Auckland: IEEE2015. doi: 10.1109/ICIEA.2015.7334442
- HobbyTronics. (2019). *Displaying float variables in arduino*. Retrieved from <http://www.hobbytronics.co.uk/arduino-float-vars> (Last accessed 25 April 2019)
- Hofland, B., Arefin, S. S., Van der Lem, C., & Van Gent, M. R. A. (2018). Smart rocking armour units. In *Proc. 7th international conference on the application of physical modelling in coastal and port engineering and science*. Santander, Spain: Coastlab18.
- <http://forum.arduino.cc>. (2019). *Why is the sd library slow?* Retrieved from <http://forum.arduino.cc/index.php?topic=49649.msg354701#msg354701> (Last accessed 30 April 2019)
- <https://github.com>. (2019a). *Arduino fat16/fat32 library*. Retrieved from <https://github.com/greiman/SdFat> (Last accessed 29 April 2019)

- <https://github.com>. (2019b). *Tinycircuits/tinycircuits-tinyshield-memory-eprom-asd2202*. Retrieved from <https://github.com/TinyCircuits/TinyCircuits-TinyShield-Memory-EEPROM-ASD2202/tree/master/examples> (Last accessed 25 April 2019)
- Kirkegaard, J., Wolters, G., Sutherland, J., Soulsby, R., Frostick, L., McLelland, S., ... Gerritsen, H. (2011). *Users guide to physical modelling and experimentation - experience of the hydralab network*. Taylor and Francis Group, 6000, Broken Sound Parkway, NW, Suite 300 Boca Raton, FL 33487-2742: CRC press.
- Le, T. N. (2016). *Rocking revisited 1, rocking of a single cube on a breakwater slope* (Unpublished master's thesis). Delft University of Technology, Delft, The Netherlands.
- Reedijk, B., & Muttray, M. (2009). Design of concrete armour layers. *Hansa International Maritime Journal*, 6, 111-118.
- Stančin, S., & Tomažič, S. (2011). Angle estimation of simultaneous orthogonal rotations from 3d gyroscope measurements. *Sensors(Basel)*, 11(9), 8536–8549. doi: 10.3390/s110908536
- Van der Meer, J. W., & Heydra, G. (1991). Rocking armour units: Number, location and impact velocity. *Coastal Engineering*, 15, 21-39.
- Verhagen, H. J., van Roode, F., & d'Angremond, K. (2008). *Breakwaters and closure dams* (2nd ed.). VSSD.
- [www.arduino.cc](http://www.arduino.cc). (2019). *Arduino 2019*. Retrieved from <https://www.arduino.cc/> (Last accessed 30 April 2019)
- Zwanenburg, S. (2012). *The influence of the wave height distribution on the stability of single layer concrete armour units* (Unpublished master's thesis). Delft University of Technology, Delft, The Netherlands.
- Zwanenburg, S., Uijttewaal, W., Ten Oever, E., & Muttray, M. (2014). The influence of the wave height distribution on the stability of interlocking single layer armour units. In *From sea to shore – meeting the challenges of the sea*. ice publishing. doi: 10.1680/fsts.59757.0508